[redacted]

CENTRAL RESEARCH LIBRARY
DOCUMENT COLLECTION

MARTIN MARIETTA ENERGY SYSTEMS LIBRARIES
3 4456 0349581 2

ORNL-1625
Progress

# AEC RESEARCH AND DEVELOPMENT REPORT

LABORATORY RECORD
1954

## METALLURGY DIVISION

## SEMIANNUAL PROGRESS REPORT

FOR PERIOD ENDING OCTOBER 10, 1953

DECLASSIFIED
CLASSIFICATION CHANGED TO
BY AUTHORITY OF AEC-6-12-62
BY ... Bowman 8-10-62

CENTRAL RESEARCH LIBRARY
DOCUMENT COLLECTION
LIBRARY LOAN COPY
DO NOT TRANSFER TO ANOTHER PERSON
If you wish someone else to see this document, send in name with document and the library will arrange a loan.

OAK RIDGE NATIONAL LABORATORY
OPERATED BY
CARBIDE AND CARBON CHEMICALS COMPANY
A DIVISION OF UNION CARBIDE AND CARBON CORPORATION
UCC
POST OFFICE BOX P
OAK RIDGE, TENNESSEE

[redacted]

This document contains Restricted Data as defined in the Atomic Energy Act of 1946. Its transmittal or the disclosure of its contents in any manner to an unauthorized person is prohibited.

[redacted]

[redacted]

ORNL-1625

This document consists of 90 pages.

Copy 6 of 146 copies. Series A.

Contract No. W-7405-eng-26

# METALLURGY DIVISION

# SEMIANNUAL PROGRESS REPORT

## for Period Ending October 10, 1953


J. H. Frye, Jr., Director

EDITED BY

W. H. Bridges


DATE ISSUED

~~DEC 3 1 1953~~


OAK RIDGE NATIONAL LABORATORY
Operated by
CARBIDE AND CARBON CHEMICALS COMPANY
A Division of Union Carbide and Carbon Corporation
Post Office Box P
Oak Ridge, Tennessee


[redacted]


MARTIN MARIETTA ENERGY SYSTEMS LIBRARIES

3 4456 0349581 2

[redacted]



*INTERNAL DISTRIBUTION*

1. C. E. Center
2. Biology Library
3. Health Physics Library
4. Metallurgy Library
5-6. Central Research Library
7. Reactor Experimental Engineering Library
8-12. Laboratory Records Department
13. Laboratory Records, ORNL RC
14. C. E. Larson
15. W. B. Humes (K-25)
16. L. B. Emlet (Y-12)
17. A. M. Weinberg
18. E. H. Taylor
19. E. J. Murphy
20. E. D. Shipley
21. J. H. Frye, Jr.
22. F. C. VonderLage
23. R. C. Briant
24. J. A. Swartout
25. S. C. Lind
26. F. L. Culler
27. A. H. Snell
28. A. Hollaender
29. M. T. Kelley
30. K. Z. Morgan
31. T. A. Lincoln
32. A. S. Householder
33. C. S. Harrill
34. C. E. Winters
35. D. S. Billington
36. D. W. Cardwell
37. E. M. King
38. A. J. Miller
39. D. D. Cowen
40. P. M. Reyling
41. W. H. Bridges
42. G. C. Williams
43. L. K. Jetter
44. E. J. Boyle
45. W. D. Manly
46. C. D. Susano
47. W. W. Parkinson
48. R. J. Gray
49. H. A. Yakel
50. D. C. Vreeland
51. E. E. Stansbury
52. G. P. Smith
53. J. E. Cunningham
54. R. S. Crouse
55. R. E. Adams
56. J. H. Erwin
57. J. O. Betterton, Jr.
58. W. O. Harms
59. G. M. Adamson
60. E. S. Bomar
61. R. J. Beaver
62. T. W. Fulton
63. W. J. Fretague
64. R. B. Oliver
65. J. T. Howe
66. T. H. Blewitt
67. C. R. Boston
68. J. H. Crawford, Jr.
69. J. C. Wilson
70. H. W. Savage
71. E. E. Hoffman
72. W. J. Leonard
73. J. A. Milko
74. J. M. Warde
75. P. M. Uthe
76. E. C. Cruetz (consultant)
77. E. P. Wigner (consultant)
78. W. W. Grigorieff (consultant)
79. R. W. Johnson
80. J. A. Lane

[redacted]

[redacted]

*EXTERNAL DISTRIBUTION*

81-88. Argonne National Laboratory
89-96. Atomic Energy Commission, Washington
97. Battelle Memorial Institute
98-101. Brookhaven National Laboratory
102. Brush Beryllium Company (N. W. Bass)
103-106. Carbide and Carbon Chemicals Company (Y-12 Plant)
107-108. Knolls Atomic Power Laboratory
109-110. General Electric Company, Richland
111-113. General Electric Company (ANPP)
114. Hanford Operations Office
115. Phillips Petroleum Company
116-119. Los Alamos Scientific Laboratory
120. Massachusetts Institute of Technology (Kaufmann)
121-122. New York Operations Office
123. Patent Branch, Washington
124. duPont Company, Wilmington
125-139. Technical Information Service, Oak Ridge
140-143. University of California Radiation Laboratory, Berkeley
144. Westinghouse Electric Corporation
145. Atomic Energy Commission, Pittsburgh Area Office
146. Atomic Energy Commission, Schenectady Operations Office

[redacted]

[redacted]

Reports previously issued in this series are as follows:

| | |
|---|---|
| ORNL-28 | Period Ending March 1, 1948 |
| ORNL-69 | Period Ending May 31, 1948 |
| ORNL-407 | Period Ending July 31, 1949 |
| ORNL-511 | Period Ending October 31, 1949 |
| ORNL-583 | Period Ending January 31, 1950 |
| ORNL-754 | Period Ending April 30, 1950 |
| ORNL-827 | Period Ending July 31, 1950 |
| ORNL-910 | Period Ending October 31, 1950 |
| ORNL-987 | Period Ending January 31, 1951 |
| ORNL-1033 | Period Ending April 30, 1951 |
| ORNL-1108 | Period Ending July 31, 1951 |
| ORNL-1161 | Period Ending October 31, 1951 |
| ORNL-1267 | Period Ending January 31, 1952 |
| ORNL-1302 | Period Ending April 30, 1952 |
| ORNL-1366 | Period Ending July 31, 1952 |
| ORNL-1437 | Period Ending October 31, 1952 |
| ORNL-1503 | Period Ending January 31, 1953 |
| ORNL-1551 | Period Ending April 10, 1953 |

[redacted]

[redacted]

## CONTENTS


SUMMARY . . . . . 1

PHYSICAL METALLURGY OF REACTOR MATERIALS . . . . . 4
- Thorium Creep and Stress-Rupture Tests . . . . . 4
- Impact Strength of Thorium . . . . . 6
- Radiation Damage of Thorium . . . . . 6
  - LITR irradiation experiments . . . . . 6
  - MTR irradiation experiments . . . . . 7
- ORNL Graphite Reactor Slug Failures . . . . . 7

HRP METALLURGY . . . . . 9
- Fracture Behavior of Titanium and Zirconium . . . . . 9
- Physical Metallurgy of Titanium and of Zirconium Alloys . . . . . 9
  - Commercial titanium . . . . . 9
  - Bureau of Mines titanium . . . . . 11
  - Zirconium-aluminum system . . . . . 11
  - Zirconium-indium system . . . . . 12
  - Zirconium-tin alloys (Zircalloy II) . . . . . 13
- Welding of Stainless Steels . . . . . 14
- Dynamic Corrosion of Welded Stainless Steel Specimens . . . . . 14
- Stress-Corrosion Cracking of Type 347 Stainless Steel . . . . . 15
- Selective Oxidation of Austenitic Stainless Steels . . . . . 17

ANP METALLURGY . . . . . 19
- Static Corrosion . . . . . 19
  - Corrosion by fluorides . . . . . 19
  - Corrosion by liquid metals . . . . . 22
  - Miscellaneous corrosion tests . . . . . 26
- Dynamic Corrosion . . . . . 26
  - Effect of time on fluoride corrosion . . . . . 26
  - Effect of temperature on fluoride corrosion . . . . . 30
  - Effect of fuel purity . . . . . 30
  - Effect of additives to the fluoride mixtures . . . . . 31
  - Effect of a graphite insert . . . . . 31
  - Preferential attack on type 316 stainless steel . . . . . 31
  - Nickel as a container material . . . . . 32
  - Loop cleaning . . . . . 32
- Physical Chemistry . . . . . 33
  - Sodium oxidation . . . . . 33
  - Interfacial equilibriums in the copper-bismuth system . . . . . 35
  - Mass transfer in liquid lead . . . . . 36
  - Hydroxide chemistry . . . . . 40


[redacted]

[redacted]


Sodium combustion . . . . . 45
Brazing . . . . . 45
High-conductivity-fin heat exchanger . . . . . 45
Nickel-phosphorus and nickel-chromium-phosphorus brazing alloys . . . . . 48
Heat exchanger fabrication . . . . . 51
Fabrication . . . . . 52
ANP radiator . . . . . 52
Special alloys . . . . . 54
Columbium research . . . . . 55
Tubular fuel elements . . . . . 55
G-E control rod . . . . . 55
ARE pump seals . . . . . 56
Shield plates . . . . . 58
Mechanical Properties of Inconel . . . . . 58

UPR METALLURGY . . . . . 59
Diffusion Studies on Barrier Materials . . . . . 59
Silicon-aluminum alloys as barriers . . . . . 59
Barriers containing beryllium . . . . . 60
52S aluminum alloy as a barrier . . . . . 60
SAP aluminum alloy as a barrier . . . . . 60
Magnesium as a barrier . . . . . 60
Chromium alloys as barriers . . . . . 60
Cerium alloys as barriers . . . . . 60
Nickel as a barrier . . . . . 61
Alloys of vanadium, columbium, and molybdenum with thorium as barriers . . . . . 61
Alloy of tin with thorium as a barrier . . . . . 61
Titanium as a barrier . . . . . 61
Roll Cladding Studies . . . . . 61
Heat treatment of alclad thorium plates at 150 and 200°C . . . . . 61
Assembly of thorium feed components . . . . . 63

CERAMICS . . . . . 68
Petrographic Examination of Fluoride Fuels . . . . . 68
Insulating End Cap Development . . . . . 69
Cermets . . . . . 69
$UO_2$ Investigations . . . . . 70
$ThO_2$ Investigations . . . . . 70
Rare Earth Oxide Investigations . . . . . 70
Ceramic Containers for Radioactive Strontium . . . . . 71
Glass-Type Pump Seals (ANP) . . . . . 71
Ceramic Container for Use in Fuel Studies (ANP) . . . . . 71

METALLOGRAPHY . . . . . 72


[redacted]

[redacted]


FABRICATION METALLURGY . . . . . 75
MTR Experimental Studies . . . . . 75
Alclad $UO_2$ and Aluminum Powder Fuel Plates . . . . . 76
Transverse tensile strength of core material . . . . . 78
Density of core material . . . . . 78
Segregation in core material . . . . . 79
Uranium-Aluminum Alloy Products . . . . . 80
MTR replacement fuel and control rod elements . . . . . 80
LITR replacement fuel and control rod elements . . . . . 80
Fuel elements for BORAX experiment . . . . . 81
BSR fuel elements . . . . . 81
Fuel and control elements for Tower Shielding Facility . . . . . 81
Extrusion of enriched uranium-aluminum alloy rod stock for "J" slugs . . . . . 81
Fabrication of alclad uranium-aluminum alloy tube for Chalk River . . . . . 81
Miscellaneous Fabricational Work . . . . . 82


[redacted]

# METALLURGY DIVISION SEMIANNUAL PROGRESS REPORT

## SUMMARY


### PHYSICAL METALLURGY OF REACTOR MATERIALS

Continuation of work on the creep and stress-rupture behavior of thorium has produced definite evidence of the occurrence of strain-aging at a temperature of 300°C. Prestressing of Ames thorium bars followed by holding at constant stress has resulted in doubling of the yield strength when the bars are finally loaded to rupture. Interrupted tensile tests have also shown a yield-point effect after each stress cycle.

Impact testing of Ames thorium and iodide thorium has demonstrated the sensitivity to carbon content of the change from brittle to ductile fracture with increasing temperature of testing. Round, subsize specimens of iodide thorium show no reduction of impact strength in the temperature range from −196°C to 180°C. Ames thorium and iodide thorium–carbon alloys with carbon contents of up to 0.21% show a very marked change in impact strength at temperatures in the range of 0 to 40°C.

Examination of discharged aluminum-silicon bonded slugs from the ORNL graphite reactor has shown that increases in length of as much as 0.183 in. have occurred in slugs which were not beta-transformed. Slugs which were transformed exhibit considerably smaller amounts of growth. It is thought that the ruptures which have been observed have resulted from leaks in the slug welds or cans and have not been caused by growth of the uranium.

### HRP METALLURGY

Experimental studies of the notch-brittle fracture behavior of titanium and zirconium are being carried out to assist in the evaluation of the suitability of these materials for the construction of lined vessels and of zirconium alloy core tanks.

Fatigue and impact properties of titanium and zirconium alloys are being studied, particularly as these properties may be influenced by methods of production and relative purity of the original material, as well as by exposure to corrosion in simulated operating environments. The possibility of introducing hydrogen into the metal during corrosion exposure, cathodic treatment, or heat treatment and thus modifying the impact behavior is being studied. The work of other investigators, which established the absence of a ductile-to-brittle fracture transition in high-purity arc-melted iodide titanium, has been confirmed, and it has been established that, at least on a laboratory scale, a good quality of selected titanium sponge, such as that obtained from the Bureau of Mines, when arc melted, swaged, and vacuum annealed, does not exhibit brittle transition down to liquid nitrogen temperatures.

A comparison of the behavior of welded austenitic stainless steels prepared according to various modifications of commercial welding practice and exposed to simulated homogeneous reactor corrosion environments has indicated the importance of further study of the effects of modification of metallurgical factors.

Because of its importance in the design and fabrication of heat exchangers to ensure long-time integrity, some work is being done to determine the relation of composition and other metallurgical factors to the susceptibility of austenitic stainless steels to stress-corrosion cracking.

Selective oxidation of austenitic stainless steels by pretreatment in moist hydrogen has developed protective films which, in some cases, have improved corrosion resistance in simulated reactor environments. This problem is being studied further in an effort to establish practical optimum pretreatments and to provide surfaces consistently resistant to corrosion attack.

### ANP METALLURGY

Studies have been made to determine the influence of varying the carbon and oxygen contents of stainless steels on their resistance to attack by fluorides under static or modified dynamic corrosion conditions in a rocking furnace. Under the conditions of the tests, there was no measurable change in the resistance to corrosion of the stainless steels. Inconel alloys of varying purity were prepared in the laboratory and tested in fluoride mediums for 100 hr at 815°C. The alloys prepared in the laboratory were not significantly different from the commercial alloys with respect to attack by the fluorides. In the temperature range of 420 to

1090°C, Inconel in contact with fluoride 14 showed no systematic variation in depth of attack with temperature.

Spinner tests of stainless steels and nickel-base alloys in sodium have been completed at 815°C and a velocity of 405 fpm. Surface layers were quite apparent on the nickel-base alloys and 300 series stainless steel, but they were negligible on the 400 series stainless steel.

A method has been found to eliminate the deposit found in the hot leg of thermal convection loops containing molten fluorides to which zirconium hydride has been added. When the hydride was added to the fill pot and filtered before being charged to the loop, no deposit was observed and, yet, an inhibiting action was obtained.

It was shown that type 316 stainless steel is preferentially attacked by fluorides in the presence of Inconel. Attack was practically nil on the Inconel, while an adjoining type 316 stainless steel section was severely attacked.

At low temperature, 1250°F, a reduction in attack of Inconel by fluorides was found. At 1500 and 1650°F, there was no difference in attack in loops operated for 500 hr, but with loops operated only 100 hr, more attack was observed at the higher temperature.

It now appears that attack of Inconel by fluorides continues after 250 hr of circulation, even though the rate is markedly decreased. Mass transfer of chromium becomes quite apparent with the longer operating times. Graphite immersed in molten fluorides in Inconel was shown to cause carburization of the Inconel vessel.

Additional studies on the mass transfer of container materials in liquid lead, made with the use of small thermal convection loops, have given the following results: a loop containing type 410 stainless steel was operated for 545 hr with only a small amount of mass transfer; loops containing nickel and Nichrome V plugged after 2 and 12 hr, respectively; a loop containing chromium metal plugged in approximately 100 hr; a nickel-iron alloy (30% Ni–70% Fe) caused plugging of a loop after 275 hr of operation.

The combustion of sodium has been studied by spraying molten sodium at 800°C into air. Additions of mercury of about 70 mole % have a pronounced retarding effect on the combustion of sodium.

A systematic study of corrosion of nickel by sodium hydroxide at elevated temperatures has been initiated, and a rational explanation of corrosion behavior at 900°C under vacuum is made on the basis of mass-action laws.

By the use of a low-melting Nicrobraz, high-conductivity fins can be brazed to tubes either in a longitudinal or transverse array. Since it has been found that preplacing the brazing alloy on the brazed joint in the form of wire or washers is advantageous, a technique for the preparation of low-melting-point Nicrobraz shapes and for preplacing them by using acryloid cement has been developed.

A new brazing alloy series (nickel-phosphorus and nickel-chromium-phosphorus) has been developed and is now being studied. Phosphorus additions to nickel and to nickel-chromium alloys are extremely effective in lowering the melting points, and phosphorus is advantageous for reactor applications because it has a low cross section for the absorption of thermal neutrons. A further advantage is the possibility of preplacing the alloy by convenient plating techniques. The tubing can be plated with a nickel strike followed by a nickel-phosphorus coating by using the "electroless" plating technique, and a chromium plate can be added on top of the nickel-phosphorus alloy. It was found that the addition of chromium to the basic nickel-phosphorus alloy is desirable because the chromium increases resistance to air oxidation and sodium corrosion and produces greater joint strength.

In actual radiator fabrication, Nicrobraz is not so desirable a brazing alloy as is a nickel-chromium-silicon alloy such as G-E alloy No. 62. In the fabrication technique found to be most effective, the heat exchanger is brought to 900°C to equalize temperature, quickly heated to the brazing temperature, held for the brazing time, and furnace cooled. Nicrobraz cannot be used for this cycle because, while being held at 900°C, the boron will diffuse out of the alloy and the melting point of the remaining alloy will be too high. The nickel-chromium-silicon brazing alloy in undergoing the same thermal treatment gives a good braze.

The tendency of the nickel-chromium-silicon alloy to crack as a result of thermal shock has been determined by thermally cycling a test radiator assembly from 1000°C to room temperature. Only one small leak occurred after a severe water-quench from 1000°C.

A program for developing a drawing technique for tubular fuel elements has been initiated. Twelve tubes containing cores of type 302 stainless steel, iron, and nickel with 20 and 30% $UO_2$ were reduced from 0.750 in. in diameter with a 0.042-in. wall to 0.250 in. in diameter with a 0.015-in. wall. Plug drawing is being tried.

To give copper the oxidation resistance necessary for use as a high-conductivity fin material, plates of chromium and nickel deposited by the thermal decomposition of the carbonyls were tried without success. Copper clad with Inconel and with types 310 and 446 stainless steel has been under study. The claddings of types 310 and 446 stainless steel seem to offer oxide protection and to be free of the serious interdiffusion experienced with Inconel-clad copper.

The creep and stress-rupture data for both coarse- and fine-grain Inconel tested in fluoride fuels at 815°C have been completed for the stress range of 2500 to 7500 psi. Specimens have now been in test for 1000 hr at 1500 and 2000 psi.

## UPR METALLURGY

Results of short-time diffusion tests indicate the improbability of finding a potential barrier material to prevent the interaction between thorium and aluminum at elevated service temperatures. Numerous commercial materials, as well as various thorium and aluminum alloys, have been tested, but, to date, none have shown any promise.

In the manufacture of alclad thorium plates, the rolling temperature must be confined to the 260 to 400°C temperature range to ensure a sound metallurgical bond that is free of intermetallic compound formation. Initial tests for evaluating the thermal behavior of such plates at 150 and 200°C for periods of up to ten weeks were inconclusive and must be repeated. Unfortunately, the test plates were prepared at 450°C, and they show the presence of intermetallic compound formation in the as-rolled condition.

A cheap and apparently sound method for construction of the thorium parallel-plate type of unit is described. Preliminary results on evaluation of several mechanical joints for use in assembly of the box-type unit are also given.

## CERAMICS

Petrographic investigations continue in connection with ANP fuel investigations. Development work is in progress on insulating end caps for Hanford-type slugs. Work progresses on the development of siliconized silicon carbide-base fuel elements, and a design for a gas-cooled reactor embodying these elements has been proposed. Fabrication of high-density $UO_2$ for fuel element service has been carried out in cooperation with the Westinghouse PWR fuel element program. Fabricational studies of the production of $ThO_2$ shapes for breeder service are being carried out. A study of the mechanism of the densification of $ThO_2$ has been undertaken. An investigation of the ceramic properties of selected rare earth oxides is under way. Work is being carried out on the development of a ceramic container for radioactive strontium. Developmental work was started on a glass-type pump seal for ANP. Fabricational work is under way on the production of a ceramic container for use in ANP fuel studies.

## METALLOGRAPHY

A program has been undertaken to establish the carbide precipitation range in Inconel of varying carbon contents.

## FABRICATION METALLURGY

Density determinations on the alclad sintered $U_3O_8$–aluminum powder core fuel plate show values of 3.09, 3.31, and 3.66, respectively, for core material containing the equivalent of 20, 30, and 40 wt % uranium as $U_3O_8$. The tensile strength of the sintered $U_3O_8$–aluminum powder core material is several factors lower than that of the wrought uranium-aluminum alloy product.

Brazing studies indicate that braze-clad material can be used in the construction of MTR-type fuel elements and that a worthwhile saving in fabrication and chemical processing costs will result. Preplacement of the brazing alloy will reduce the amount of silicon required for brazing the 19-plate element by 60%. Arrangements are complete for Alcoa to supply the new product which will be designated as brazing sheet M-315.

Ten complete core loadings of the thin-side-wall fuel elements were fabricated and delivered to the MTR site. An observed gain in $\Delta k/k$ of 1.56% was measured upon operation of the reactor with the new 19-plate elements in the clean state. The gain was somewhat lower than the calculated value of 2%. The gain calculated for a 20-plate element

fabricated with braze-clad side-plate material is 3.7%.

The 28 special elements needed by ANL for the BORAX Experiment were constructed and forwarded to Arco. Additional replacement fuel units were fabricated for the LITR and the BSR.

Sufficient rod stock of 7.5 wt % uranium–aluminum alloy was extruded and drawn to prepare a batch of 200 "J" slugs for Hanford.

The possibility of fabricating an alclad enriched uranium–aluminum alloy tube for service in the NRX reactor was investigated. Exploratory work conducted on 20% normal uranium alloy material indicated that a composite tube, 1.36 in. in outside diameter with a $\frac{1}{8}$-in. wall thickness, clad inside and out with $\frac{1}{16}$-in.-gage aluminum tubing, could easily be fabricated.

# PHYSICAL METALLURGY OF REACTOR MATERIALS

E. J. Boyle

## THORIUM CREEP AND STRESS-RUPTURE TESTS

R. B. Oliver

In a previous report,[1] the presence of a possible aging phenomenon in thorium was reported. In the investigation of this behavior, tensile and creep tests have been made on extruded bars of Ames thorium and on a few specimens of swaged iodide thorium.

Tensile specimens were machined from bars extruded at a rate of 32 fpm at 850°C with a reduction ratio of 12 to 1. Tensile testing was carried out at 300°C in vacuum. One specimen was loaded directly to rupture, while two other specimens were unloaded and reloaded after a 3-min rest period. The resultant stress-strain curves are shown in Fig. 1. It will be noted that no increase in ultimate strength occurred, but a yield-point effect resulted after each stress cycle. The transitory type of yield point and the discontinuous yielding usually observed during loading are similar to the strain-aging effects described in the literature[2,3] and explained as true strain-aging of the Cottrell type.

A second series of tests was made on specimens machined from the same extruded rod of Ames thorium. These were tested at 300°C in vacuum in a lever-arm creep machine. One specimen was loaded directly to rupture; one was loaded to 4000 psi, allowed to creep for 800 hr, and loaded to rupture; and three more were loaded to 18,000 psi and allowed to creep for 200, 400, and 900 hr, respectively, before being loaded to rupture. Table 1 summarizes the results of these tests.

[1] R. B. Oliver, *Met. Semiannual Prog. Rep. Apr. 10, 1953*, ORNL-1551, p. 4-6.

[2] V. A. Phillips, A. J. Swain, and R. Eborall, *J. Inst. Metals* 81, 625 (August 1953).

[3] V. A. Phillips, *ibid.*, p. 649.

TABLE 1. EFFECT OF PRESTRAINING ON AMES THORIUM

| ORIGINAL STRESS (psi) | TIME AT STRESS (hr) | ELONGATION AFTER PRESTRAIN (%) | YIELD AFTER PRESTRAIN (psi) | ULTIMATE STRESS (psi) | ELONGATION (%) | |
|---|---|---|---|---|---|---|
| | | | | | Total | Net |
| * | | | 12,000 | 19,300 | 21 | 21 |
| 4,000 | 800 | 0.2 | 10,000 | 20,600 | 12 | 11.8 |
| 18,000 | 200 | 18.6 | 20,000 | 21,300 | 30 | 11.4 |
| 18,000 | 400 | 23.0 | 20,000 | 21,000 | 33 | 10.0 |
| 18,000 | 900 | 18.6 | 20,000 | 21,500 | 31 | 14.4 |

*Specimen loaded directly to rupture.

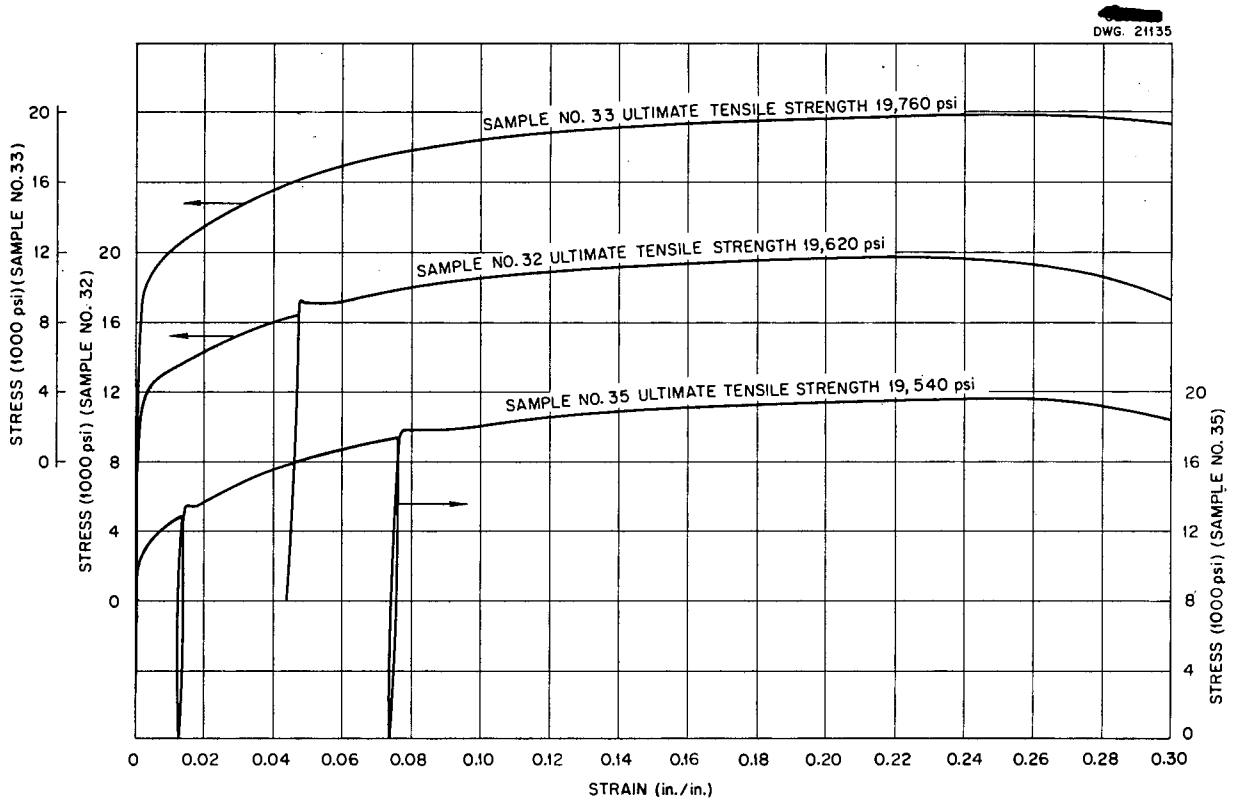


**Fig. 1. Stress-Strain Curves for Ames Thorium from Billet A-320.** Specimens extruded at 850°C at a rate of 32 fpm; tested in vacuum at 300°C; crosshead speed, 0.05 in./min. Curve 1: specimen loaded directly to rupture. Curves 2 and 3: specimens loaded, unloaded for 3 min, and reloaded to rupture.

It is interesting to note that stressing to 4000 psi and aging does not appreciably increase the yield strength. However, prestressing to 18,000 psi nearly doubles the yield strength. Also, if the net elongation after aging is compared with the elongation of a specimen loaded directly to rupture, a marked decrease of ductility is observed.

In Fig. 2, a specimen loaded directly to rupture and one prestressed to 18,000 psi, held for 400 hr, and then loaded to rupture are compared. It will be noted that prestressing and aging increases the ultimate strength by about 10%. Precipitation and/or strain-aging would seem to be indicated.

In a few preliminary tests on iodide thorium, creep behavior very similar to that of Ames thorium has been observed but at considerably lower stress levels. Prestressing, prior to loading to rupture, results in decreased elongation without a significant increase in ultimate strength.

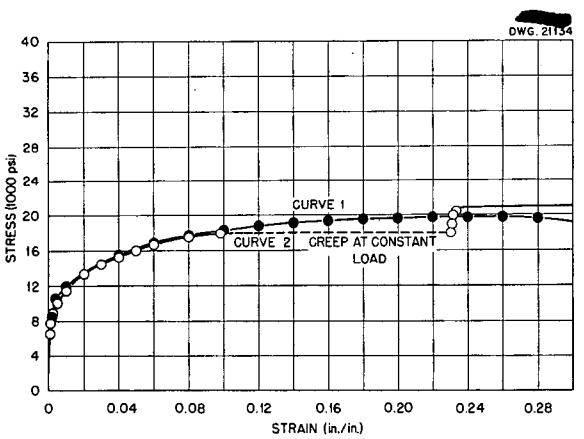


**Fig. 2. Comparison of a Specimen of Ames Thorium from Billet A-320 Loaded Directly to Rupture (Curve 1) with a Specimen Prestressed to 18,000 psi, Held for 400 hr, and Then Loaded to Rupture (Curve 2).** Specimens extruded at 850°C at a rate of 32 fpm; tested in vacuum at 300°C.

## IMPACT STRENGTH OF THORIUM

J. A. Milko

The impact behavior of thorium as determined on standard Charpy V-notch bars was reported previously.[4] These tests were made over the temperature range of −195 to 240°C, and they indicated that a transition in fracture from brittle to ductile occurred in the range from 0 to 180°C. It was noted that specimens fractured below 0°C showed complete fracture, while those broken above this temperature exhibited considerable amounts of flow in the vicinity of the notch.

In reviewing the literature,[5,6] it has been noted that face-centered-cubic metals, such as copper and aluminum, and their precipitation hardenable alloys do not show a transition in impact strength at low temperatures. Since thorium is a face-centered-cubic metal, it was decided to reinvestigate the impact behavior of thorium and also to study the effects of additions of carbon and nitrogen.

The impact specimens of Ames thorium were all obtained from one lot of metal. A 3-in.-dia billet was extruded to $\frac{5}{8}$-in.-dia rod which was swaged to 0.217 in. in diameter. Cylindrical impact specimens, 0.204 in. in diameter with a 45-deg V-notch having a 0.164-in. root diameter, were machined from the swaged rod. When it was found that the notch was not severe enough to result in complete fractures, a notch having a root diameter of 0.050 in. was adapted for all subsequent tests.

The iodide thorium specimens were prepared from arc-melted ingots, 4 in. in length and about 0.5 in. in diameter, which were swaged to 0.217-in.-dia rod.

The results of impact tests on Ames thorium annealed for 30 min at 750°C prior to testing are shown in Fig. 3. All values plotted are the average of four tests. In confirmation of earlier tests, it will be noted that there is a transition from brittle to ductile fracture in the temperature range from 0 to 180°C. Incomplete fracture occurred in specimens tested at temperatures above 80°C.

Results of tests made on iodide thorium specimens are also plotted in Fig. 3. All specimens were annealed for 30 min at 650°C prior to testing. The results show clearly that, in contrast to the Ames thorium, there is no transition in impact behavior – all specimens showed ductile fractures over the entire temperature range. Such behavior is characteristic of face-centered-cubic metals such as aluminum and copper.

Finally, the results of tests on alloys of iodide thorium with additions of 0.16 and 0.21% carbon are shown in Fig. 3. The values for those specimens tested at the higher temperatures are not quantitatively significant because they were taken at the limit of the machine, that is, 50 in.-lb. Several interesting observations can be made from these tests: carbon additions to iodide thorium cause transition behavior in impact properties; the transition occurs at lower temperatures than for Ames thorium, which contains considerably less carbon; and the impact strength of iodide thorium–carbon alloys is lower than that of Ames thorium at very low temperatures and significantly higher at high temperatures. These facts suggest strongly that the impact behavior of Ames thorium is determined by the content of carbon and other impurities, such as nitrogen, rather than by carbon content alone.

## RADIATION DAMAGE OF THORIUM

R. E. Adams
R. H. Kernohan, Solid State Division

Detailed descriptions of experiments planned for studying the effects of radiation on thorium have been given in previous reports.[7] The status of the experiments is presented below.

**LITR Irradiation Experiments.** Tensile, hardness, and impact specimens and cylindrical specimens for study of a variety of the physical properties of thorium were exposed for six months in the LITR at an estimated flux of $4 \times 10^{12}$ neutrons/cm$^2$·sec. The tensile and impact test specimens were removed from the reactor on June 9, 1953, and the hardness and cylindrical test specimens were removed on August 11, 1953. The specimens will be tested as soon as laboratory facilities for working with radioactive materials are available; it is estimated that most of the tests can be started within one or two months.

[4] D. E. Hamby (ed.), *Interim Report on Metallurgy of Thorium and Thorium Alloys*, ORNL-1090 (Dec. 7, 1951).

[5] R. M. Brick, J. R. Low, Jr., and C. H. Lorig, *Behavior of Metals at Low Temperatures*, American Society for Metals, Cleveland, 1953.

[6] P. L. Teed, *The Properties of Metallic Materials at Low Temperatures*, Chapman & Hall, London, 1950.

[7] R. E. Adams and R. H. Kernohan, *Met. Quar. Prog. Reps. for Jan. 31, 1953*, ORNL-1503, p. 4, and *for Apr. 10, 1953*, ORNL-1551, p. 4.

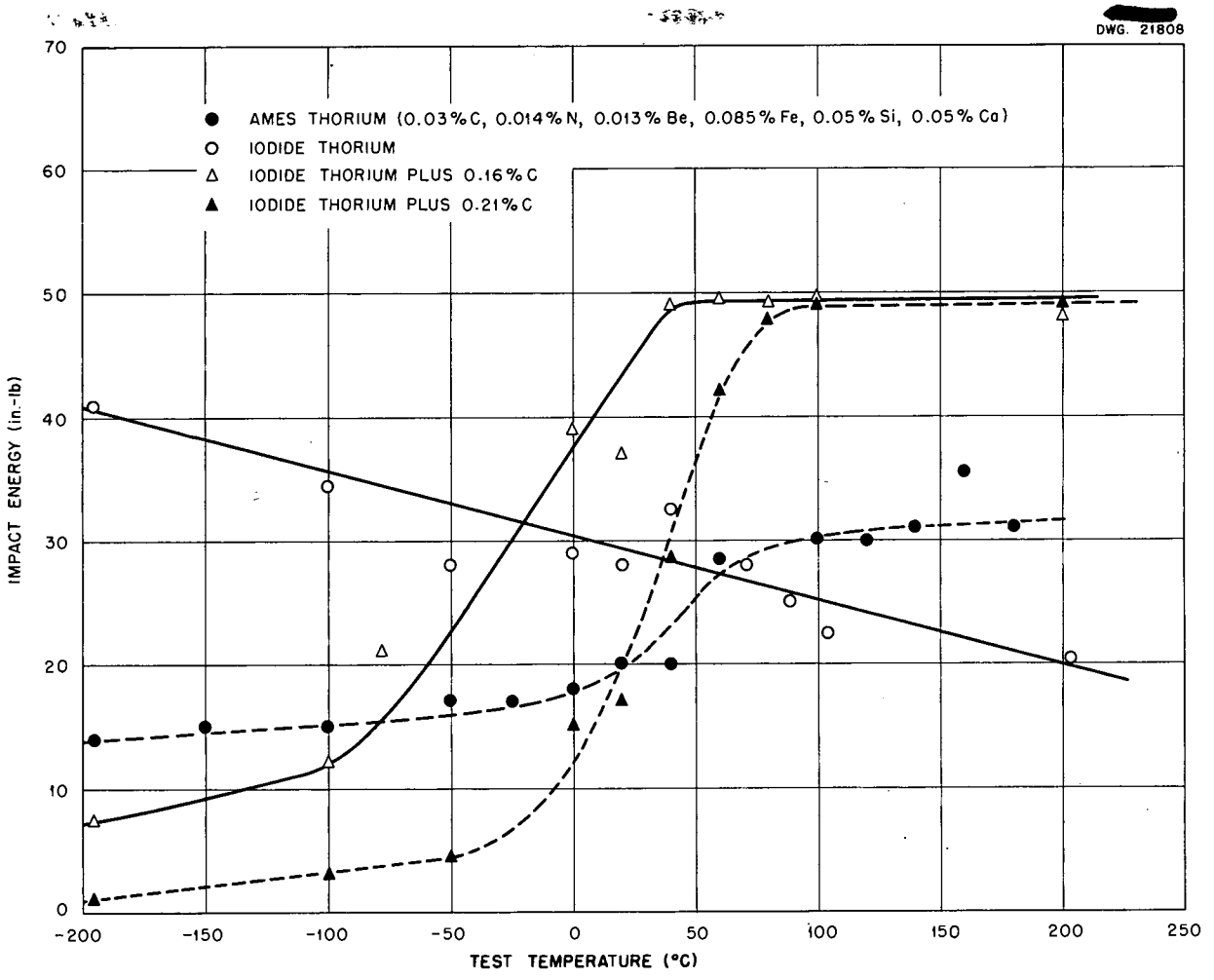


**Fig. 3. Impact Strength of Thorium.**

**MTR Irradiation Experiments.** Irradiation of thorium impact, tensile, and cylindrical test specimens, similar to those exposed in the LITR, was started in the MTR on August 26, 1953. The specimens are submerged in liquid NaK to provide good heat transfer to the zirconium capsules. Exposures of six months and one year will be made.

## ORNL GRAPHITE REACTOR SLUG FAILURES

R. E. Adams

Seventeen of the aluminum-silicon bonded slugs with which the ORNL graphite reactor was recharged on April 1, 1952 have ruptured. A program of examination of the ruptured slugs and of associated slugs from the discharged channels has been carried on.

It has been noted that the frequency of ruptures is highest at the center of the reactor. The maximum number of ruptures occurred in the maximum temperature zone rather than in the zone of highest flux. The cause or causes of rupture have not been fixed with certainty, but all available evidence indicates that the ruptures are the result of air having entered the aluminum cans through undetected holes in the welds or in the cans. Three hundred and fifteen slugs exposed for periods of up to 464 days have been examined, and no instances of incipient failure of the cans have been found that might indicate other causes of failure.

Figure 4 shows a typical ruptured slug. Usually, both the end cap and the bottom section of the slug can are pushed out, and large oxide-filled blisters appear along the length of the slug.

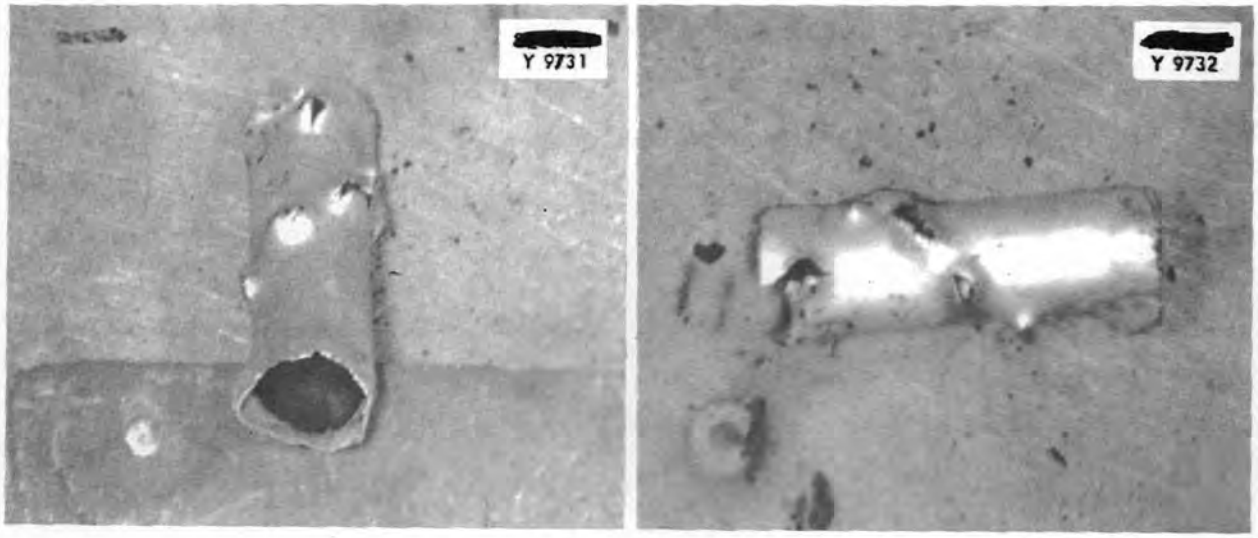


**Fig. 4. Typical Ruptured Slug.**

Some data have been obtained on the growth of irradiated slugs as affected by beta transformation of the uranium. The specifications for all slugs called for complete beta transformation of the uranium, but it was found by examination of sample lots of each batch of slugs that a significant number of slugs which were not transformed because of an error in manufacturing had been put into the reactor. Table 2 gives the changes in length which have been measured.

The values in Table 2 were obtained from measurements of the canned slugs. Three of the slugs were stripped, and the uranium cores were measured to determine whether all the growth occurred in the uranium or whether a "ratcheting" effect as a result of differential thermal expansion of the aluminum and the uranium was a contributing factor in the growth. Table 3 gives the results obtained. Since it was found that the length of the uranium core was greater than that of the canned slug, it is

**TABLE 2. GROWTH OF ORNL GRAPHITE REACTOR FUEL SLUGS**

| RUPTURE NO. | PERCENTAGE OF SAMPLE LOT SHOWING BETA TRANSFORMATION | TIME IN REACTOR (days) | NO. OF SLUGS MEASURED | GROWTH (in.) | | | GROWTH RATE* (in./year) | |
|---|---|---|---|---|---|---|---|---|
| | | | | Min. | Max. | Avg. | Max. | Avg. |
| 4 | 0 | 195 | 10 | 0.010 | 0.043 | 0.024 | 0.080 | 0.045 |
| 8 | 0 | 419 | 15 | 0.013 | 0.099 | 0.045 | 0.086 | 0.039 |
| 13 | 0 | 464 | 40 | –0.002 | 0.183 | 0.063 | 0.144 | 0.050 |
| 7 | 25 | 363 | 16 | 0.013 | 0.085 | 0.043 | 0.086 | 0.043 |
| 3 | 87 | 189 | 10 | 0.000 | 0.022 | 0.011 | 0.042 | 0.021 |
| 5 | 100 | 203 | 34 | 0.001 | 0.021 | 0.008 | 0.037 | 0.014 |
| 14 | 100 | 245 | 34 | –0.006 | 0.009 | 0.002 | 0.015 | 0.003 |
| 9 | 100 | 385 | 52 | –0.002 | 0.014 | 0.006 | 0.012 | 0.005 |
| 15 | 100 | 455 | 10 | 0.004 | 0.043 | 0.012 | 0.034 | 0.009 |

*Calculated from growth measured at time of discharge.

evident that the length measurements were not accurate to better than 0.010 inch. It is significant, however, that all the growth occurred in the uranium.

TABLE 3. COMPARISON OF GROWTH OF CANNED SLUG WITH GROWTH OF ITS URANIUM CORE

| SLUG NO. | GROWTH OF CANNED SLUG (in.) | GROWTH OF URANIUM CORE (in.) |
|---|---|---|
| A | 0.183 | 0.189 |
| B | 0.089 | 0.099 |
| C | 0.183 | 0.189 |

On the basis of the data obtained to date, the following conclusions about the behavior of aluminum-silicon bonded graphite reactor slugs appear to be justified.

1. Slugs which have not been beta transformed grow in length at a maximum rate of about 0.040 to 0.140 in./year. Slugs which have been beta transformed show much lower growth rates, that is, maximum rates of 0.010 to 0.040 in./year.

2. It appears likely that the ruptures which have occurred to date were caused by air in the cans rather than by growth of the uranium cores. However, if the present rate of growth of nontransformed slugs continues, ruptures resulting from growth of the uranium may occur in these slugs in less than five years.

# HRP METALLURGY

E. C. Miller

## FRACTURE BEHAVIOR OF TITANIUM AND ZIRCONIUM

A. R. Olsen

Although the literature search for information on the notch-brittle fracture behavior of titanium and of zirconium has not been entirely completed, sufficient information was found to permit the selection of a testing procedure. A modification of the Kinzel notched-bar slow-bend test[1] as used at Lehigh University was selected. The test consists of centrally loading a freely supported beam, which contains a machined notch in the center of the tension side, and obtaining a load-deflection curve through failure.

To date, only a preliminary survey of the effect of temperature on the ductile-energy absorption of a zirconium-tin alloy (97.5% Zr–2.5% Sn) has been made. The results agree quite well with those reported by others in this group for modified Izod impact tests on the same material, that is, a ductile-to-brittle transition in the range 125 to 200°C.

These tests will be continued, and other criteria[2] for evaluating the ductile-to-brittle transformation will be investigated. These will include deflection at maximum load, energy absorption after maximum load, per cent of contraction below the root of the notch, and fracture appearance.

[1] A. B. Kinzel, *Trans. Am. Soc. Metals* 40, 27-82 (1948).

## PHYSICAL METALLURGY OF TITANIUM AND OF ZIRCONIUM ALLOYS

W. J. Fretague A. R. Olsen

R. G. Berggren

Reactor Experimental Engineering Division

J. J. Woodhouse, Solid State Division

**Commercial Titanium.** Impact tests have been performed over the temperature range from −195.6°C to +300°C on commercial titanium (Ti-75A, heat L782, item 24) specimens in the as-swaged condition and in the as-swaged and cathodically treated condition. Figure 5 is a plot of the data obtained. A comparison of these data with those presented in a previous report[3] for annealed commercial

[2] C. J. Osborn, A. F. Scotchbrook, R. D. Stout, and B. G. Johnston, *Welding J. (N.Y.)* 28, 24-S to 33-S (1949).

[3] W. J. Fretague, A. R. Olsen, and R. G. Berggren, *Met. Semiannual Prog. Rep. Apr. 10, 1953*, ORNL-1551, p. 13.

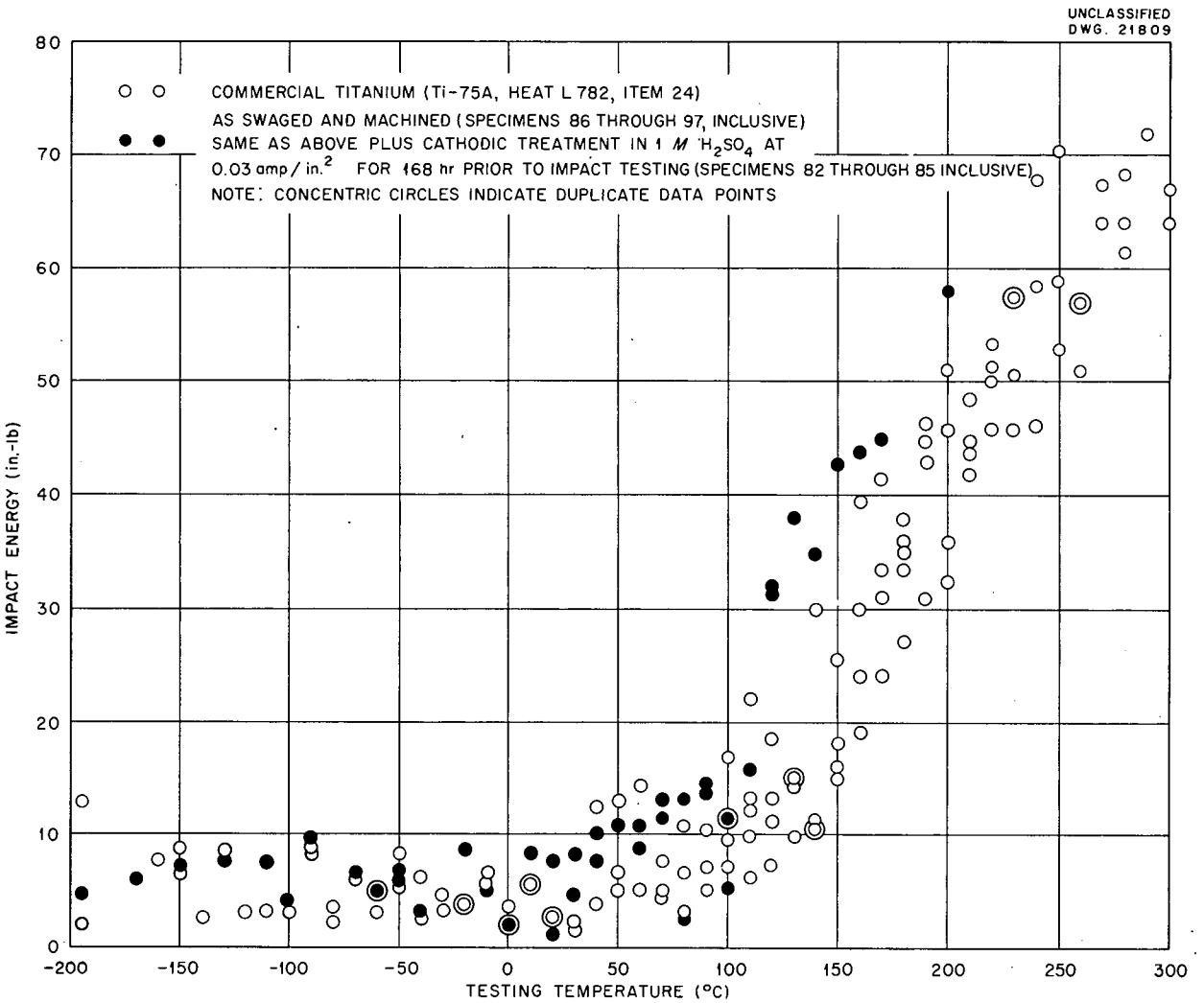


**Fig. 5. Impact Tests of Commercial Titanium.**

titanium (Ti-75A, heat L782, item 24) shows a transition temperature for the as-swaged material that is approximately 50 to 75°C higher than that for the annealed material.

Fatigue tests have been completed on hot-rolled and annealed Ti-75A sheet fatigue specimens that were exposed in uranyl sulfate solution (300 g of uranium per liter) for 200 hr at 250°C. Table 4 gives the complete history of the specimens prior to testing and the results obtained in fatigue tests. Results for other specimens in this series of tests were reported previously.[4]

To determine the effect of the oxide films present on the surface of commercial titanium on the rate of adsorption of hydrogen by titanium, a specimen of Ti-75A plate was heated in a hydrogen atmosphere at 250°C for one month. Metallographic examination of this specimen revealed considerably more of the titanium-hydrogen phase than was present in a similar sample of the as-received plate. Further experiments in a hydrogen-free atmosphere are planned to determine whether the difference in microstructure will result from the thermal treatment alone.

A sample of commercial titanium (Ti-75A, heat X922) was obtained from a thermocouple well that had been assembled in a titanium bomb and irradiated in contact with uranyl sulfate solution (292.5 g of uranium per liter) in hole C-44 of the LITR. The

[4] *Ibid.*, p. 15, Table 4.

TABLE 4. FATIGUE PROPERTIES OF HOT-ROLLED AND ANNEALED Ti-75A SHEET EXPOSED TO URANYL SULFATE SOLUTION CONTAINING 300 g OF URANIUM PER LITER AT 250°C

| SPECIMEN NO. | SPECIMEN HISTORY PRIOR TO TESTING | STRESS (psi) | NUMBER OF CYCLES BEFORE FAILURE |
|---|---|---|---|
| 9 | Hot rolled at 850°C from $\frac{1}{4}$-in.-thick plate to 0.032-in.-thick sheet. Surface ground. Vacuum annealed for 1 hr at 600°C and furnace cooled. Exposed to uranyl sulfate solution containing 300 g of uranium per liter. Initial gas pressure in bomb at room temperature was 100 psi $O_2$ and 200 psi $H_2$. Test run for 72 hr at 250°C; at end of run total pressure was 1200 psi. Repressurized and run 128 hr at 250°C. Final total pressure 50 psi. Specimen blanks exposed on both sides to uranyl sulfate. Machined into sheet-fatigue specimens. | 44,200 | $1.63 \times 10^5$ |
| 10 | | 45,000 | $8.6 \times 10^4$ |
| 11 | Same as for specimens 9 and 10 except that only one side of each specimen blank was exposed to uranyl sulfate solution. | 44,480 | $6.5 \times 10^4$ |
| 12 | | 44,550 | $7.9 \times 10^4$ |

pressure of hydrogen and oxygen gas (present in a 2-to-1 ratio) varied from 1000 to 2500 psi total at the temperatures employed during the test (190 to 260°C). Vacuum fusion analyses for hydrogen, oxygen, and nitrogen were performed on a sample cut from the irradiated thermocouple well and on a sample cut from a Ti-75A bar of heat X922 in the as-received condition. Table 5 lists the results obtained. Metallographic samples were obtained and are being examined for evidences of the titanium-hydrogen phase in the microstructure.

**Bureau of Mines Titanium.** Impact tests have been performed at room temperature and at liquid-nitrogen temperature on arc-melted, swaged, vacuum-annealed, and machined specimens of Bureau of Mines titanium (lot 1056, R83A). The data obtained are presented in Table 6. It appears that, for the temperature range investigated, there is no transition from ductile-to-brittle fracture in this higher purity titanium.

**Zirconium-Aluminum System.** Three alloys of zirconium-aluminum were prepared by arc melting Grade I crystal-bar zirconium with high purity aluminum, (99.99+% Al, R84A) to determine the crystal structure and mechanical properties of the zirconium-aluminum compound (22.82 wt % Al) formed in the solid state by the peritectoid reaction:[5]

$$Zr_4Al_3 + Zr_2Al_3 = Zr\text{-}Al; \text{ at } 1250 \pm 50°C .$$

Table 7 lists the nominal compositions of the three alloys prepared.

Available information[6] on the gamma phase (50-50 at. % Ti and Al) in the titanium-aluminum system indicates that the gamma phase has an ordered face-centered-tetragonal crystal structure with the axial ratio (c/a) very close to unity. The frequent similarity of behavior of titanium and zirconium when alloyed with other metals prompted this investigation into the crystal structure and mechanical properties of zirconium-aluminum alloys at or near the 50-50 at. % zirconium-aluminum composition.

All the alloys listed in Table 7 cracked on cooling from the molten condition. Unsuccessful attempts have been made to remelt these alloys under conditions designed to give slower cooling rates. Present plans are to remelt the alloys, cold work then slightly, and homogenize them at 1250°C for a period sufficient to allow the peritectoid reaction to occur. Following this thermal treatment, representative metallographic and x-ray diffraction samples will be obtained prior to further fabrication treatments.

[5] Armour Research Foundation, *Phase Diagrams of Zirconium-Base Binary Alloys*, p. 131-143, COO-89 (Apr. 14, 1952).

[6] E. S. Bumps, H. D. Kessler, and M. Hansen, *Trans. Am. Inst. Mining Met. Engrs.* 194, 609-614 (1952).

TABLE 5. OXYGEN, NITROGEN, AND HYDROGEN ANALYSES OF COMMERCIAL TITANIUM

| SAMPLE NO. | SAMPLE HISTORY | SAMPLE WEIGHT (g) | OXYGEN (wt %) | NITROGEN (wt %) | HYDROGEN (wt %) |
|---|---|---|---|---|---|
| N1255 | Ti-75A from heat X922 irradiated in uranyl sulfate solution (reference test Ti-5, V-13) | 0.2663 | 0.11 | 0.004 | 0.027 |
| N1258 | As-received Ti-75A from heat X922 | 0.586 | 0.021 | 0.008 | 0.020 |

TABLE 6. IMPACT ENERGY VS. TESTING TEMPERATURE DATA FOR ARC-MELTED, SWAGED, AND VACUUM-ANNEALED BUREAU OF MINES TITANIUM

| SPECIMEN NO. | NOTCH NO. | SCALE USED (in.-lb) | TEMPERATURE (°C) | IMPACT ENERGY (in.-lb) | REMARKS |
|---|---|---|---|---|---|
| B-1-1 | 1 | 0 to 200 | 33 | 96 | Did not break |
| | 2 | 0 to 200 | −195.6 | 127 | Did not break |
| B-1-2 | 1 | 0 to 200 | 32 | 94 | Did not break |
| | 2 | 0 to 200 | −195.6 | 72 | Did not break |
| | 3 | 0 to 200 | −195.6 | 120 | Did not break |
| B-1-3 | 1 | 0 to 100 | 22 | 85 | Did not break |
| | 2 | 0 to 100 | −195.6 | 98 | Did not break |
| | 3 | 0 to 200 | 32 | 95 | Did not break |
| | 4 | 0 to 200 | −195.6 | 78 | Did not break |
| B-2-4 | 1 | 0 to 200 | 26 | 127 | Did not break completely |
| | 2 | 0 to 200 | −195.6 | 144 | Did not break completely |
| B-3-4 | 1 | 0 to 200 | 26 | 113 | Did not break completely |
| | 2 | 0 to 200 | −195.6 | 146 | Did not break completely |

TABLE 7. NOMINAL COMPOSITION OF ARC-MELTED ZIRCONIUM-ALUMINUM ALLOYS

| MELT NO. | ALLOY NO. | ALUMINUM (wt %) |
|---|---|---|
| 1 | IZA-22.82 | 22.82 |
| 2 | IZA-21.32 | 21.32 |
| 3 | IZA-24.32 | 24.32 |

**Zirconium-Indium System.** Mention was made in the previous report[7] of an experiment designed to determine the properties of a zirconium-indium alloy. Attempts to hot swage the alloy at 700°C were unsuccessful; the alloy crumbled into a number of small pieces and exhibited the general appearance of a "hot-short" material. Metallographic examination of samples of the hot-swaged alloy revealed a structure that was not appreciably different from the single-phase structure observed in the as-melted sample. Homogenizing the as-cast material at 1100°C for five days did not seem to alter the structure, since it still had the appearance

[7] W. J. Fretague, A. R. Olsen, and R. G. Berggren, *Met. Semiannual Prog. Rep. Apr. 10, 1953*, ORNL-1551, p. 16-17.

of a single-phase alloy. The fragments of the hot-swaged alloy have been remelted, and the melt will be homogenized at 1100°C before any further attempts are made to fabricate it.

**Zirconium-Tin Alloys (Zircalloy II).** Impact tests were performed on four specimens of Zircalloy II machined from ¼-in.-thick plates of two heats (F879 and F909) received from WAPD. One specimen from each heat was 0.204 in. in diameter and 6¾ in. in length with six 45-deg circumferential V notches machined at intervals of 1 in. along its length to a depth of 0.020 in. and a radius of 0.005 in. at the root of the notch. The remaining specimen from each heat was 0.200 in. square and 6¾ in. long with 0.040-in.-deep 45-deg V notches with a 0.005-in. root radius machined perpendicular to the rolling plane at intervals of 1 in. along the length. Table 8 lists the data obtained and Fig. 6 is a graphical representation of the results.

TABLE 8. IMPACT-ENERGY VS. TESTING-TEMPERATURE DATA FOR AS-RECEIVED ZIRCALLOY II SPECIMENS

| SPECIMEN NO. | NOTCH NO. | SCALE USED (in.-lb) | TEMPERATURE (°C) | IMPACT ENERGY (in.-lb) |
|---|---|---|---|---|
| F879 (round) | 1 | 0 to 100 | 35 | 4 |
| | 2 | 0 to 100 | −195.6 | < 1 |
| | 3 | 0 to 100 | −100 | 1 |
| | 4 | 0 to 100 | 60 | 4.5 |
| | 5 | 0 to 100 | 120 | 9 |
| | 6 | 0 to 100 | 200 | 28.5 |
| F909 (round) | 1 | 0 to 100 | 35 | 11 |
| | 2 | 0 to 100 | −195.6 | 4 |
| | 3 | 0 to 100 | −100 | 4.5 |
| | 4 | 0 to 100 | 60 | 9 |
| | 5 | 0 to 100 | 120 | 11 |
| | 6 | 0 to 100 | 200 | 36.5 |
| F879 (square) | 1 | 0 to 25 | 30 | 15.25 |
| | 2 | 0 to 50 | 60 | 15.5 |
| | 3 | 0 to 50 | −195.6 | 3 |
| | 4 | 0 to 50 | −100 | 3.5 |
| | 5 | 0 to 50 | 120 | 27 |
| | 6 | 0 to 100 | 200 | 64.5 |
| F909 (square) | 1 | 0 to 25 | 30 | 17.5 |
| | 2 | 0 to 50 | 60 | * |
| | 3 | 0 to 50 | −195.6 | 4 |
| | 4 | 0 to 50 | −100 | 6 |
| | 5 | 0 to 50 | 120 | 34 |
| | 6 | 0 to 100 | 200 | 62 |

*Pendulum hit thermocouple.

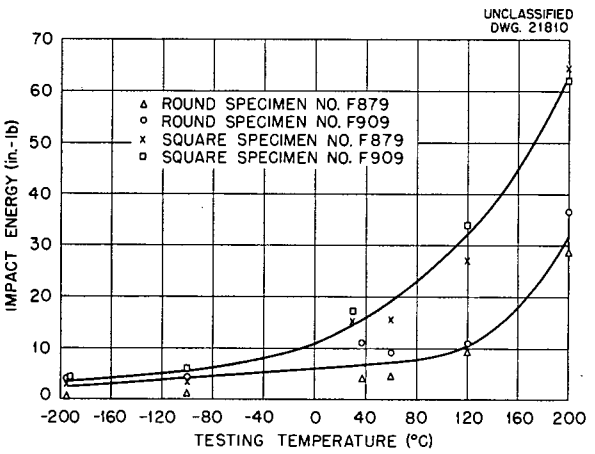


**Fig. 6. Impact Tests of Zirconium-Tin Alloys.**

Specimens of Zircalloy II obtained from ⅜-in.-dia rods that were swaged to 0.217-in.-dia rods, sand blasted, pickled, vacuum annealed at 750°C for 2 hr, and furnace cooled prior to machining were exposed to uranyl sulfate solution (4 g of uranium per liter) for 400 hr at 300°C in a loop. These specimens will be impact tested in the near future.

In addition, approximately 20 lb of ⅜-in.-dia Zircalloy II rods was given a treatment similar to that described for the loop specimens. These rods were prepared for the HRP Dynamic Corrosion Group, and they will be used for corrosion test pins.

## WELDING OF STAINLESS STEELS

W. J. Leonard

Types 347 and 304 L stainless steel in heavy sections have been welded in all possible combinations with types 347, 347 "modified fully austenitic," and 308 L stainless steel welding rod. The mechanical, physical, and metallurgical characteristics of these welds are being evaluated by appropriate tests.

Sintered compounds of powdered iron of known volume percentages in electrolytic copper were made to obtain calibration curves for use in Magnegage determinations of the ferrite content of stainless steels.

Sample pins for dynamic corrosion tests in loops are being taken from all weldments and given various heat treatments for corrosion resistance evaluations of the heat-treated and as-welded condition of each weld.

Samples of type 347 stainless steel of various chemical composition ranges have been vacuum melted into buttons about 1 in. in diameter and slow cooled in an attempt to simulate the solidification of weld metal. The buttons were sectioned and are being studied microscopically to evaluate the role of segregation in welds as related to crater cracking and localized loss of corrosion resistance in type 347 stainless steel weld metal.

## DYNAMIC CORROSION OF WELDED STAINLESS STEEL SPECIMENS

W. O. Harms W. J. Leonard

At the request of the HRP Dynamic Corrosion Group, an attempt was made to evaluate the results of dynamic corrosion tests of 126 welded, austenitic stainless steel, pin-type specimens. The 0.203-in.-dia by 1.375-in.-long specimens were machined from ¼-in. welded plates and were tested under conditions which included (1) oxygen-pressurized solutions containing 5, 15, 40, and 300 g of uranium per liter as uranyl sulfate with additions in some cases of sulfuric acid, copper sulfate, and/or potassium chloride, (2) flow rates from approximately 10 to 80 fps, (3) exposure for periods of from 90 to more than 1000 hr, and (4) temperatures from 125 to 250°C.

The evaluation program was designed as a survey for comparing combinations of various austenitic stainless steels heliarc welded with type 347 stainless steel. The base metal combinations investigated were types 347-347, 304-304, 321-321, 304 L-304 L, and 304-347 stainless steel. Five special welds were also included: four of type 347 stainless steel welded with (1) type 307 lime-coated stainless steel rod, (2) unshielded type 347 bare stainless steel rod, (3) type 310 lime-coated stainless steel rod, and (4) type 347 lime-coated stainless steel rod, and one of type 304 L stainless steel heliarc welded with type 308 L stainless steel rod.

The corroded specimens were electrolytically defilmed in inhibited 5% sulfuric acid and were examined microscopically in this condition. Representative specimens have been submitted for metallographic examination, and the results will be reported at a later date. The soundness of the welds was tested by subjecting each pin to a 180-deg bend test.

The data were separated into 23 groups on the basis of comparable test conditions and have been reported in detail elsewhere.[8] The evaluation of these data may be summarized as follows.

1. Unqualified statements as to the general superiority of one combination of base metals and weld cannot be made because the relative corrosion resistance of a given combination varied with test conditions and not all combinations were represented in each of the 23 sets of conditions.

2. The five sets of pins involving other than type 347 stainless steel heliarc welds were tested in only one run; no differences were observed among them or between them and the nonwelded austenitic stainless steel pins tested in the same run.

3. A comparison of welded and nonwelded specimens under each of the 23 sets of conditions showed that, on the basis of average defilmed weight loss, nonwelded specimens were (*a*) better than the best welded specimens in 12 cases, (*b*) worse than the worst welded specimens in two cases, and (c) intermediate between the best and worst welded specimens in nine cases. The superiority of the nonwelded specimens was most pronounced at moderate flow rates (10 to 20 fps) in uranyl sulfate solutions (40 g of uranium per liter) with 0.042 *M* sulfuric acid and in uranyl sulfate solutions containing 300 g of uranium per liter.

4. It was observed that welded specimens were more susceptible to the deleterious effects of sulfuric acid additions to the solution than were nonwelded specimens. For instance, in uranyl sulfate solutions containing 40 g of uranium per liter, and under otherwise comparable conditions, the weight losses of welded pins in the solutions containing 0.042 *M* sulfuric acid were as much as 17 times greater than the weight losses of those in solutions containing only 0.005 *M* sulfuric acid. By comparison, the attack on nonwelded pins was greater by a factor of only 3.

5. Preliminary microscopic examination has indicated that, in general, the difference in the behavior of various combinations under the same or different test conditions is not attributable to abnormal effects within the structure of either the base metals or the welds.

6. Since the composition of the weld rod used is balanced so as to deposit an alloy containing some ferrite, all welds were found to be more or less magnetic. In many cases, it was observed that if the weld was strongly magnetic the corrosion was more severe. Of the base metals studied, only type 321 stainless steel was magnetic, and, in most cases, specimens involving type 321 stainless steel were inferior to others in a given group. In the low-temperature tests with uranyl sulfate solutions containing 300 g of uranium per liter, the attack on type 321 stainless steel base metal was noticeably greater than the attack on the welds. In the tests at 250°C with uranyl sulfate solutions containing 40 g of uranium per liter, however, the opposite was observed.

7. All but one specimen passed the bend test. The single failure was due to a void which existed in the original weld and therefore was not due to selective attack in the corrosion test.

Further study of the dynamic corrosion of welded specimens is being made. Specimens for this study have been machined from welds made in a welding development program in which 1-in. and 1¼-in. plates of types 347 and 304 L stainless steel were joined with types 347, 308 L, and 347 "modified fully austenitic" stainless steel welding rods in all possible combinations. Complete chemical composition data, metallurgical histories, and results of physical tests on these welds are known. The machined pins have been given various heat treatments and are to be electrolytically polished before being tested in a loop under one set of conditions. The test results are expected to reflect the effects of chemical composition and heat treatment only, because the other variables are thought to be standardized.

## STRESS-CORROSION CRACKING OF TYPE 347 STAINLESS STEEL

E. C. Miller W. O. Harms

Preliminary experiments have been performed in the study of the effects of plastic deformation and subsequent heat treatment on the stress-corrosion cracking of austenitic stainless steels. The purpose of this work is to obtain a clearer understanding of the relation which is reported to exist between transgranular stress-corrosion cracking and martensite-forming susceptibility in these steels. If found to be significant, such a relation

[8] W. O. Harms and W. J. Leonard, *HRP Quar. Prog. Rep. July 31, 1953*, ORNL-1605, p. 112.

would require consideration, for example, in the development of specifications for composition, forming, and heat treatment of heat exchanger tubes and tube sheets.

Three-inch lengths of annealed ¼-in. type 347 stainless steel tubing having a 1/32-in. wall thickness were crimped at the ends, twisted through 90 deg, and bent through 95 to 100 deg at the midpoint at four temperatures: –320, 75, 212, and 400°F. All specimens were tested in the as-worked condition, and, in addition, the subzero-worked specimens were tested after partial stress relief and full annealing at 750 and 1900°F, respectively. Two of the subzero-worked and heat-treated specimens were elastically stressed by a stud-and-nut arrangement through the crimped ends of the specimens.

The corrosion tests were performed in boiling 42% magnesium chloride solutions under conditions of total reflux. Specimens were removed every ½ hr and examined microscopically at 30X for evidence of cracks. The results of these tests are summarized in Table 9.

The severely stressed specimens (Nos. 5 and 6) showed the best stress-corrosion resistance under the test conditions employed, and those worked at room and higher temperatures (Nos. 7 through 14) were the least resistant. The specimens worked at –320°F (in liquid nitrogen) were strongly magnetic at the ends and in the bend. Specimens heated to 750°F remained magnetic; however, those which were fully annealed and those which were deformed at room and higher temperatures without subsequent heat treatment were not magnetic. The observed magnetism is believed to be due to the presence of pseudomartensite (or martensitically formed chromium-nickel ferrite) formed during plastic deformation and subzero cooling. This hypothesis is being checked by metallographic examination, and the results will be reported later.

These observations can be interpreted according to a theory proposed recently by Edeleanu,[9] who,

[9] C. Edeleanu, *J. Iron Steel Inst. (London)* 173 (Part 2), 140 (1953).

TABLE 9. EFFECT OF COLD-WORKING TEMPERATURE AND SUBSEQUENT HEAT TREATMENT ON THE STRESS-CORROSION CRACKING OF TYPE 347 STAINLESS STEEL TUBING

| SPECIMEN NO. | COLD-WORKING TEMPERATURE (°F) | REHEATING TEMPERATURE (°F) | ELASTIC STRESS | FIRST CRACK | |
|---|---|---|---|---|---|
| | | | | Time (hr ± ½ hr) | Location |
| 1 | –320 | 1900 | | 18 | Crimped end |
| 2 | –320 | 1900 | * | 5 | Bend |
| 3 | –320 | 750 | | 5 | Crimped end |
| 4 | –320 | 750 | * | 5 | Bend |
| 5 | –320 | | | 25 | Bend |
| 6 | –320 | | | 30 | Bend |
| 7 | 75 | | | 2 | Bend |
| 8 | 75 | | | 2 | Bend |
| 9 | 75 | | | 2½ | Bend |
| 10 | 75 | | | 2 | Bend |
| 11 | 212 | | | 2 | Bend |
| 12 | 212 | | | 2 | Bend |
| 13 | 400 | | | 2 | Bend |
| 14 | 400 | | | 2 | Bend |

*Specimens 2 and 4 elastically stressed.

on the basis of a rather extensive experimental study, concluded that transgranular stress-corrosion cracking of austenitic chromium-nickel steels is due to preferential attack on small quantities of pseudomartensite formed during straining. According to this theory, the corrosion in materials containing large quantities of this phase would not be concentrated on any particular plate and would be less likely to lead to rapid penetration; if only small quantities were present, the corrosion would probably be more localized and penetration would proceed rapidly.

It will be noted that specimen 2, which was subzero worked, fully annealed, and elastically stressed, showed less stress-corrosion resistance than specimen 1, which was treated similarly but tested without elastic stress. Comparison of specimens 3 and 4, however, indicates that the effect of elastic stress may be less significant in material which is subzero worked and subsequently stress-relieved at 750°F. The elastically stressed specimens cracked at the bend, while the as-heat-treated specimens cracked at the crimped end. Future work is to include a closer study of the effects of elastic stress.

Prior to the tests in boiling 42% magnesium chloride solutions, several subzero-worked specimens with and without elastic stress were tested in the less severe medium of 3% sodium chloride solution with either 1.5 or 0.15% sodium dichromate, and they showed no cracking after exposure periods of as long as 384 hours. Since Edeleanu, using annealed U-bend specimens elastically stressed at room temperature, reported cracking in these solutions after 27 to 45 hr, these observations appear to lend further support to the theory proposed by him.

It should be emphasized that the evidence cited here in support of the "pseudomartensite" theory of stress-corrosion cracking in austenitic stainless steels is by no means conclusive. However, the results of these preliminary tests do indicate that the relation between plastic deformation and subsequent heat treatment on the one hand and stress-corrosion cracking on the other may not be simple, and it therefore warrants further investigation.

## SELECTIVE OXIDATION OF AUSTENITIC STAINLESS STEELS

E. C. Miller W. O. Harms

It was found recently that pretreatment in moist hydrogen increased considerably the corrosion resistance of austenitic stainless steel in certain HRP loop environments. Consideration of the pretreatment conditions and of the information contained in the literature indicated that selective oxidation by the limited moisture content had produced a very thin, tenacious film of highly protective oxide which served as a barrier to lessen diffusion and oxidation of the specimens when exposed to oxygen-pressurized uranyl sulfate solutions in the dynamic tests.

The initial observations were made on four pin-type specimens of type 347 stainless steel machined from special heats with varying columbium-to-tantalum ratios which were heated in slightly moist hydrogen at 1000°F. The defilmed weight changes of these specimens, which were covered with a light-blue temper film as the result of this treatment, are compared in Table 10 with corresponding data for as-machined wrought austenitic stainless steels.

A series of austenitic stainless steel pins was then pretreated at 1000°F for 24 hr in a hydrogen atmosphere containing approximately 6 vol % water vapor. These pins were loop tested in uranyl sulfate containing 15 g of uranium per liter plus 0.016 M sulfuric acid for 200 hr at 250°C and at flow rates of 15 to 16, 36, and 58 fps. Coupon-type specimens of type 304 L stainless steel were also pretreated in this manner and tested in the same run in the velocity range of 10 to 80 fps. The results of the pin tests are shown in Fig. 7. It is clear from these data that if there is a failure in the film, the pretreatment may be wholly ineffective, but, if the film forms in a continuous and uniform manner, it may retain its protective qualities even at fairly high flow rates.

Type 304 L stainless steel pins were also pretreated at 900, 1150, 1300, 1850, and 1950°F in hydrogen containing 6% water vapor and tested at 36 fps in this run. The pins treated at 1950°F

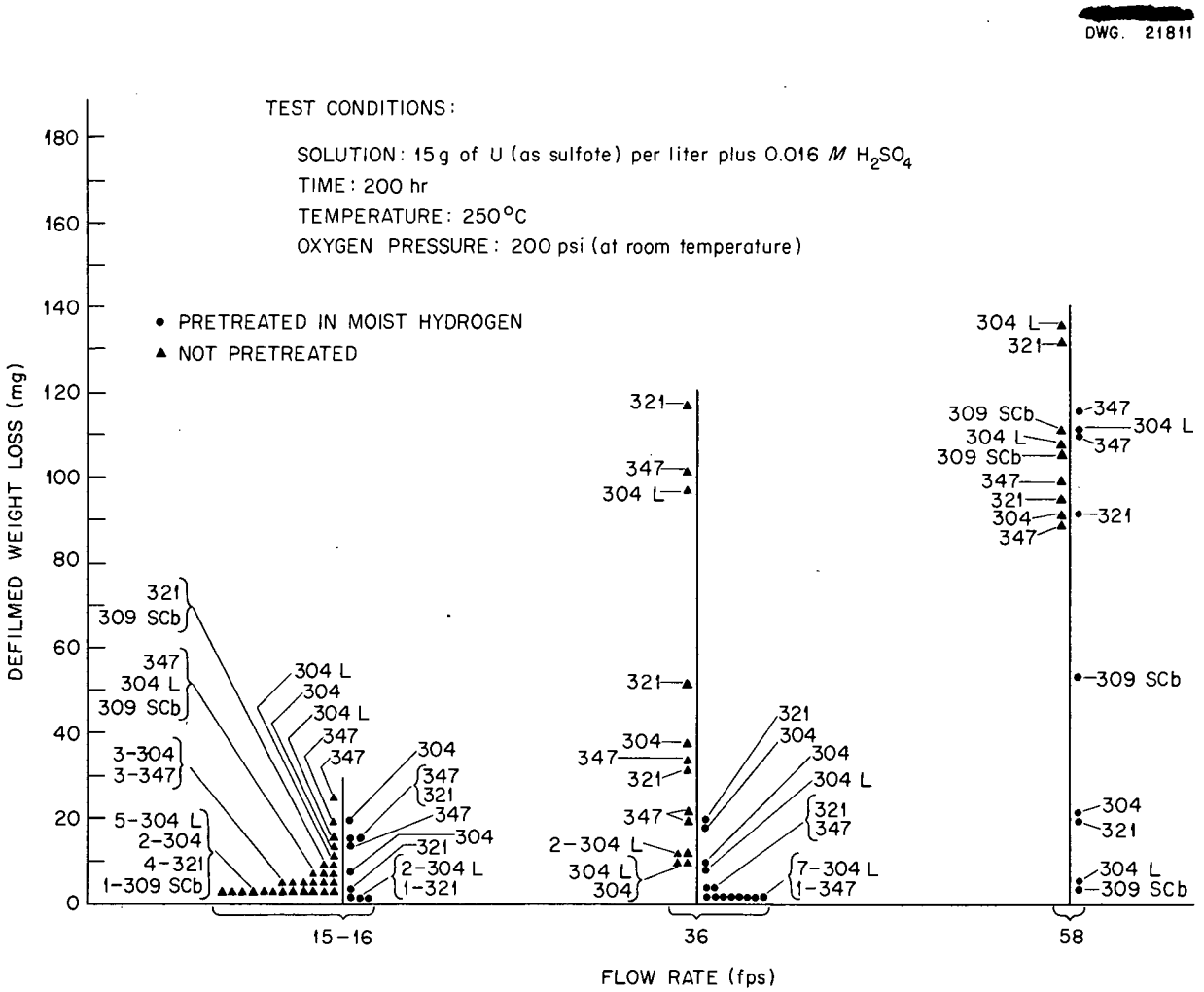


**Fig. 7. Effect of Moist Hydrogen Pretreatment on Corrosion Resistance of Wrought Austenitic Stainless Steels in Dynamic Loop Tests.** Symbol notations indicate number of specimens tested and type of stainless steel.

failed, but the others exhibited marked improvement in corrosion resistance. The 1500°F pretreatment gave the best results under these conditions. Pretreated coupon-type specimens showed better corrosion resistance than did the as-machined coupons tested previously under similar conditions. This comparison is not considered conclusive, however, because discontinuities and lack of uniformity were observed in the pretreatment films on these specimens prior to the test.

Pretreated specimens have been submitted for electron diffraction studies and chemical analyses of the films. Additional work in progress includes (1) determination of the optimum combination of temperature, time, and moisture content to produce by pretreatment in moist hydrogen the most tenacious and resistant film; (2) further evaluation of the corrosion resistance of these films in high-velocity and turbulent solutions; (3) investigation of methods for enriching the chromium content on stainless steel surfaces to lessen the net surface impoverishment which may exist after selective oxidation; and (4) consideration of practical methods of economical application of such films if they appear to have real value.

TABLE 10. DYNAMIC CORROSION TESTS OF TYPE 347 STAINLESS STEEL PINS PRETREATED IN MOIST HYDROGEN AT 1000°F FOR 24 hr AND TESTED IN URANYL SULFATE SOLUTION
(40 g of Uranium per Liter)

| LOOP RUN NO. | PIN NO. | ADDITIONS TO URANYL SULFATE SOLUTION | EXPOSURE TIME (hr) | SOLUTION FLOW RATE (fps) | DEFILMED WEIGHT CHANGE OF PRETREATED PINS (mg) | AVERAGE DEFILMED WEIGHT CHANGE OF MACHINED AUSTENITIC STAINLESS STEEL PINS IN SAME RUN (mg) |
|---|---|---|---|---|---|---|
| I-4 | 2125 | 200 psi $O_2$ | | | | |
| | | 0.1 M $CuSO_4$ | 499 | 14 | −0.1 | −24.5 |
| | 2127 | 0.005 M $H_2SO_4$ | | | +1.2 | |
| II-14 | 2029 | 200 psi $O_2$ | 113 | 13 | −10.5 | −20.5 |
| | 2031 | | | | −10.7 | |

## ANP METALLURGY

### STATIC CORROSION

D. C. Vreeland E. E. Hoffman

#### Corrosion by Fluorides

In an attempt to determine the effect of various carbon, oxygen, and nitrogen contents of stainless steels on resistance to attack by fluorides, static corrosion tests were made on eight specimens of stainless steels. Two specimens were commercial stainless steel, types 304 and 305, while the other six specimens were stainless steels cast and extruded at MIT. Three of these special steels contained 18% chromium and 12% nickel, while the other three contained 18% chromium and 8% nickel. Each of the eight specimens was contained in a capsule machined from the same material as the specimen, with the exception of the specimen of type 305 stainless steel which was contained in tubing of type 304 stainless steel. The specimens were tested in fluoride 14 for 100 hr at 816°C. The compositions of the steels and the results of the tests are shown in Table 11. Insofar as can be determined from these tests, variations of carbon, oxygen, and nitrogen contents within the ranges covered by the specimens tested had no measurable effect on the resistance to corrosion.

Static tests were run on several specimens of high-purity Inconel prepared in the Metallurgy Division. The nominal analysis of this Inconel was 15% chromium, 78% nickel, and 7% iron. Details of casting, extruding, chemical analyses, and test results are given in Table 12. The specimens, contained in commercial Inconel tubing, were tested in fluoride 14 at 816°C for 100 hours. In general, the as-cast, low-carbon specimens had fewer subsurface voids than did the extruded specimens, but attack of the extruded specimens was not excessive. In the one instance in which the as-cast and the extruded material from the same ingot were tested, no significant differences in corrosion were observed. The attack on the arc-cast specimen containing 1.6% carbon was the most severe, but the depth of attack of this specimen was only slightly greater than that of the low-carbon specimens. With the exception of the arc-cast, high-carbon material, the laboratory-melted alloys were not significantly different from commercial alloys with respect to attack by the fluoride.

Static corrosion tests of Inconel in fluoride 30 were made at seven different temperatures covering the range 800 to 2000°F. The duration of each

TABLE 11. STATIC CORROSION OF STAINLESS STEELS IN FLUORIDE 14 AFTER 100 hr AT 816°C

| MATERIAL | COMPOSITION (wt %) | | | | | ASTM GRAIN SIZE | DEPTH AND TYPE OF ATTACK | PHASE CHANGE |
|---|---|---|---|---|---|---|---|---|
| | Cr | Ni | C | $N_2$ | $O_2$ | | | |
| Type 304 stainless steel | ~18 | ~ 8 | ~0.1 | ~0.02 | ~0.01 | 8 to 9 | Subsurface voids 2 to 3 mils deep | Decarburization 1 to 2 mils deeper than voids; some phase transformation |
| Type 305 stainless steel | ~18 | ~12 | ~0.1 | ~0.02 | ~0.01 | 7 | Intergranular attack and some subsurface voids 2 to 4 mils deep | Same as above |
| Special steel* | 18.24 | 12.32 | 0.151 | 0.0044 | 0.021 | 5 to 7 | Subsurface voids, some intergranular 2 to 4 mils deep, attack 10 mils deep in one place along carbide segregation | Same as above |
| | 18.55 | 12.44 | 0.006 | 0.0039 | 0.015 | 2 to 4 | Mainly intergranular attack 3 to 5 mils in depth; one 10-mil-deep area along grain boundary | Phase change deeper than attack along grain boundaries |
| | 18.03 | 8.52 | 0.011 | 0.096 | 0.018 | 2 to 5 | Mostly intergranular attack; some subsurface voids 3 to 4 mils deep; one stringer attacked to 6 mils | Some phase change noted |
| | ~18 | ~12 | 0.001 | 0.2 | | 2 to 4 | Mostly subsurface voids, some intergranular to a depth of 5 to 7 mils | Same as above |
| | 18.51 | 8.20 | 0.007 | 0.0031 | 0.031 | 2 to 4 | Mostly intergranular attack, some subsurface voids 3 to 7 mils deep | Same as above |
| | 18.55 | 8.43 | 0.193 | 0.0055 | 0.017 | 4 to 6 | Both subsurface voids and grain boundary attack 2 to 4 mils in depth, tended to be deeper along carbide segregation | Same as above |

*Prepared at MIT.

TABLE 12. STATIC CORROSION OF LABORATORY-MELTED INCONEL TESTED IN FLUORIDE 14 AT 816°C FOR 100 HOURS

| MATERIAL | COMPOSITION (wt %) | | | | | | METALLOGRAPHIC NOTES |
|---|---|---|---|---|---|---|---|
| | C | S | Ti | Mn | Al | Mg | |
| As cast in graphite mold | 0.03 | 0.026 | 0.2 | 0.03 | 0.01 | | Isolated areas of subsurface voids to 2.5 mils both within grains and along grain boundaries |
| Extruded; glass lubricant used | | | 0.25 | 0.032 | 0.1 | 0.05 | Attack more general than above, predominantly subsurface voids at grain boundaries to a depth of 3 mils |
| As cast in graphite mold | 0.01 | 0.007 | | 0.25 | 0.15 | | A few scattered areas of subsurface voids to 2.5 mils both within grains and along grain boundaries |
| Extruded; lubricated with graphite and oil | 0.03 | 0.017 | | 0.25 | 0.15 | | A few scattered subsurface voids to 1.5 mils; one grain boundary attacked to 3 mils in depth |
| As cast in copper mold | | | | 0.25 | 0.15 | | Occasional scattered subsurface voids to 3 mils both within grains and along grain boundaries |
| Extruded; glass lubricant used | | | | | | 0.05* | Attack more general than above; subsurface voids to 2.5 mils both within grains and along grain boundaries |
| As cast in graphite mold | 0.031 | 0.008 | | 0.25 | | | Occasional grain boundary attack to 2 mils in depth |
| Extruded, glass lubricant used | No additions made | | | | | | Attack more general than above; subsurface voids to 3 mils both within grains and along grain boundaries |
| As arc cast | 1.6 | | | | | | Most heavily attacked of this series of specimens; attack took place along carbides, with some decarburization up to 4 mils in depth |

*Nominal composition; no chemical analysis made.

test was 100 hours. Within the range 800 to 1400°F, the depth of attack appeared to be independent of temperature, the depth of attack being approximately 0.5 mil. Within the range 1600 to 2000°F, there was no systematic variation in depth of attack with temperature, but the depth of attack was slightly (from 2 to 4 mils) greater than at lower temperatures. Metallographic notes on these tests are presented in Table 13.

Since fluoride 31 is used to descale Inconel loops and because buildup of zirconium oxide in the fluoride with successive cleanings had been reported, static corrosion tests were run with fluoride 31 to which 0.75 and 1.5% $ZrO_2$ had been added. There was possibly a slight increase in depth of attack by the fluorides containing zirconium oxide during the 100-hr test at 1500°F, but for the short times and at the temperatures

TABLE 13. TEMPERATURE-DEPENDENCE TESTS OF INCONEL EXPOSED IN FLUORIDE 30 FOR 100 HOURS

| TEST TEMPERATURE °F | TEST TEMPERATURE °C | METALLOGRAPHIC NOTES |
|---|---|---|
| 800 | 427 | Subsurface voids in a few places to 0.5 mil |
| 1000 | 538 | Subsurface voids of erratic occurrence to a depth of 0.5 mil in most places and to a maximum depth of 1 mil |
| 1200 | 649 | Very little attack; subsurface voids in a few places to 0.5 mil |
| 1400 | 760 | Attack in only one place on specimen to 0.5 mil |
| 1600 | 871 | Erratic attack; subsurface voids to a maximum of 2 mils |
| 1800 | 982 | Fairly regular attack in the form of subsurface voids to a maximum depth of 4 mils; depth of attack less than 4 mils in most places |
| 2000 | 1093 | Subsurface voids to 2 mils |

used for descaling, no measurable increase in attack as a result of the zirconium oxide in the fluoride should be expected.

Another series of ARE descaling tests on Inconel has been run. The objectives in this series of tests were to check the lowest temperature at which fluoride 31 will remove oxide from Inconel and to determine the amount of attack which takes place during descaling. Static tests were run in fluoride 31 with Inconel specimens that had been oxidized for 24 hr at 1500°F. Results of these tests can be seen in Fig. 8. All specimens were completely descaled, except the specimen treated at 950°F. From this series of tests, it appears that a temperature of 1000°F could be recommended for descaling Inconel. However, in a previous test, descaling was not accomplished after 4 hr at 1000°F, and perhaps it would be better to recommend a temperature of 1100°F. In the previous test, the specimens were electropolished before they were oxidized, and it is thought that because of this treatment the oxide layer may have been more adherent. Specimens which had been oxidized and then descaled were examined metallographically to determine the amount of attack. The results are given in Table 14. It appears that only very light attack is to be expected during the usual short time of descaling.

Several tests were completed on the NACA-type whirligig. The attack of Inconel by fluoride 30 at velocities of 6 and 10 fps was no greater than the attack that occurred during static tests. Additions of titanium formed a surface layer which appeared to inhibit attack. Additions of nickel fluoride and chromium fluoride appeared to increase attack. Detailed results of the tests are shown in Table 15. Figure 9 shows some of the small globular crystals which were found attached to the tube wall in the test in which nickel fluoride was added. Chemical analysis revealed the composition of the crystals to be 92.34% nickel, 6.53% iron, 0.99% chromium, and 0.14% manganese.

### Corrosion by Liquid Metals

Several spinner tests of various materials in sodium at a temperature of 816°C and a speed of 405 fpm have been completed. The materials tested were types 310, 410, and 430 stainless steel, Inconel X, and Nichrome V. As in the spinner tests run in the past, attack seemed to be more severe than that encountered in static tests with molten sodium. Surface layers were quite apparent on Inconel X, Nichrome V, and type 310 stainless steel and less apparent or absent on the types 430 and 410 stainless steel. Weight changes were least on the types 410 and 430 stainless steel. A spinner test in which the specimens were not rotated was also run with Inconel X. This test was run because it had been suggested that attack in the spinner test might possibly be due mainly to impurities in the sodium or in the atmosphere rather than to the velocity of test.. The time and

temperature employed in this static test were the same as those used in the dynamic tests. Much lighter attack and less weight change were noted on these specimens than on the Inconel X specimens that were run at 405 fpm, and it is believed that most of the attack on specimens in spinner tests is due to velocity effects. The test results are listed in Table 16.

Static tests of types 309, 316, 347, and 430 stainless steel have been run in lithium. Extreme

UNCLASSIFIED
Y-9553

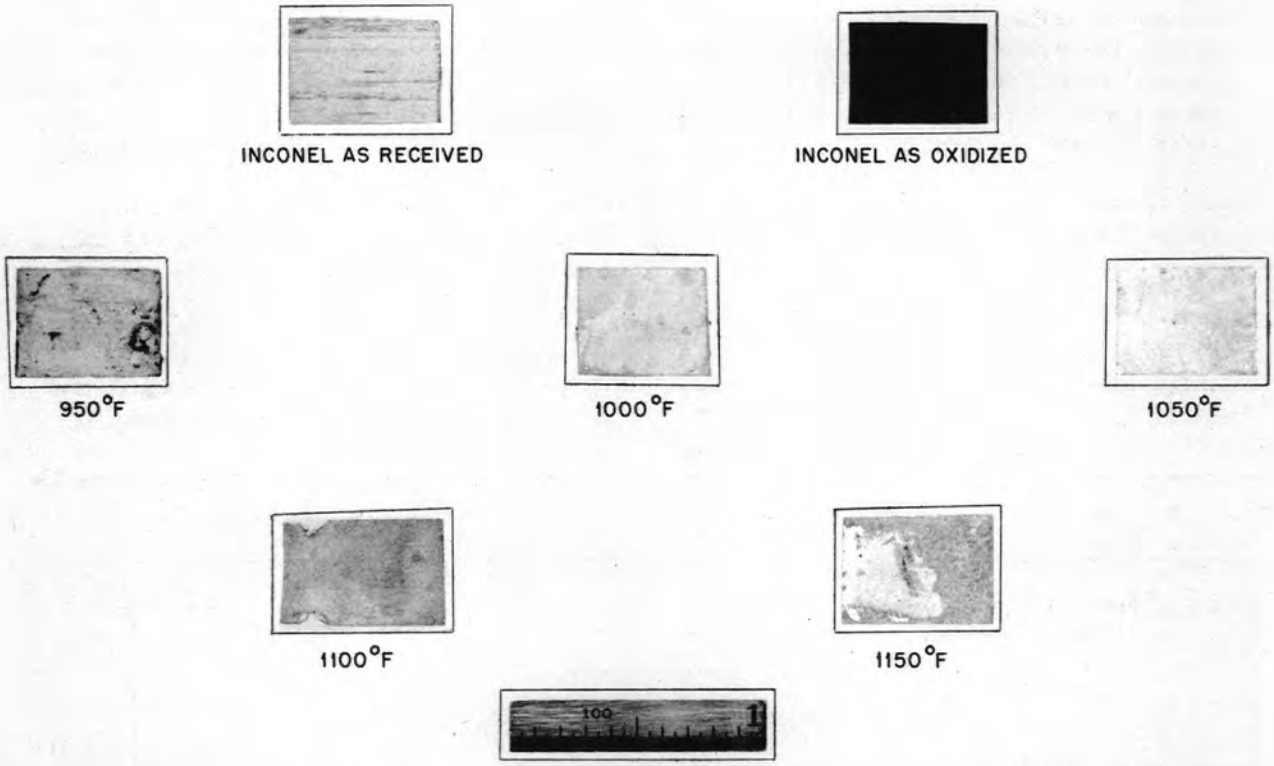


**Fig. 8. Descaling of Oxidized Inconel by Fluoride 31.** Specimens treated for 4 hr at indicated temperatures.

**TABLE 14. ATTACK ON INCONEL DURING DESCALING**

| OXIDATION AND DESCALING TREATMENT | METALLOGRAPHIC NOTES |
|---|---|
| Oxidized 24 hr at 1200° F; descaled 100 hr at 1500° F in seesaw furnace | Subsurface voids to a maximum depth of 1.5 mils, less in many places |
| Oxidized 24 hr at 1500° F; descaled 100 hr at 1500° F in seesaw furnace | Same as above |
| Oxidized 24 hr at 1500° F; descaled 4 hr at 950° F in static test | Very few subsurface voids to a maximum depth of 0.5 mil |
| Oxidized 24 hr at 1500° F; descaled 4 hr at 1150° F in static test | Same as above |

TABLE 15. RESULTS OF WHIRLIGIG TESTS

| TEST MATERIALS AND CONDITIONS | METALLOGRAPHIC NOTES |
|---|---|
| Inconel exposed to fluoride 30; solution velocity 10 fps for 100 hr; hot zone at 816°C, cold zone at 710°C | Very few subsurface voids and no change in tube-wall thickness |
| Inconel exposed to fluoride 30; solution velocity 6 fps for 100 hr; hot zone at 816°C, cold zone at 705°C | Intergranular attack and subsurface voids to a maximum depth of 0.5 mil |
| Inconel exposed to fluoride 27 plus 0.7% Ti; solution velocity 6 fps for 14 hr with hot zone at 816°C and cold zone at 635°C, 10 hr with hot zone at 700°C and cold zone at 575°C, 76 hr with hot zone at 816°C and cold zone at 610°C | Subsurface voids to a maximum depth of 0.5 mil; surface layer of ~0.1 mil at many places; cold zone appeared to have suffered a little less attack than did the hot zone |
| Inconel exposed to fluoride 30 plus 5% $NiF_2$; solution velocity 10 fps for 100 hr; hot zone at 816°C, cold zone at 710°C | Several small globular crystals in hot zone; tubing attacked rather severely, subsurface voids 2 to 10 mils in depth; many voids filled with blue-gray material |
| Inconel exposed to fluoride 30 plus 5% $CrF_2$; solution velocity 10 fps for 100 hr; hot zone at 816°C, cold zone at 716°C | Small amount of metallic crystals in hot zone; heavy attack in the form of subsurface voids to 4 to 6 mils in cold zone and 6 to 8 mils in hot zone; blue-gray material in some voids |

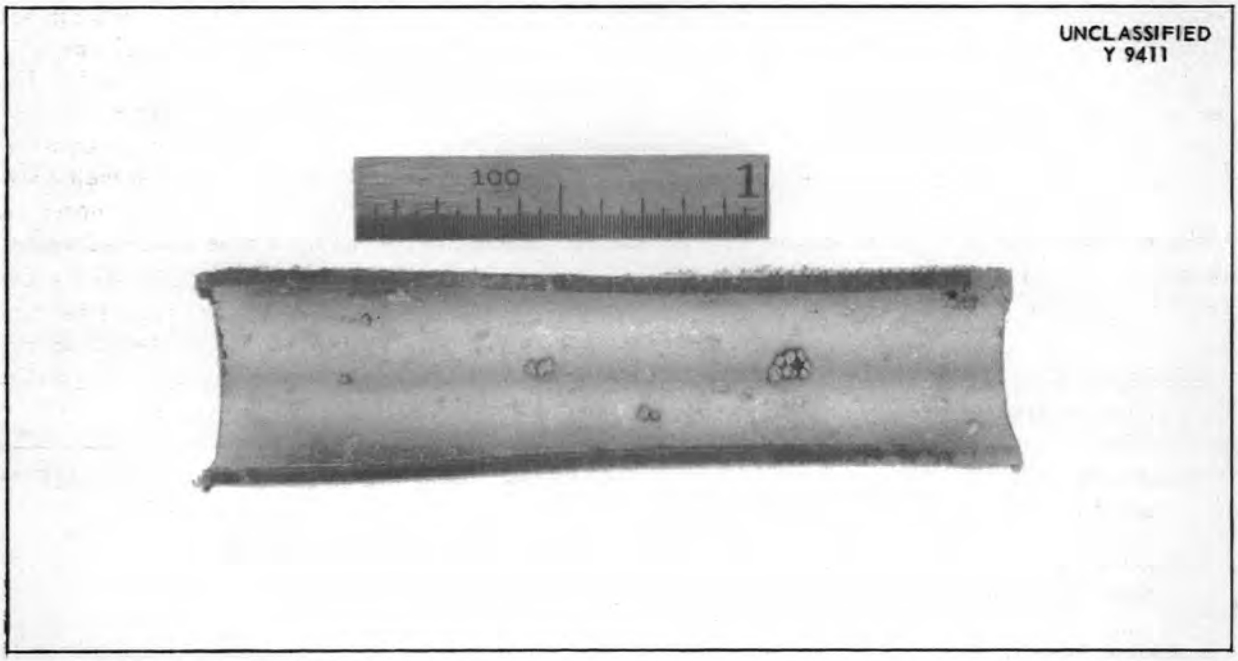


**Fig. 9. Sectioned Whirligig Tubing Showing Globular Crystals Found After Testing with Fluoride 30 to Which $NiF_2$ Had Been Added.**

TABLE 16. RESULTS OF SPINNER TESTS OF VARIOUS MATERIALS

| MATERIAL | SPECIMEN NO. | WEIGHT CHANGE (%) | METALLOGRAPHIC NOTES |
|---|---|---|---|
| Type 310 stainless steel | 1 | +1.16 | Intergranular attack 0.5 to 1 mil in depth; some evidence of surface layer |
| | 2 | +1.15 | |
| | 3 | +1.15 | |
| Type 410 stainless steel | 1 | −0.02 | Roughening and intergranular attack 0.5 to 1 mil in most places; intergranular attack to 3 mils at one place on leading edge |
| | 2 | −0.13 | |
| | 3 | −0.03 | |
| Type 430 stainless steel | 1 | +0.07 | Fairly uniform intergranular attack to 0.5 mil in most places, maximum of 1 mil in a few places; some slight evidence of a surface layer in a few places |
| | 2 | +0.07 | |
| | 3 | +0.04 | |
| Nichrome V | 1 | +0.97 | Up to 1 mil of attack (intergranular voids) beneath a surface layer of 0.5 mil |
| | 2 | +0.90 | |
| | 3 | +0.93 | |
| Inconel X | 1 | +3.22 | One-mil surface layer with intergranular attack to 2 mils beneath it |
| | 2 | +2.96 | |
| | 3 | +3.22 | |
| Inconel X (static test) | 1 | +0.051 | Light intergranular attack and voids to a depth of about 0.25 mil; apparently, no surface layer present |
| | 2 | +0.056 | |
| | 3 | +0.056 | |

care was taken in regard to the details of these tests which were run for 400 hr at 1000°C. Types 309 and 316 stainless steel exhibited corrosion resistance superior to that of types 347 and 430 stainless steel. Both types 347 and 430 showed evidence of mass transfer on a macro scale. The types 309 and 316 stainless steel specimens had small weight losses, very little, if any, mass transfer, and not over 1 to 2 mils of attack. Details of these tests are listed in Table 17.

A series of beryllium oxide specimens were received from the Ceramic Department for testing in sodium, lithium, and lead. These specimens were approximately $\frac{1}{2} \times \frac{1}{4} \times \frac{1}{4}$ in. and were cut from 2-in. hexagonal blocks hot pressed by the Norton Company. One half the specimens were tested as cut from the original block, and one half were tested after having been refired for 2 hr at 1800°C. The refired specimens had a higher density and a lower apparent porosity than did the specimens which were not refired. Results of these tests are presented in Table 18. As can be seen from the weight and dimensional change data, the refired beryllium oxide apparently had greater resistance to attack than did the specimens that were not refired. The one exception appeared in the sodium test in which the refired specimen showed greater weight change than did the as-received specimen. However, even in this test, the refired specimen was more dimensionally stable, as can be seen from the measurements listed in Table 18. The weight gains in sodium and lithium are presumed to be due to absorption of these metals. The specimens tested in lead appeared to be affected the least. Edges of the specimens appeared to be just as sharp after testing as before. The tests were run with Inconel tubes for containing the sodium and Armco iron tubes for containing the lithium and the lead. The test period was 100 hr and the test temperature was 1000°F.

TABLE 17. RESULTS OF STATIC TESTS OF VARIOUS STAINLESS STEELS IN LITHIUM AT 1000°C FOR 400 HOURS

| TYPE OF STAINLESS STEEL | WEIGHT CHANGE ($g/in.^2$) | NOTES |
|---|---|---|
| 309 | −0.0022 | No evidence of mass transfer upon opening tube; metallographic examination revealed a white phase in grain boundaries throughout the specimen; 0.5-mil crystals attached to the surface in some areas; 0.25 mil of intergranular attack in scattered areas |
| 316 | −0.0037 | No evidence of mass transfer upon opening tube, but surface had etched appearance; metallographic examination revealed very little attack; voids in some grain boundaries to a depth of 1 to 2 mils; fine precipitate all around the specimen in a band approximately 1 mil from surface; 4 to 5 mils of intergranular penetration in a few areas in vapor zone of tube |
| 347 | +0.0076* | Large amount of mass transfer on both tube and specimen, mainly at bath-level line; specimen heavily attacked intergranularly to a depth of 10 to 11 mils at one end; attack on rest of specimen did not exceed 0.5 mil; tubing attacked 1 to 2 mils; fine precipitate 1 mil under surface |
| 430 | No data | Few small crystals attached to surface of tube; surface of specimen had small grains and was attacked intergranularly to a depth of 4 to 5 mils; tubing attacked 2 to 3 mils |

*Crystals clinging to specimen.

### Miscellaneous Corrosion Tests

Static screening tests have been run with type 330 stainless steel (14 to 16% Cr, 34 to 37% Ni, 1.25% Si) in fluoride 30, lithium, lead, sodium, and sodium hydroxide. The tests were run for 100 hr at 816°C. Welded tubing was used in these tests, since seamless tubing was not available. The tests indicated that type 330 stainless steel is no more suited for use in these environments than are other grades of the 300 series stainless steels. Details of the results of these tests are listed in Table 19.

Static tests were run in sodium to check the corrosion resistance of type 316 stainless steel T joints brazed from samples plated with nickel and phosphorus by the "Electroless" process. These tests were run for 100 hr at 816°C. From the results of these tests, it appears that the nickel-phosphorus braze will not have satisfactory corrosion resistance under these conditions. The addition of chromium to the nickel-phosphorus braze produces a joint with better resistance to attack. Figure 10 shows an as-brazed joint, Fig. 11 shows a similar joint tested in sodium, and Fig. 12 illustrates a chromium-plated nickel-phosphorus brazed joint tested in sodium. Results of these tests are given in Table 20.

## DYNAMIC CORROSION

G. M. Adamson

### Effect of Time on Fluoride Corrosion

When the previous report was prepared, it was thought that the depth of attack of fluorides on Inconel remained essentially constant after 250 hours. During this period, a series of loops was filled from a single batch of fluorides which were then circulated for various times. The data from this series of tests, as well as other comparable data, are plotted in Fig. 13. The curve shows that

TABLE 18. RESULTS OF TESTS OF BERYLLIUM OXIDE IN LIQUID LEAD, SODIUM, AND LITHIUM

| SAMPLE NO. | BERYLLIUM OXIDE TREATMENT | TESTED IN | POROSITY (%, apparent) | DENSITY ($g/cm^3$) | WEIGHT BEFORE TEST (g) | WEIGHT AFTER TEST (g) | WEIGHT CHANGE (g) | WEIGHT CHANGE (%) | WEIGHT CHANGE ($g/in.^2$) | DIMENSIONS BEFORE TEST (in.) | DIMENSIONS AFTER TEST (in.) |
|---|---|---|---|---|---|---|---|---|---|---|---|
| B | Unfired | Lead | 12.41 | 2.58 | 1.3541 | 1.3533 | −0.0008 | −0.06 | −0.0013 | 0.500*<br>0.256**<br>0.255*** | 0.500<br>0.256<br>0.255 |
| H | Refired at 1800°C for 2 hr | Lead | 0.44 | 2.72 | 1.2956 | 1.2954 | −0.0002 | −0.02 | −0.0003 | 0.484<br>0.250<br>0.251 | 0.484<br>0.250<br>0.251 |
| D | Unfired | Sodium | 4.30 | 2.68 | 1.3878 | 1.4041 | +0.0163 | +1.09 | +0.0256 | 0.498<br>0.256<br>0.252 | 0.500<br>0.258<br>0.254 |
| E | Refired at 1800°C for 2 hr | Sodium | 0.79 | 2.73 | 1.1302 | 1.1465 | +0.0163 | +1.44 | +0.0289 | 0.463<br>0.243<br>0.240 | 0.464<br>0.243<br>0.240 |
| C | Unfired | Lithium | 9.58 | 2.63 | 1.2755 | 1.2975 | +0.0220 | +1.83 | +0.0361 | 0.491<br>0.247<br>0.249 | 0.497<br>0.251<br>0.252 |
| F | Refired at 1800°C for 2 hr | Lithium | 0.38 | 2.76 | 1.3105 | 1.3300 | +0.0195 | +1.49 | +0.0317 | 0.488<br>0.252<br>0.249 | 0.489<br>0.253<br>0.249 |

*Length **Width ***Thickness

TABLE 19. RESULTS OF STATIC TESTS OF TYPE 330 STAINLESS STEEL IN VARIOUS MEDIA AT 826°C FOR 100 HOURS

| CORRODANT | METALLOGRAPHIC NOTES |
|---|---|
| Fluoride 30 | Subsurface voids to 2 to 4 mils |
| Lithium | Subsurface voids to 1 to 2 mils; mass transfer crystals ¼ mil thick noted at several places on surface |
| Lead | Few scattered voids to a depth of 2 mils |
| Sodium | Light intergranular attack to 1 to 2 mils confined mostly to welded area of specimen |
| Sodium hydroxide | 20-mil oxide plus metal layer on specimen |

while a change in slope takes place at around 250 hr, some increase in depth of attack is found after this time. The data point that shows this increase of attack was taken from the single loop operated for 2850 hr and therefore the increase of attack should be confirmed. A flat curve would fit the other points equally well. This loop was scheduled to run for 3000 hr, but by mistake, it was turned off at 2850 hours. It is thought that the initial steep portion of the curve is caused by a reaction between the chromium in the Inconel and contaminants in either the fuel or the loop. The second phase of the reaction possibly represents the partial reduction of uranium tetrafluoride by chromium metal.

When the 3000-hr loop was studied in more detail, several unusual things became apparent. In the trap at the bottom of the cold leg, a metallic mass that formed a layer ¼ in. thick was found. This mass was located just above the liquid-solid interface and was made up of dendritic crystals. The metal was identified spectrographically as

**TABLE 20. RESULTS OF STATIC CORROSION OF NICKEL-PHOSPHORUS BRAZING ALLOY ON TYPE 316 STAINLESS STEEL TESTED IN SODIUM AT 816°C FOR 100 HOURS**

| SPECIMEN | METALLOGRAPHIC NOTES |
|---|---|
| 0.0014 in. of nickel-phosphorus alloy on type 316 stainless steel | As brazed – very good joint, no voids; after test – small voids in fillet and completely across joint |
| 0.000056 in. of chromium on 0.0079 in. of nickel-phosphorus alloy on type 316 stainless steel | As brazed – good joint, but several small voids present 2 mils beneath surface in fillet; after test – scattered voids throughout fillet to a depth of 14 mils |
| 0.00013 in. of chromium on 0.0011 in. of nickel-phosphorus alloy on type 316 stainless steel | As brazed – good joint with a few voids near surface of fillet (2 to 3 mils); after test – only a few more voids than in the as-brazed sample, voids in fillet to a depth of 3 to 4 mils |

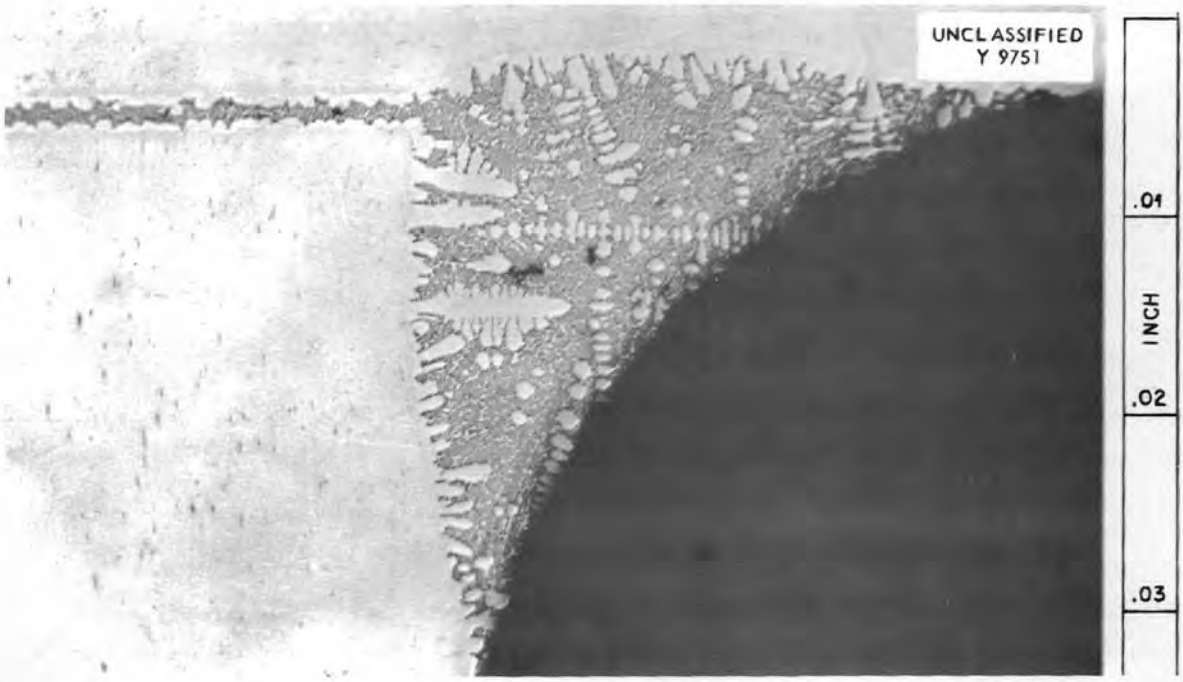


**Fig. 10. "Electroless" Nickel-Phosphorus Brazed Type 316 Stainless Steel T Joint, As-Brazed. 100X**

chromium. No layer or deposit was found on the walls of the cold leg. When the fluorides in the loop were analyzed, the chromium content was found to vary from 350 to 550 ppm. With a maximum attack of 18 mils, a value of about 2000 ppm of chromium was expected. A satisfactory explanation for the presence of the chromium, as metal, in the trap has not been found. All the accepted reactions have been written in the other direction with chromium metal going to chromium fluoride. One possibility is that some of these reactions are temperature sensitive and at least partially reverse in the cold leg.

The traps from several standard 500-hr loops were sectioned longitudinally and a careful search was made for metal. In almost every case, some metal could be found just above the liquid-solid interface. The deeper the attack, the greater was the amount of metal that could be found. It is now apparent that some chromium metal mass transfers in all Inconel loops in which fuzrna 30 is circulated.

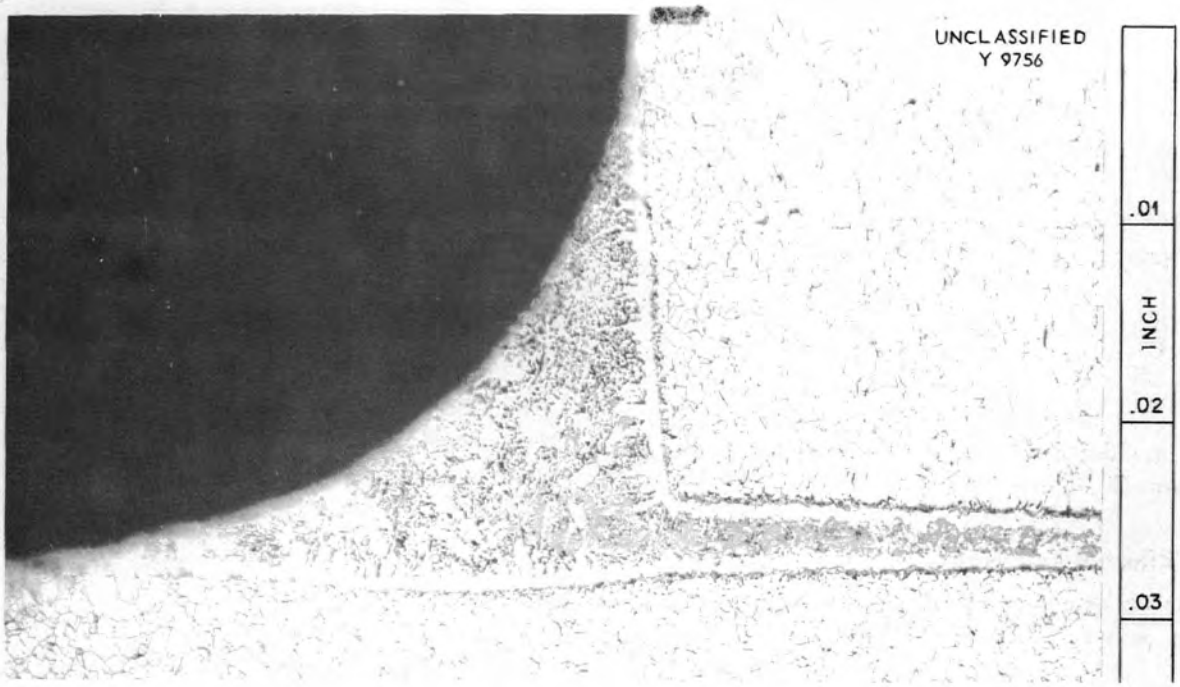


**Fig. 11. "Electroless" Nickel-Phosphorus Brazed Type 316 Stainless Steel T Joint Tested in Sodium for 100 hr at 816°C.** 100X

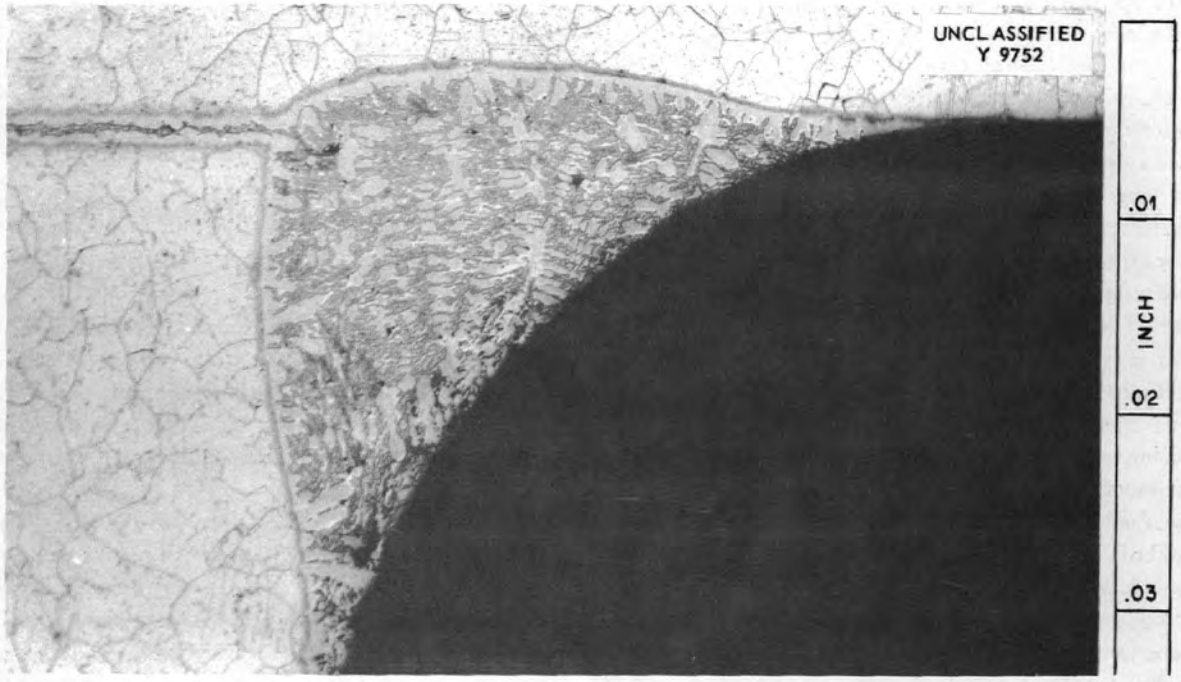


**Fig. 12. Chromium-Coated "Electroless" Nickel-Phosphorus Type 316 Stainless Steel T Joint Tested in Sodium for 100 hr at 816°C.**

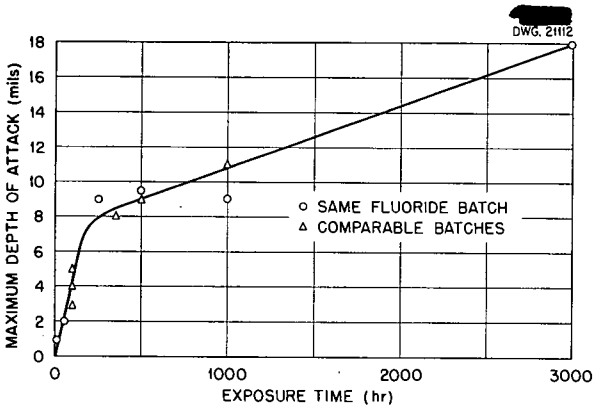


**Fig. 13. Depth of Attack of Inconel Loop by Fuzrna 30.** Tested at 1500°F.

### Effect of Temperature on Fluoride Corrosion

As an extension of work previously reported, a loop was operated with a hot-leg temperature of 1250°F. The attack was moderate-to-heavy subsurface void formation to a depth of 3 mils. The voids were small and evenly distributed. Six inches below the hot-leg section, no attack was found. The low corrosion measurements were substantiated by the fact that chromium did not build up in the fluoride solution during circulation. Since the attack was low in the upper section of the loop and completely absent in other sections, it seems likely that attack may be eliminated by operating at a slightly lower maximum temperature. Loops are being operated to confirm these results, and one is being operated at an even lower temperature, that is, 1200°F in the hot leg. Because of operational characteristics, 1200°F is about the lowest temperature that may be investigated in the thermal loops.

As previously mentioned, very little difference in maximum depth of attack was found when loops were operated at 1650°F instead of at 1500°F for 500 hours. After 100 hr of operation, however, the maximum attack in the loop operated at 1650°F was 7 mils, while in a loop operated at 1500°F, it was only 4 mils. After 100 hr at 1500°F, the holes were small and evenly distributed, that is, similar to those found at low temperatures after 500 hr of operation. When the loop was operated at 1650°F, the holes were larger and were concentrated in the grain boundaries. These tests show that attack is initially more rapid at higher operating temperatures and that it tends to level off at about the same depth during prolonged operation, irrespective of operating temperature.

### Effect of Fuel Purity

From both the metallurgical work and that done by the Materials Chemistry Division, it appeared that the nickel and iron fluorides and the residual hydrogen fluoride caused the major portion of the attack. However, data accumulated during this period indicate that possibly an additional, as yet unknown, factor also causes appreciable attack.

The fluorides circulated in loop 310 were prepared in the laboratory in a special graphite-lined pot. The iron and nickel impurities were reduced to 50 and 230 ppm, respectively. The maximum attack measured when this batch was circulated in an Inconel loop was 9 mils, which is a normal value.

A group of loops was filled at various times from a single 50-lb batch (EE-92) of fluorides made in the pilot plant. Considerable variation was reported in the iron, nickel, and chromium analyses of the samples taken as the loops were filled; however, reasonable values appear to be 50 ppm of nickel and 500 ppm of iron – both of which are normal. The production log also showed an average value for the hydrogen fluoride. Every loop filled from this batch produced much more attack than was expected. Two loops run under essentially standard conditions showed maximum penetrations of over 15 mils. As yet, the Chemistry Division has been unable to discover anything unusual in this batch of fluorides.

Two loops were operated to demonstrate the feasibility of "conditioning" the fluorides by circulating them in another Inconel system before they are used. Loop 334 was filled with a batch of fuzrna 30 that had previously been circulated 240 hr in loop 333. Loop 333, which was one of those filled from batch EE-92, showed a maximum penetration of 14 mils in its short period of operation. When the fluorides from loop 333 were transferred to loop 334 and circulated for 500 hr, the light, scattered attack found was to a maximum depth of only 5 mils. While this is not complete elimination of attack, it is a big reduction. It is likely that better handling and cleaning procedures would reduce the attack even further.

### Effect of Additives to the Fluoride Mixtures

Previously, when zirconium hydride was added to the coolant (a nonuranium-bearing fluoride mixture), the depth of attack was reduced, but a layer was deposited on the hot-leg wall. For loop 308, which was run during this period, the zirconium hydride was added to the fluorides in the fill pot. The fluoride batch was agitated for 3 hr at 1200°F and then transferred to the loop through a micrometallic grade G filter. After operation for 500 hr at 1500°F, no layer could be found in the hot leg of the loop. The hot-leg attack had been reduced to a maximum penetration of 2.5 mils, which is the same attack as that obtained with previous zirconium hydride additions and is a large reduction from that found in the standard loops. No change in analysis of the fluoride mixture could be detected after the hydride addition.

Several attempts were made previously to reduce attack by adding chromium metal to the fluorides before they were circulated, but these attempts resulted in very little, if any, improvement. In an attempt to improve dissolution, –325 mesh electrolytic chromium powder was used in these tests. For loop 323, the chromium was added to the charge pot as fairly coarse chromium-metal flakes. Light subsurface void formation with a maximum penetration of 4 mils was found in the hot leg. This loop was also filled from fluoride batch EE-92, which produced 15 mils of attack in the standard loops; so definite improvement was obtained. A thin, continuous metal deposit was found in the cold leg, and thus there is evidence that this procedure results in increased chromium mass transfer. The chromium content was actually lower in the final fluoride mixture than it was in the original batch.

### Effect of a Graphite Insert

Inconel loop 294 was operated with a graphite rod inserted in the center of the upper portion of the hot leg. Results obtained with this loop show that, under these conditions, Inconel may be carburized. Opposite the graphite rod in the hot leg, carbides were found in the Inconel grain boundaries to a depth of almost one-half the pipe-wall thickness. The carbides were also found in the cold leg but only to a depth of 15 mils. In the cold leg, the carbides were evenly dispersed and not, primarily, concentrated in the grain boundaries as they were in the hot leg. The hot-leg attack in this loop was heavier than usual and extended to 13 mils. The mechanism of this carburization is not understood.

Visually, it appeared that the graphite rod was covered with a complete metallic coating. Under the microscope, it could be seen that this layer was actually a collection of nonmetallic particles; each particle was covered with a thin, metallic skin. These particles had penetrated the graphite to a depth of 17 mils. Spectrographic analyses showed the presence of chromium, zirconium, and sodium; the iron and nickel contents were low. A diffraction pattern revealed the presence of only the fuel. Thus it appears that the layer consisted of clumps of fuel covered with chromium metal. While attack was deeper than usual, the chromium content in the fluoride was lower. The deposit was probably caused by a temperature drop across the pipe.

### Preferential Attack on Type 316 Stainless Steel

One Inconel loop was operated with a type 316 stainless steel section 6 in. long welded into the upper part of the hot leg. The Inconel showed only very light and widely scattered subsurface void formation to 3 mils, and the depth of attack decreased near the stainless steel joint. The joining type 316 stainless steel showed a very rough surface, with some areas spalling off. Heavy attack that was primarily intergranular in nature extended to a depth of 12 mils. Figure 14 shows both the Inconel and the type 316 stainless steel surfaces across the top weld. In the center of the insert, the attack decreased to 8 mils. The Inconel below the stainless steel also showed a reduction in attack. In the cold leg, a well-diffused surface deposit 0.3 mil thick was found. It appears therefore that stainless steel is attacked preferentially in fluorides in the presence of Inconel.

While it may be possible to protect an Inconel system by using stainless steel, such a combination does not look promising. The major difficulty expected to be encountered in such a system would be mass transfer. The major benefit derived from this loop is the warning against obtaining corrosion data from a loop in which any stainless steel is present.

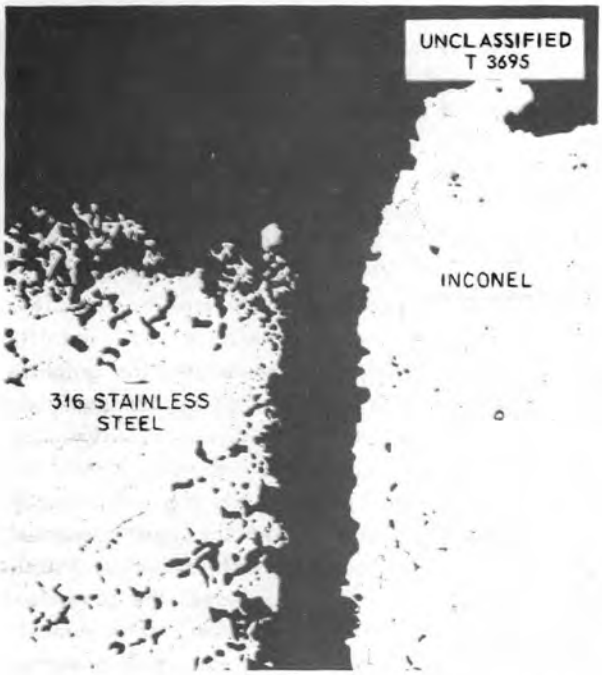


**Fig. 14. Inconel–Type 316 Stainless Steel Interface in Hot Leg of a Thermal Convection Loop in Which Fuzrna 30 Was Circulated for 500 hr at 1500°F.** 100X

### Nickel as a Container Material

A batch of fuzrna 30 was circulated 500 hr at 1500°F in a nickel loop that had been cleaned with hot, dry hydrogen. After circulation, a few metallic crystals were found in the trap and in the fluorides in the lower portion of the cold leg. An extremely thin layer was found metallographically on the cold-leg wall surface. The hot-leg surface was smooth and highly polished. No attack was discernible under the microscope (Fig. 15). The wall of the hot leg measured 2 mils thinner than that of the cold leg. This variation in thickness is within commercial tolerances and therefore no definite conclusion can be drawn; however, it is felt that some even removal had taken place. The amount of mass transfer found with this system was many times less than that found when fluoride mixtures containing lithium and potassium, instead of zirconium, were circulated in nickel. This test will be repeated and more care will be taken in cleaning and handling in an effort to eliminate all mass transfer.

### Loop Cleaning

A cleaning step is now being used to remove the metallic oxides from the welds and from the pipe

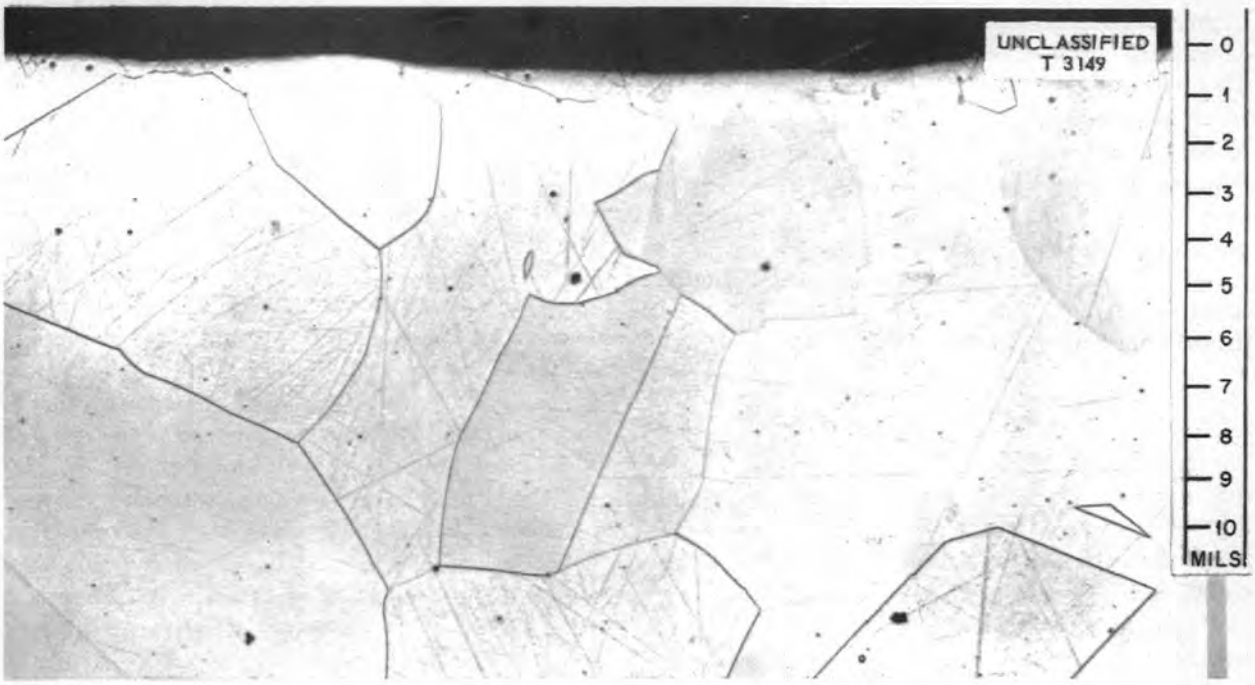


**Fig. 15. Hot Leg of Nickel Thermal Convection Loop in Which Fuzrna 30 Was Circulated for 500 hr at 1500°F.** 250X

surface. In the cleaning step, a batch of non-uranium-bearing fluoride mixture with otherwise the same composition as that of the uranium-bearing fluoride mixture is circulated thermally for 2½ hr and then drained from the loop. For tests of this procedure, three hot-leg temperatures were tried: 1200, 1400, and 1500°F. The weld discoloration was removed in all cases, as far as could be determined visually or metallographically, and no visible attack had taken place. In using this cleaning method, if the loop did not drain completely or if the cleaning material deposited on the walls, any remaining oxides would be converted from the structural metal oxides to zirconium oxide. The Materials Chemistry Division has shown that zirconium oxide will not produce attack on Inconel.

Insufficient results are available to determine whether this loop cleaning will result in a significant decrease in corrosion depth. The first loop seemed to indicate that it would, but the results for the second loop were questionable. Other variables were involved in both loops.

## PHYSICAL CHEMISTRY

G. P. Smith

### Sodium Oxidation

J. V. Cathcart

A study has been made of the oxidation rate of sodium at room temperature, both in dry oxygen and in the presence of water vapor. The presence of water vapor appeared to accelerate the oxidation rate, although the extent of this effect is still not clear. The most striking result was the protective nature of the oxide film formed in dry oxygen. It was found that the oxide film thickness increased rapidly during the first few minutes of oxidation and thereafter remained virtually constant. As discussed below, this result is at variance with the generally accepted theory of the oxidation of sodium; however, the oxidation rate has not been adequately tested in the past.

A manometric technique was employed in making the rate measurements. The apparatus, as shown in Fig. 16, consisted of two pyrex-glass bulbs, $A_1$ and $A_2$, each of which had a volume of about 30 $cm^3$. The two bulbs were separated by a thin-walled, glass break-off tip. Side arms on the bulbs were connected through appropriate stop-

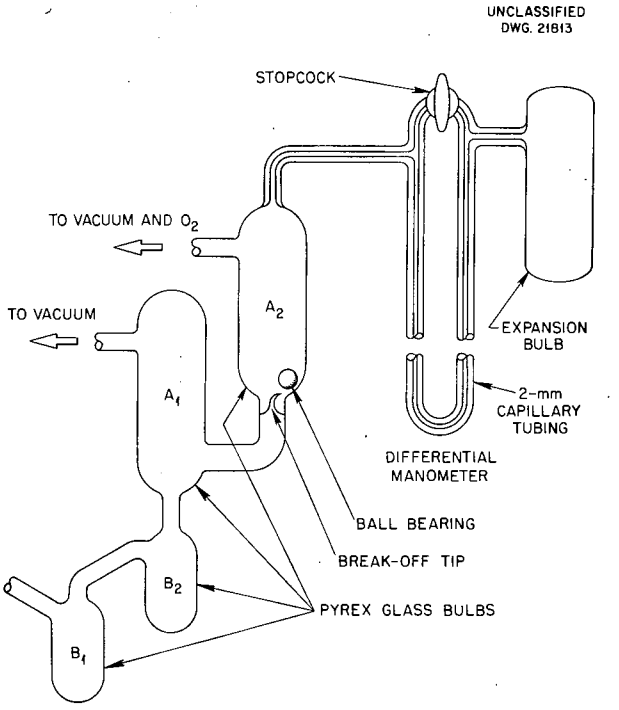


**Fig. 16. Apparatus for Measuring Oxidation Rate of Sodium.**

cocks to vacuum and oxygen lines. Two smaller glass bulbs, $B_1$ and $B_2$, were connected in series and sealed to the bottom of bulb $A_1$. A differential manometer was connected at the top of bulb $A_2$. The manometer was made of 2-mm pyrex-glass capillary tubing, and Octoil-S diffusion pump oil was used as the manometric fluid. The two arms of the manometer were separated by a stopcock, and the closed arm of the manometer was provided with an expansion bulb. Pressure changes of 0.01 mm Hg could be detected with this manometer.

About 1 g of sodium was introduced into bulb $B_1$, and the entire apparatus was evacuated to a pressure of approximately $10^{-6}$ mm Hg. The sodium was first distilled into bulb $B_2$ and then evaporated onto the walls of bulb $A_1$. During the final evaporation of the sodium, the walls of bulb $A_1$ were kept cool with a piece of wet cloth. First, bulb $B_2$ was sealed off under vacuum with a hand torch, and then the side arm connecting bulb $A_1$ to the vacuum pump was similarly sealed off. Bulb $A_2$ was then filled with oxygen to a pressure of about 400 mm Hg, and its side arm was sealed off. The oxygen had previously been purified by passing it

over hot cupric oxide and drying it in a liquid-nitrogen trap.

At this point, the apparatus consisted only of bulbs $A_1$ and $A_2$ and the manometer. With the stopcock open, the break-off tip separating bulbs $A_1$ and $A_2$ was crushed with a stainless steel ball bearing to admit oxygen into bulb $A_1$ at an initial pressure of approximately 200 mm Hg. The stopcock was then closed, and manometer readings were taken at measured time intervals.

In experiments in which the effect of water vapor was studied, a small bulb filled with water was attached to the side arm of bulb $A_2$. The water in this bulb was allowed to remain in contact with the oxygen in bulb $A_2$ overnight to saturate the oxygen with water vapor. The water bulb was then sealed off from the remainder of the system, and the experiment was performed in the manner described above.

The data from two typical experiments in which sodium was oxidized in dry oxygen are plotted in Fig. 17. The quantity $\Delta p$, which is plotted on the ordinate of the graph, represents the decrease in pressure in the system during reaction. It is related, approximately, to the thickness of the oxide film through the Ideal Gas Law. If it is assumed that the oxide formed is $Na_2O$, the thickness of the oxide film, in angstroms, is given by

$$\text{Film thickness} = 4.86 \times 10^5 \frac{\Delta p V}{ART},$$

where

$\Delta p \equiv$ decrease in pressure in reaction chamber, in mm of Octoil,

$V \equiv$ volume of reaction chamber, in $cm^3$,

$A \equiv$ area of sodium film (product of the apparent area and its roughness factor), $cm^2$,

$R \equiv$ gas constant, in $cm^3 \cdot atm/mole \cdot deg$,

$T \equiv$ temperature of reaction chamber, in °K.

Since in any given experiment $V$ and $T$ are constant, $\Delta p$ differs from film thickness by a constant factor. In comparing the results of several experiments, it was necessary to correct $\Delta p$ values for the variations which occurred from experiment to experiment in the volume of the reaction bulb and the area of the sodium film. The $\Delta p$ values shown in Fig. 17 have all been corrected to a film area of 65 $cm^2$ and a volume of 60 $cm^3$. For these values of $A$ and $V$, a change of pressure of 1 mm of Octoil is equivalent to an increase in film thickness of approximately 20 Å. On this basis, it may be seen that the limiting film thickness obtained for dry oxygen was about 220 Å.

Measurements of the oxidation rate in the presence of water vapor were complicated because at least

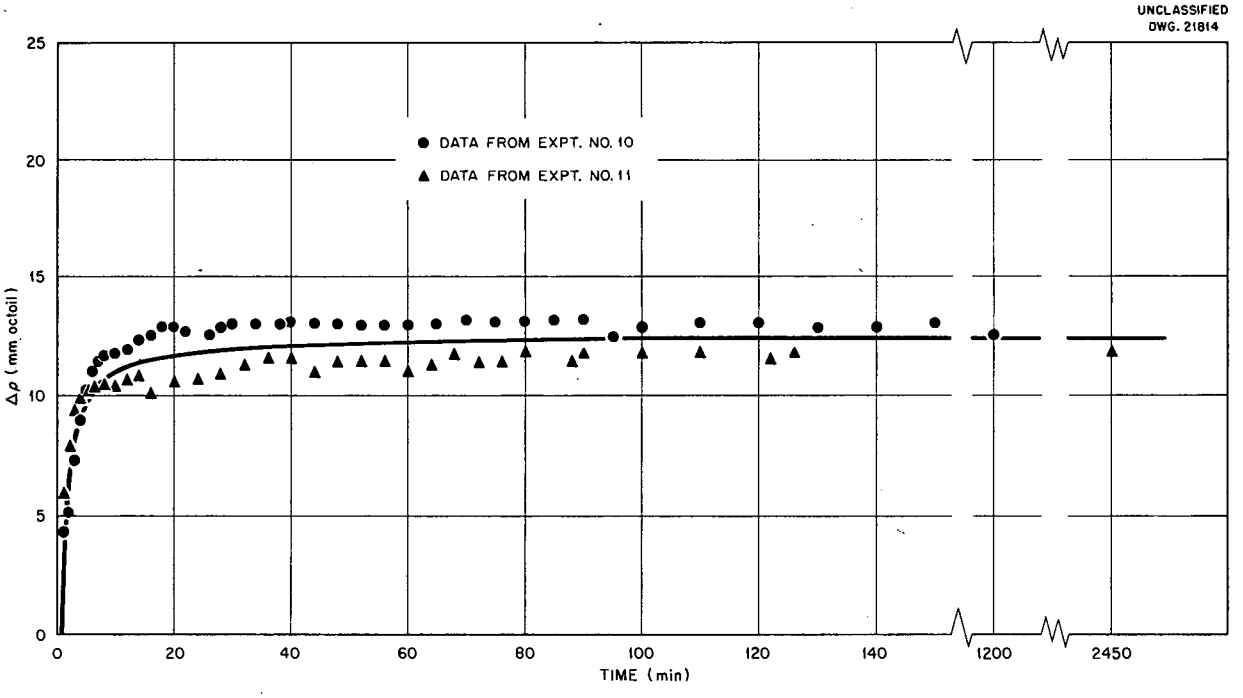


**Fig. 17. Oxidation of Sodium in Dry Oxygen at 25°C.**

some of the water reacted directly with the sodium to produce hydrogen. The reaction was

$$2H_2O + 2Na \longrightarrow 2NaOH + H_2 .$$

Since two molecules of water were removed from the reacting gas mixture for every hydrogen molecule formed, this reaction also led to a decrease in the pressure of the system. Thus measurements of pressure changes in the reaction chamber reflected the combined effect of the reaction of sodium with both water and oxygen. More precise determinations of the quantity of hydrogen in the residual gas after the completion of an experiment will be required before the separate effects of the two reactions can be evaluated.

The thicknesses of the oxide films formed have not been reported directly for several reasons. The use of a manometric method for following the oxidation process makes it inherently impossible to determine accurately the time corresponding to zero film thickness. Approximately 10 to 20 sec was required to admit oxygen to the system and to begin reading the manometer. Because the reaction between sodium and oxygen is initially very rapid, it is quite likely that even this short period of time was sufficient for the formation of an appreciable oxide film. Although the magnitude of this error cannot be accurately determined by manometric techniques, it is believed, on the basis of the behavior of other metals in early stages of oxidation, that this error probably does not exceed 25 to 50 Å.

A second limitation in the experimental results exists because no measurements were made of the surface roughness of the sodium film. In calculating approximate film thicknesses, a surface roughness factor of unity was assumed. Again, however, the error from this assumption is probably not very large, since the relatively high surface tension and the atomic mobility of sodium at room temperature make a large roughness factor unlikely.

Other small errors were introduced in measuring the volumes of the reaction bulbs and the areas of the sodium films. The volumes were obtained by immersing the reaction bulb in a vessel filled with water and weighing the displaced water. From the weight of the bulb and the known density of pyrex glass, the actual volume of the reaction bulb was calculated. The areas of the sodium films were calculated from the known dimensions of the bulbs.

Although the absolute values reported for the oxide thicknesses are somewhat uncertain, the discrepancies do not in any way obscure the essential result of the experiments: namely, the demonstration of the protective nature of the oxide film formed on sodium in dry oxygen at room temperature.

In most theoretical treatments of the oxidation of metals, it is stated that the density of an oxide relative to that of the parent metal determines the mechanism of oxidation.[1] The oxides of the alkali metals have densities which are greater than those of the parent metals. It has been assumed that a thin oxide film on an alkali metal would thus always be in a state of tension which would promote crack formation in the film and constantly expose fresh metal to oxygen. On this basis, an oxidation rate which is linear with time has been predicted for the alkali metals.

The results which have been obtained for sodium demonstrate clearly the incorrectness of the above theory. Sodium formed a protective oxide film in dry oxygen at room temperature, and thus sodium is in the same general category as is copper or aluminum, for which the mechanism of oxidation is much better understood.

In addition to continuing experiments designed to show the effect of water on the oxidation rate, measurements will be made of the oxidation rate of sodium as a function of temperature. It is also hoped that it will be possible to study the structure of the oxide film to obtain additional data concerning the mechanism of oxidation.

### Interfacial Equilibriums in the Copper-Bismuth System

J. V. Cathcart W. H. Bridges

The investigations of the variation of surface free energy with crystallographic plane on copper single crystals immersed in a saturated solution of copper in bismuth have been continued. Details of the apparatus used and of the experimental procedure were previously reported.[2]

One experimental approach which may be utilized in establishing the existence of variations of surface free energy with crystallographic plane on a single crystal involves the determination of the

[1] U. R. Evans, *Metallic Corrosion, Passivity and Protection*, p. 100-114, E. Arnold & Co., London, 1946.

[2] G. P. Smith, Jr., J. V. Cathcart, and W. H. Bridges, *Met. Quar. Prog. Reps. for Apr. 30, 1952*, ORNL-1302, p. 59 and for *Jan. 31, 1953*, ORNL-1403, p. 31.

equilibrium shape of the crystal. A set of experimental conditions may be defined such that the total free energy of the crystal is minimized provided no variations of surface free energy exist over the crystal. Under these circumstances, any changes which occur on the crystal can then be ascribed to surface free energy variations.

Such a set of conditions was realized by bringing a previously saturated solution of copper in bismuth into contact with a spherical copper single crystal, the entire system being held at a rigidly controlled temperature. A sphere is the geometrical shape which minimizes surface area; hence, no changes in the surface topography of the crystal were expected unless variations of surface free energy with crystallographic plane existed over the crystal.

Experiments of the kind described above have been performed, and rearrangements of the crystal surfaces were observed to occur. These changes in surface topography have been interpreted as an indication of the existence of surface free energy differences for different crystallographic planes of a copper crystal.

Obviously, strict control of isothermal conditions was essential in this study. The experiments were conducted entirely in a stirred, constant-temperature molten-salt bath. The temperature control of the salt bath has been improved to the extent that temperature fluctuations at 400°C amounted to no more than ±0.03°C. This degree of control was obtained with a platinum resistance thermometer that operated through a Leeds & Northrup controller with a 1-ohm span. The controller was used in conjunction with a Leeds & Northrup DAT 50. The bridge resistances in the controller were thermostated for increased accuracy. The temperature of the bath was monitored with a Bureau of Standards-calibrated platinum resistance thermometer connected to a Leeds & Northrup Model G-2 Mueller bridge. A continuous record of the bath temperature was obtained by substituting a Leeds & Northrup Speedomax recorder with a full-scale span of 0.145°C for the galvanometer of the Mueller bridge.

The results obtained with this improved temperature control were in many respects similar to those reported in previous experiments. As before, a rearrangement occurred on the surface of the crystal that produced a large number of small, flat, faceted regions on the crystal surface. These areas were generally concentric with important poles on the crystals. The faceted surfaces produced brilliant, specular reflections when the crystal was rotated in a light beam, and it was possible to establish the orientations of the flat surface of the facets from the symmetry of the reflections. The (111), (110), and (320) surfaces have been identified, the (111) planes being by far the most prominent.

In an earlier experiment, a similar rearrangement of the surface of the crystal was observed. Instead of simple facet formation, however, the rearrangement caused the formation on the surface of the crystal of many very small, pyramid-like structures which possessed symmetries corresponding to their orientations on the crystal. The bounding planes of these pyramid-like structures were constituted essentially of the same crystallographic planes as those reported above. It is thought that this difference between the two experiments may have been due to the better temperature control which was attained in the more recent experiment.

The occurrence of surface rearrangement on the copper crystals was interpreted as an indication of the existence of variations in the surface free energy with the crystallographic plane on copper crystal under the experimental conditions described above. It is possible to speculate on the true equilibrium shape of a copper crystal on the basis of these surface rearrangements. It seems probable that the equilibrium crystal is bounded, at least in part, by flat surfaces. Since the (111) planes were predominant on the faceted areas of the crystal, it is likely that in the true equilibrium crystal the major portion of the surface is covered by (111) planes.

### Mass Transfer in Liquid Lead

J. V. Cathcart

Studies of the mass transfer of a variety of solid metals in liquid lead have been continued with the use of small thermal convection loops made of quartz tubing. Details of the construction and operation of the loops and of the results obtained for Inconel, columbium, molybdenum, and type 304 stainless steel were reported previously.[3] Materials tested during the period of this report included types 347, 410, and 446 stainless steel,

[3] G. P. Smith, *Met. Semiannual Prog. Rep. Apr. 10, 1953*, ORNL-1551, p. 17.

Armco iron, chromium, nickel, Nichrome V, and a nickel-iron alloy (30% Ni–70% Fe).

From the point of view of resistance to mass transfer and corrosion, the 400 series stainless steels gave, by far, the best results. A loop containing type 446 stainless steel was operated for 619 hr with hot- and cold-leg temperatures of 810 and 520°C, respectively. Although no plugging occurred in this loop, a small amount of mass transfer material collected at the bottom of the cold leg. It is presumed that had the loop been allowed to operate for a sufficiently long time, this deposit would have grown to such a size as to stop circulation of the lead. As may be seen from Fig. 18, the test specimen suffered irregular surface attack. A loop containing type 410 stainless steel was operated for 545 hr with hot- and cold-leg temperatures of 810 and 525°C, respectively. The results for this loop were comparable to those obtained with type 446 stainless steel.

The type 347 stainless steel loop plugged after 140 hr of operation with hot- and cold-leg temperatures of 800 and 500°C, respectively. Not only was there an increase in the rate of mass transfer as compared with that for the 400 series stainless steels, but there was also a considerable increase in the intergranular penetration (Fig. 19). Results obtained with type 347 stainless steel were similar to those obtained with type 304 stainless steel.

Tests were also conducted on the major constituents of these stainless steels. A loop containing Armco iron was operated for 250 hr with hot- and cold-leg temperatures of 800 and 545°C, respectively, before plugging occurred. Corrosive attack in this loop was limited to an even solution of metal from the surface of the test specimens (Fig. 20).

Somewhat poorer results were obtained with the chromium loops which plugged after an average operating time of 90 hours. The hot- and cold-leg temperatures used were again approximately 800 and 500°C, respectively. Corrosive attack was relatively slight and irregular, as shown in Fig. 21.

Pure nickel exhibited the least resistance to mass transfer of all metals tested, the loops plugging at an average time of 2 hr; hot- and cold-leg temperatures for these loops were 810 and 525°C, respectively. The nickel specimens suffered very heavy intergranular penetration, as shown in Fig. 22.

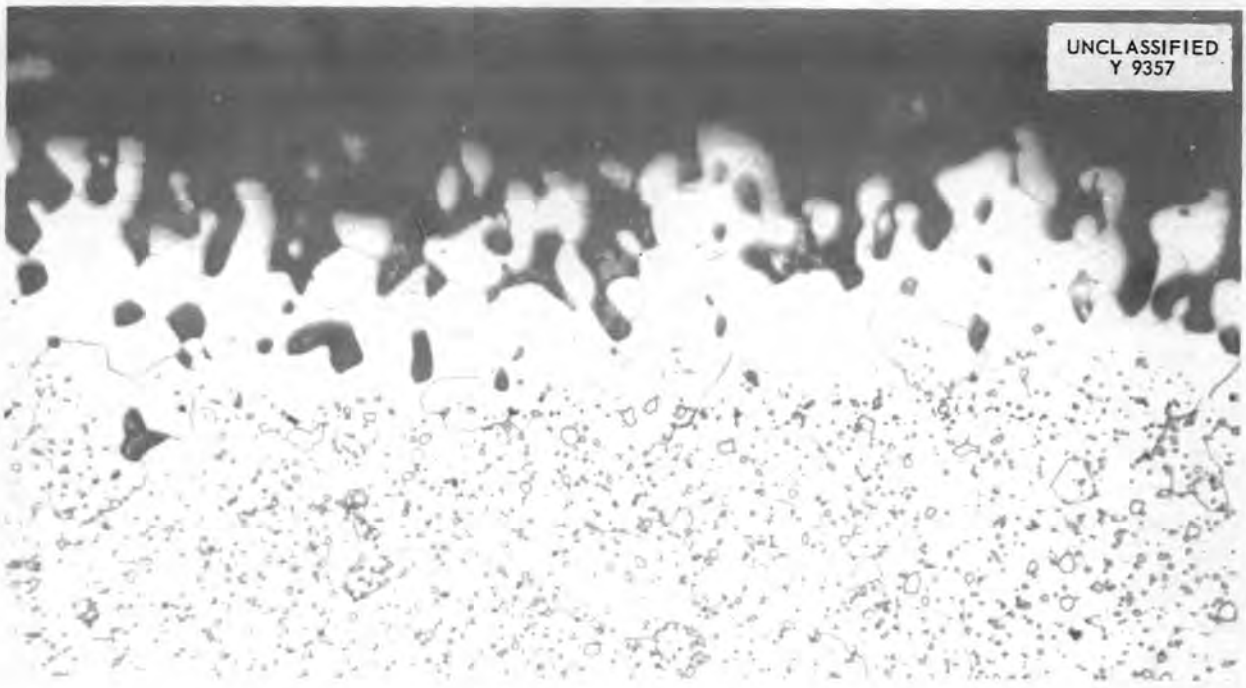


**Fig. 18. Hot Leg of Type 446 Stainless Steel Loop in Which Lead Was Circulated for 619 hr with Hot- and Cold-Leg Temperatures of 810 and 520°C.** 500X

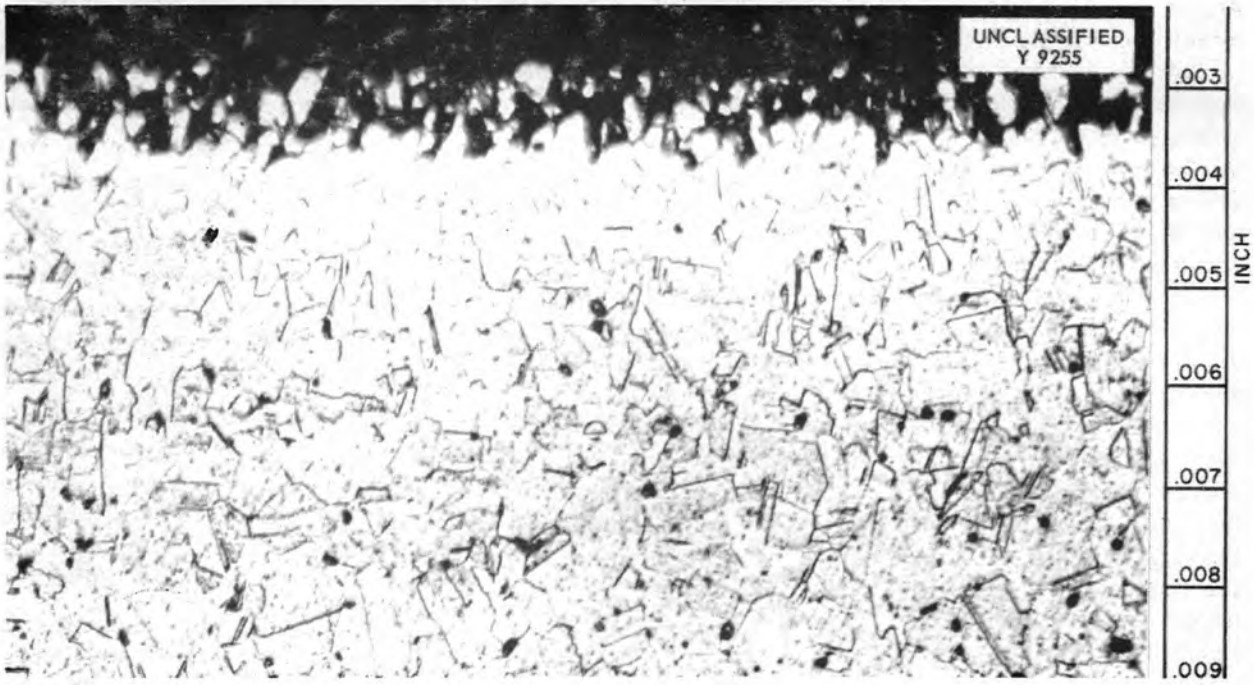


**Fig. 19. Hot Leg of Type 347 Stainless Steel Loop in Which Lead Was Circulated with Hot- and Cold-Leg Temperatures of 800 and 500°C.** Loop plugged after 140 hr of operation. 500X

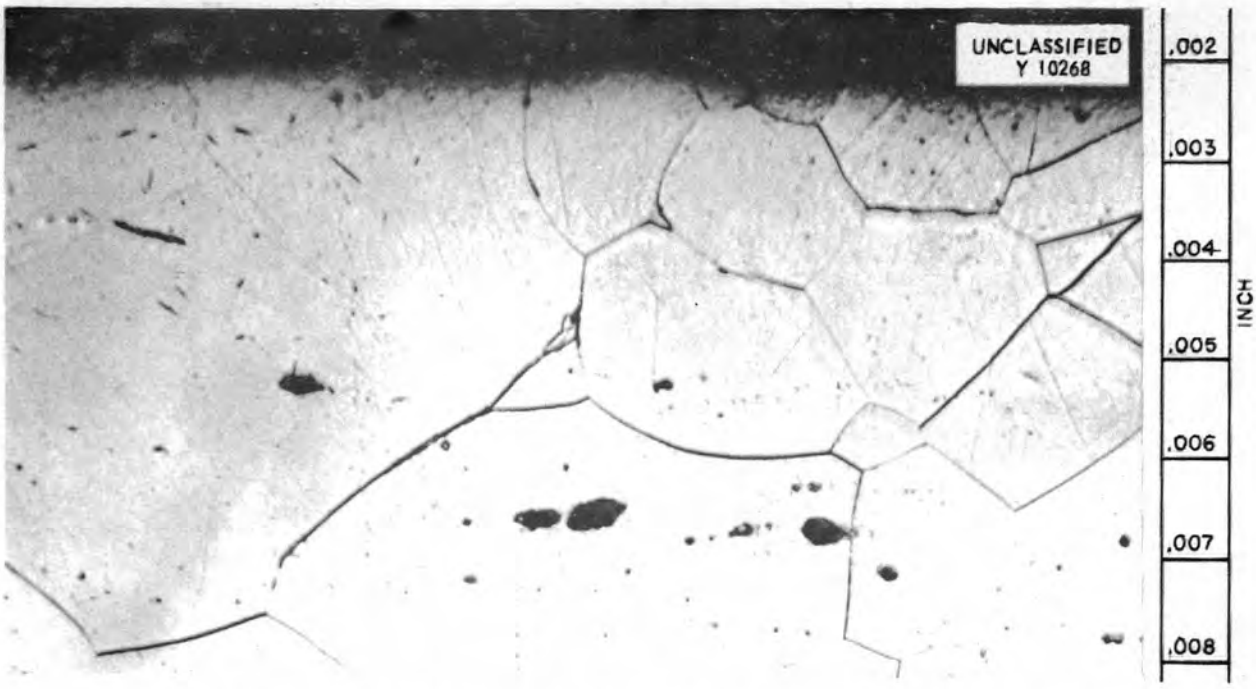


**Fig. 20. Hot Leg of Armco Iron Loop in Which Lead Was Circulated with Hot- and Cold-Leg Temperatures of 800 and 545°C.** Loop plugged after 250 hr of operation. 500X

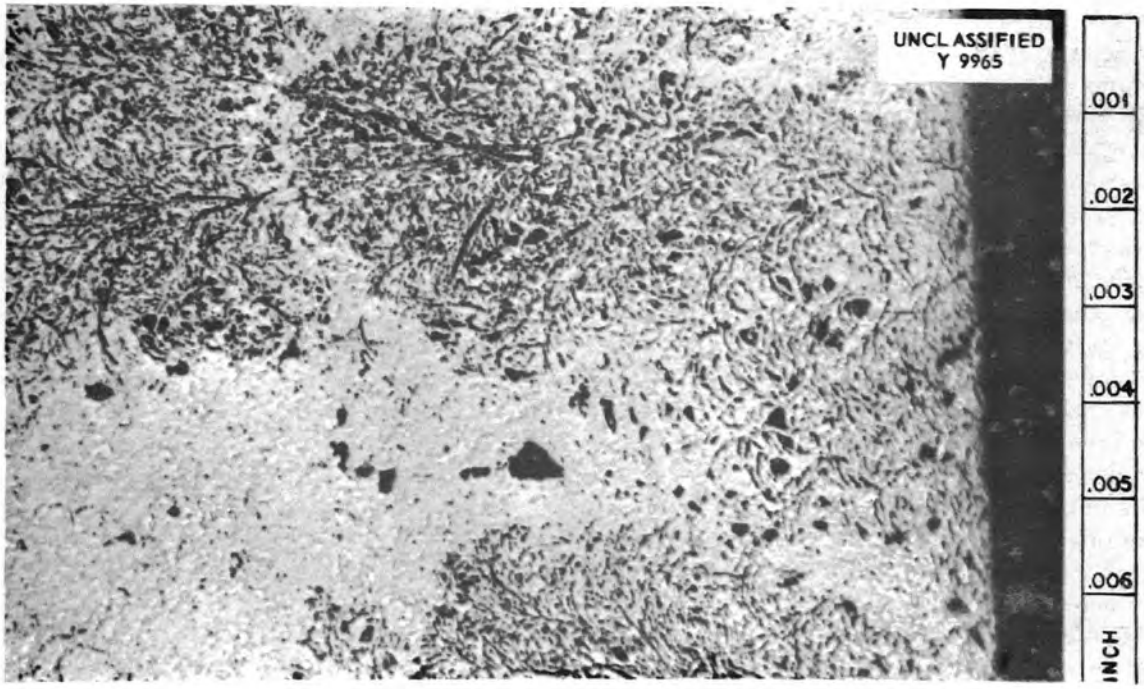


**Fig. 21. Hot Leg of Chromium Loop in Which Lead Was Circulated with Hot- and Cold-Leg Temperatures of 800 and 500°C.** The fine structure in the metal is due to the chromium tubing having been made by electrodepositing chromium onto a form. 500X

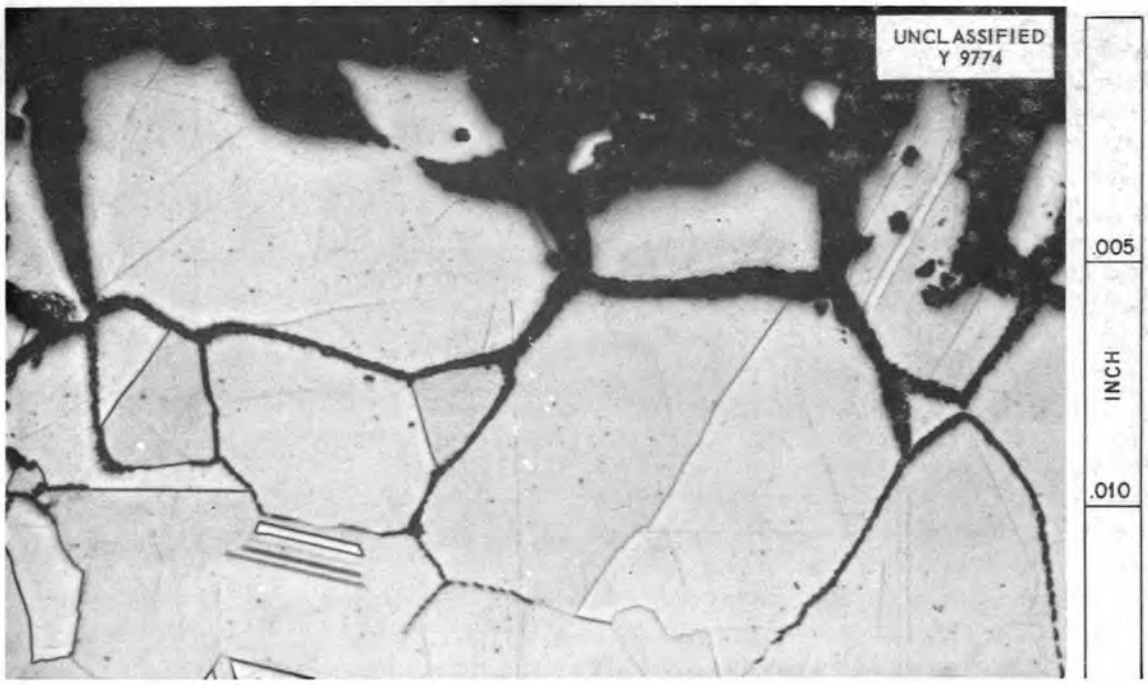


**Fig. 22. Hot Leg of Nickel Loop in Which Lead Was Circulated with Hot- and Cold-Leg Temperatures of 810 and 525°C.** 250X

In addition to the iron-chromium binary alloy represented by the 400 series stainless steels, tests were also conducted on nickel-chromium and iron-nickel alloys. Nichrome V (80% Ni–20% Cr) showed only a slight increase in resistance to mass transfer as compared with pure nickel. The loop, which was operated with hot- and cold-leg temperatures of 810 and 525°C, respectively, plugged after 12 hr of operation. As in the case of nickel, copious quantities of mass transfer material were found in the Nichrome V loops. The corrosion encountered in these loops was similar to that which occurred in Inconel, although the attack was more severe. As shown in Fig. 23, lead penetrated throughout the Nichrome sample.

The resistance to mass transfer shown by the nickel-iron alloy (30% Ni–70% Fe) was comparable to that found for pure iron. Loops were operated with hot- and cold-leg temperatures of 810 and 525°C, respectively, for approximately 275 hr before plugging occurred. Corrosion in these loops was limited to slight irregular surface attack, as shown in Fig. 24. The results for all metals tested are summarized in Table 21.

As the table illustrates, much better results were obtained with the 400 series stainless steels than with the pure metals which comprised them. The reverse tended to be the case with 300 series stainless steels. In general, alloys having a high nickel content showed poor resistance to mass transfer and underwent heavy corrosive attack. Future work will include an effort to obtain an explanation of this behavior. Tests will also be made of the effect on mass transfer in liquid lead of the addition of silicon to various stainless steels. It is also planned to test nickel-chromium-iron alloys with high chromium content.

### Hydroxide Chemistry

L. D. Dyer M. E. Steidlitz

The hydroxide chemistry studies which have been made may be divided into two categories: first, a continuation of the work previously reported[4] on the occurrence of trivalent nickel among the corrosion products formed in fused hydroxide media and, second, a preliminary examination of the catastrophic corrosion of nickel by sodium hydroxide at 900°C under a kinetic vacuum. The studies of trivalent nickel included attempts to prepare the compounds $KNiO_2$ and $RbNiO_2$, determination of additional physical and chemical properties of $LiNiO_2$ and $NaNiO_2$, and an estimation of the $Ni^{3+}$-to-$Ni^{2+}$ ratio for corrosion products in fused NaOH as a function of temperature. The studies of trivalent nickel are described below.

Attempts to make $KNiO_2$ from KOH-$KO_2$ melts in nickel tubes produced potassium-nickel-oxygen compounds in which the ratio of nickel(III) to total nickel varied up to 0.5. Passing oxygen through fused RbOH yielded only nickel(II) oxide.

The density of $NaNiO_2$ was determined pycnometrically to be 4.72 g/cm$^3$ as compared with the value of 4.74 g/cm$^3$ calculated from the crystal structure.

X-ray evidence shows that $NaNiO_2$ crystals take up moisture and $CO_2$ from the air to form a crust of $Na_2CO_3 \cdot H_2O$. In the presence of 6 *N* sulfuric acid, perchloric acid, or nitric acid, the crystals slowly

TABLE 21. RESULTS OF TESTS OF MASS TRANSFER OF VARIOUS SOLID METALS IN LIQUID LEAD

| TEST METAL | TIME FOR PLUG FORMATION (hr)[a] |
|---|---|
| Columbium | 500[b] |
| Molybdenum | 500[b] |
| Type 446 stainless steel | 619[c] |
| Type 410 stainless steel | 545[c] |
| Nickel–iron alloy (30% Ni–70% Fe) | 275 |
| Armco iron | 250 |
| Type 347 stainless steel | 140 |
| Type 304 stainless steel | 100 |
| Chromium | 90 |
| Inconel | 75 |
| Nichrome V | 12 |
| Nickel | 2 |

[a]Hot- and cold-leg temperatures for all loops were approximately 810 and 525°C, respectively.

[b]No mass transfer or corrosion observed.

[c]Circulation not stopped; small amounts of mass-transferred material noted.

[4]G. P. Smith, J. V. Cathcart, and W. H. Bridges, *Met. Quar. Prog. Rep. Oct. 31, 1952*, ORNL-1437, p. 33-35.

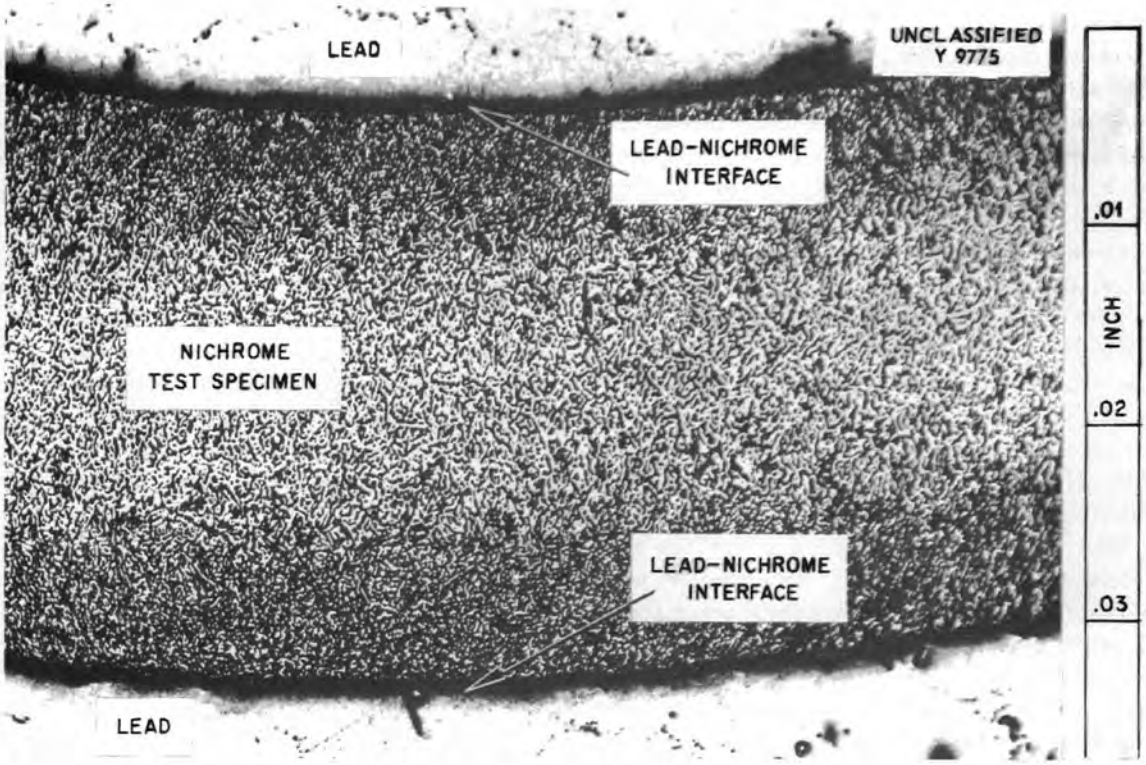


**Fig. 23. Hot Leg of Nichrome V Loop in Which Lead Was Circulated with Hot- and Cold-Leg Tem atures of 810 and 525°C.** Loop plugged after 12 hr of operation. 100X

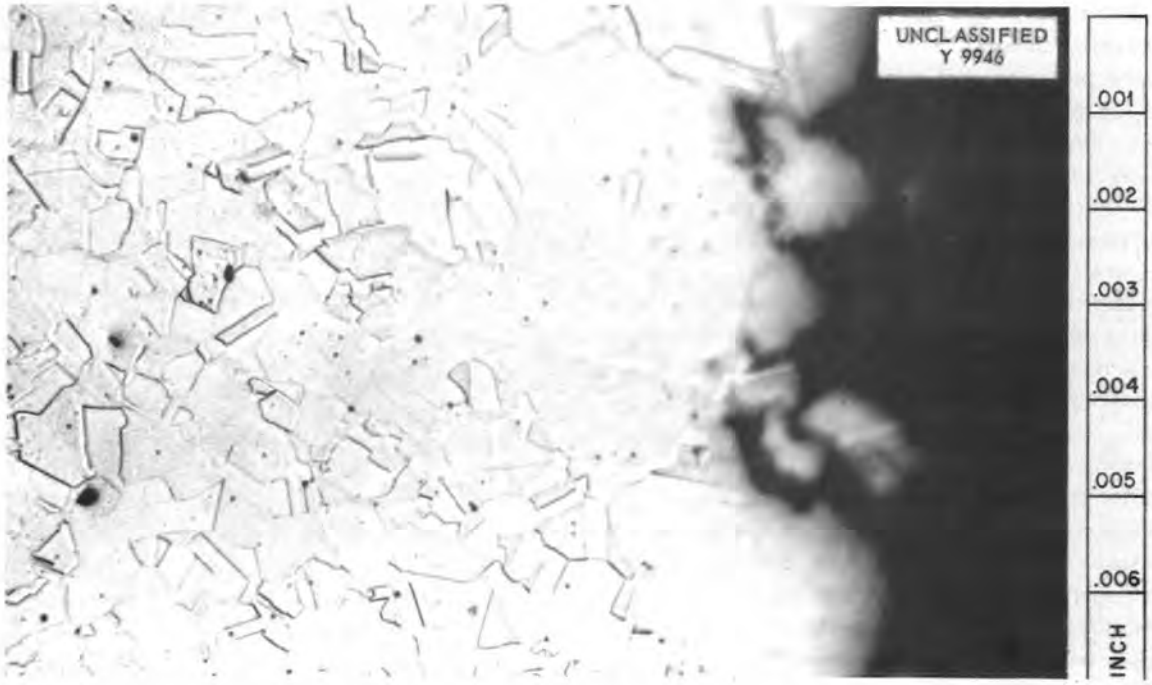


**Fig. 24. Hot Leg of Nickel-Iron (30% Ni–70% Fe) Alloy Loop in Which Lead Was Circulated with Hot- and Cold-Leg Temperatures of 810 and 525°C.** Loop plugged after approximately 275 hr of operation. 500X

dissolve and evolve oxygen. In all cases, hydrogen peroxide accelerates the dissolution. Hydrochloric acid rapidly dissolves the compound, and chlorine is evolved. Dilute acid suspensions of the compound rapidly oxidize manganous ions to manganese dioxide and permanganate and oxidize iodide to iodine, which is further oxidized to iodate.

The action of water on $NaNiO_2$ was also studied. The results of x-ray and chemical analyses of water-washed products show that $\gamma$-$NiOOH \cdot xH_2O$ and $Ni(OH)_2$ are formed and that, by cautious hydrolysis in a cold, alkaline solution, the amount of $Ni(OH)_2$ formed can be lessened greatly. An intermediate phase between $NaNiO_2$ and $\gamma$-$NiOOH \cdot xH_2O$ was indicated by some x-ray patterns of $NaNiO_2$ exposed only a few minutes to water, but this intermediate phase was not isolated. Crystals of $NaNiO_2$ are not disintegrated when they react with water but retain their gross shape. The reaction appears to occur by a solid-state diffusion process. The progress of this reaction through a crystal can be followed qualitatively by changes in the reflection of plane polarized light and other easily detected microscopic alterations. The $Ni(OH)_2$ formed in the resulting particle shows a slight distortion of its crystal structure and an epitaxical relation to the crystal lattice of NiOOH, as determined by measurements with an x-ray precession camera.

Many particles of $NaNiO_2$ possess bands which microscopically are similar in many respects to those associated with the martensitic transformation in indium-thallium alloys. X-ray studies show that these bands represent a complex twinned structure.

Several attempts to prepare $LiNiO_2$ yielded products which were deficient in trivalent nickel (approximately 75%). Small amounts of cobalt and manganese were found in these products. Cold, dilute sulfuric, perchloric, and nitric acids dissolve $LiNiO_2$ very slowly. Hydrochloric acid dissolves it rapidly and chlorine is evolved. Studies of the reaction of $LiNiO_2$ with water indicate that $LiNiO_2$ remains unchanged in cold water and slowly decomposes to nickel(II) oxide in hot water without the formation of any observed intermediate compounds. The rate of decomposition is even slower in cold 1 *N* lithium hydroxide solution.

The analysis for oxidizing power of the $NaNiO_2$ products was made by dissolving the $NaNiO_2$ in an HCl-KI mixture under an inert gas and titrating with thiosulfate the iodine released. Blank runs titrated from 0.00 to 0.05 $cm^3$ of 0.1 *N* $Na_2S_2O_3$.

The lithium compound presented a difficulty in that it would not dissolve readily in acid of the concentration ordinarily used for iodometric titrations; also the blanks sharply rose in oxidation titer and decreased in reproducibility as the acid concentration was raised. Therefore, a more elaborate method and apparatus had to be used. The following satisfactory procedure for the analysis of the $LiNiO_2$ was developed. About 0.3 g of $LiNiO_2$ was added to a two-necked reaction flask containing a stirring magnet and 3 g of KI. The apparatus was assembled as shown in Fig. 25. A vacuum pump with a liquid-nitrogen trap and

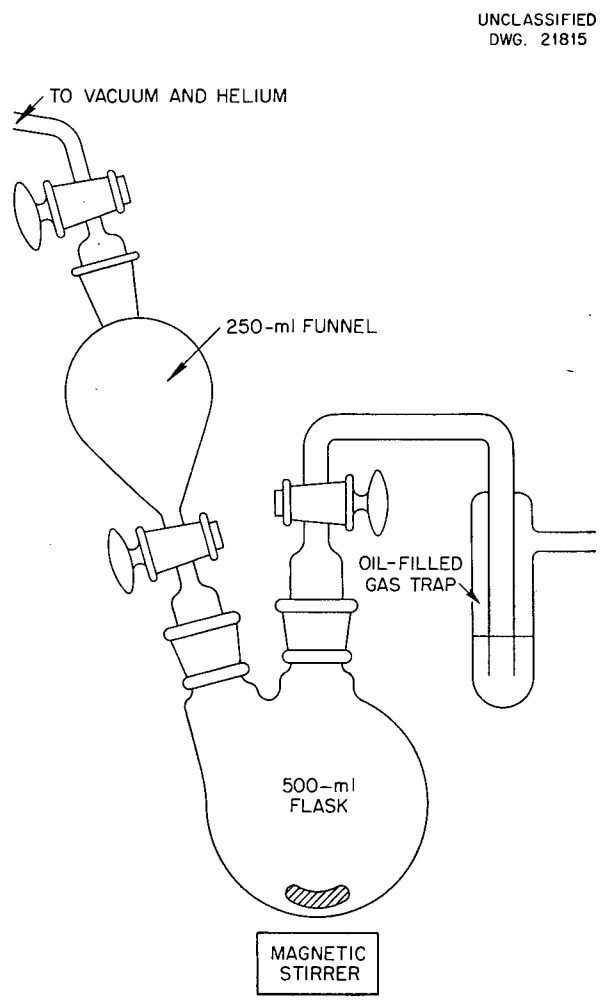


**Fig. 25. Apparatus for Determining Oxidizing Power of Sodium and Lithium Nickelate Compounds.**

a helium tank with a hot copper purifier were connected to the supply tube. After the reaction flask had been evacuated and flushed with helium several times, it was filled with helium, and the stopcock of the separatory funnel was closed. Fifty cubic centimeters of distilled 6 *N* HCl was added to the funnel, and the dissolved gases were pumped off. The 50 $cm^3$ of HCl was then forced into the reaction flask by helium pressure. After the mixture had been stirred for 2 hr, 200 $cm^3$ of 1.0 *N* NaOH was degassed the same way and added. Finally, the solution was titrated with thiosulfate. The blanks then titrated 0.01 to 0.03 $cm^3$ of 0.1 *N* $Na_2S_2O_3$.

It has been found that the $Ni^{3+}$-to-$Ni^{2+}$ ratio in solid corrosion products formed in NaOH in the presence of excess air increases as the temperature increases from 400 to 700°C and decreases as the temperature decreases over a number of temperature cycles.

It is well known that sodium hydroxide reacts relatively rapidly with nickel at 900°C if the volatile products are allowed to escape. For example, Williams[5] has shown by cautious removal of hydrogen under almost equilibrium conditions from fused caustic contained in nickel that the reaction proceeds in two steps, as follows: first,

$$NaOH + Ni \longrightarrow [Na_2O{\cdot}NiO] + H_2 ,$$

and, as soon as this reaction has gone to completion, a second reaction,

$$Ni + [Na_2O{\cdot}NiO] \longrightarrow NiO + Na ,$$

takes place. (It is to be remembered that sodium is a gas at 900°C.)

In experiments performed at this Laboratory, sodium hydroxide was heated in nickel containers at 900°C under nonequilibrium conditions. The severe corrosion which resulted is tentatively explained in terms of known reactions which serve to illustrate the complex nature of hydroxide corrosion at high temperatures.

The following experimental procedure was used. Sodium hydroxide was heated at 900°C under a kinetic vacuum in a nickel tube surrounded by a second nickel tube. In two experiments, the space between the tubes was evacuated. In a third experiment, this space was filled with hydrogen at 1 atmosphere. In all experiments, the temperature was measured by a chromel-alumel thermocouple welded to the inner tube.

The experiments in which a vacuum was maintained both inside and outside the hydroxide container were terminated after 100 hours. Copious quantities of nickel(II) oxide had formed in the melt. Metallic sodium and sodium oxide had deposited above the melt along the cooler walls of the tube. A small amount of mass transfer of nickel occurred some distance above the liquid level. In places, the walls of the tube above the liquid level were lightly grooved; thus there appeared to have been erosive attack. Corrosion at the liquid-vacuum interface was severe.

The experiment in which hydrogen pressure was maintained in the annulus was terminated after 24 hr because of tube failure. The corrosion was complex and severe. At the bottom of the tube was a polished zone devoid of hydroxide. Above this zone, there was a large plug of metallic nickel and then a zone of sodium hydroxide. Above what had been the liquid-vacuum interface, the tube wall was deeply furrowed by vertical grooves which completely pierced the tube 15 cm above the liquid level.

The following tentative explanation for the severe corrosion above the liquid level has been formulated. Because of strong surface tension forces, fused sodium hydroxide creeps up a vertical nickel surface for a considerable distance and produces an extensive thin film. This film will be referred to as the "meniscus phase," as distinguished from the bulk liquid phase. Figure 26 is a schematic diagram showing the relative positions of the tube wall and meniscus and bulk liquid phases, together with the vacuum on the interior of the tube. The relative position of the level of the bulk liquid phase, usually referred to as the vacuum-liquid interface, is shown by a dotted line. Below the dotted line, the temperature is about 900°C. Above the dotted line, the temperature progressively decreases. It is assumed that a small amount of sodium metal is formed in the system. (Metallic sodium was found in the cooler parts of the tube.) The sodium vaporizes readily at the high temperature of the vacuum-liquid interface but condenses on the cooler walls of the tube at a distance above the interface. The condensed liquid sodium drains down the tube wall and reacts with the sodium hydroxide of the meniscus phase to form sodium monoxide, as shown in the following

[5] D. D. Williams, report at the Hydroxide Committee Meeting held at Beverly, Mass. in August 1953.

UNCLASSIFIED
DWG. 21816

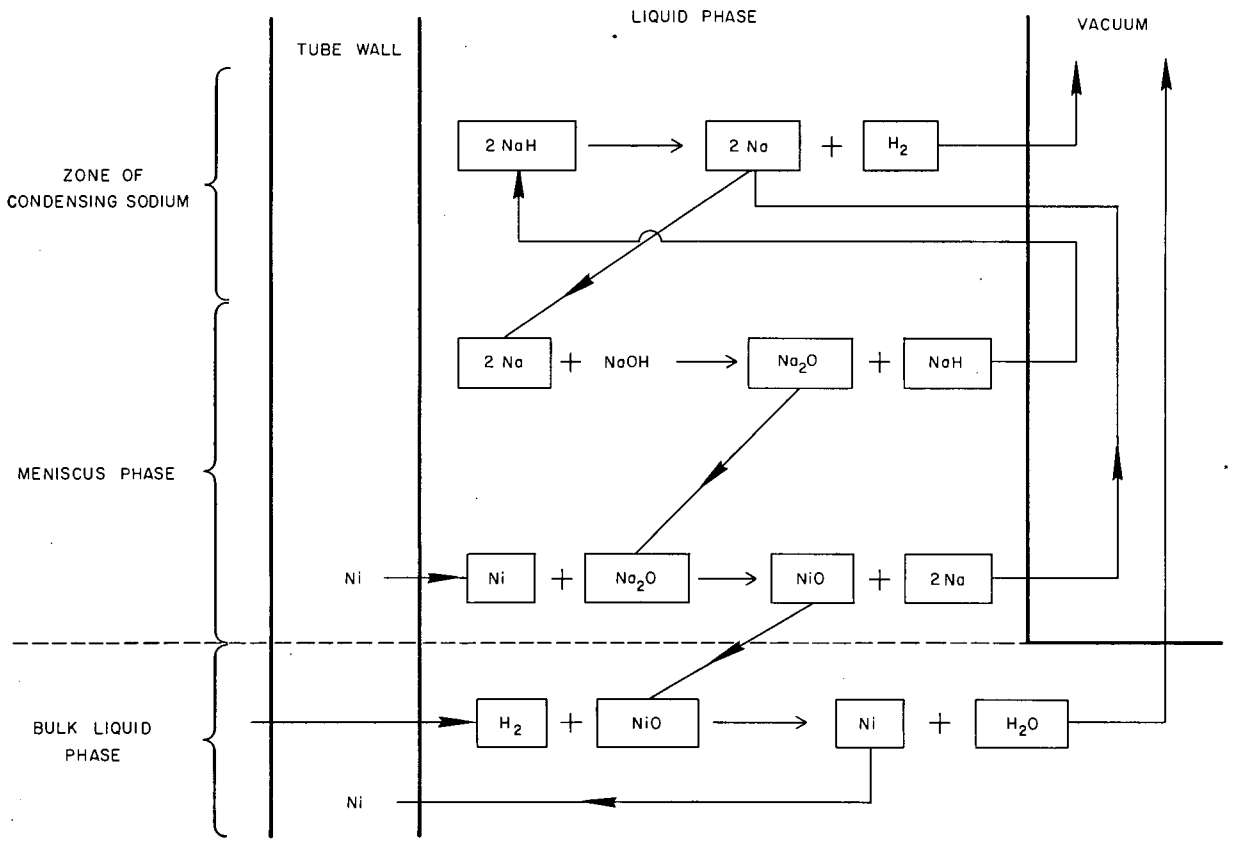


**Fig. 26. Schematic Diagram of Material Balance for Some Possible Corrosion Reactions in Fused Sodium Hydroxide.** Relative dimensions in the diagram have no significance.

equation:

$$2Na + NaOH \longrightarrow Na_2O + NaH \ . \quad (1)$$

This reaction is driven by the volatilization of sodium hydride into the vacuum. The sodium monoxide mixes with the hydroxide of the meniscus phase. As it does so, it reacts with the nickel of the tube wall to form nickel(II) oxide, as shown in the following equation:

$$Ni + Na_2O \longrightarrow NiO + 2Na \ . \quad (2)$$

This reaction is driven by the vaporization of sodium into the vacuum. The nickel(II) oxide drains into the bulk liquid phase. In the case of the tests without external hydrogen, the nickel(II) oxide collected in the bulk liquid phase. In the case of the tests with external hydrogen, the nickel(II) oxide was reduced by the hydrogen that entered the liquid phase by diffusion through the tube wall, according to the following equation:

$$H_2 + NiO \longrightarrow Ni + H_2O \ . \quad (3)$$

This reaction is driven by the escape of water into the vacuum.

In these reactions, the sodium is recycled by vaporization in the hot parts of the tube where the reaction of Eq. 2 is occurring and condensation in the cooler parts of the tube. Nickel is continuously removed from the tube wall by the formation of nickel(II) oxide in the meniscus phase. One mole of sodium hydride is formed by the reaction of Eq. 1 for every mole of nickel removed by the reaction of Eq. 2. This hydride probably condenses and then dissociates according to the reaction

$$2NaH \longrightarrow 2Na + H_2 \ . \quad (4)$$

It is proposed that this reaction occurs upon condensation of the hydride rather than in the vapor

phase, as the work of Williams[6] indicates. However, the cycle of reactions presented would go just as well if the decomposition occurred in the gas phase, and it depends, rather, on the stable character of sodium hydride in sodium hydroxide solutions, as reported by Banus,[7] to account for the decrease in stability of sodium hydride in going from a hot zone to a cooler zone. Each step of the cyclic corrosion process shown in Fig. 26 occurs in the same regular way. Each reaction is driven by the volatilization of one of the products, which should occur with ease in the thin meniscus phase, and the nonvolatile product drains down the tube wall to become a reactant in the next reaction. The order proposed for the occurrence of the reactions is in accord with the increasing temperature from top to bottom of the meniscus phase and the increasing availability of diffusing hydrogen with increasing temperature.

The sodium needed to initiate the cycle may have come from the thermal dissociation of sodium hydroxide:

$$2NaOH \longrightarrow Na_2O + H_2O \ .$$

This reaction is followed by the reduction of sodium monoxide by nickel in a region of low water fugacity or by the reactions reported by Williams for equilibrium conditions, as mentioned above.

In addition to these processes, additional mass transfer of nickel within the bulk liquid phase probably occurred in the presence of inward diffusing hydrogen, according to the mechanism of Williams.[8] This would account for the polished zone below the nickel plug.

### Sodium Combustion

M. E. Steidlitz

The apparatus for examining the combustion of sodium and some of its alloys in various atmospheres has been completed. The equipment consists of a steel box connected to a vacuum pump, a filter system, and a source of dry air. The sodium capsule is heated to a temperature of 700 to 800°C in a furnace located on top the box. The tip of the capsule is then broken off to allow a jet of molten metal to spray into the atmosphere in the box. Observations of the flammability are visual only.

A total of six runs has been made with pure sodium at 800°C in the new apparatus. Of these, two were in dry air, dew point of –43°C, and four were in room air, all at 1 atm pressure. The only observable difference in these tests was the formation of a heavier scum on the surface of the molten sodium on the floor of the box after burning in room air. This scum was effective in confining the combustion on the floor to a section at the edge of the puddle. The dry-air samples burned vigorously all over the puddle.

A series of tests on sodium-mercury mixtures has been run at 700°C. Capsules containing 50, 60, 62, 64, 66, 68, 70, 72, and 90 mole % mercury were burned in room air with the following results. With 50 mole % mercury, the combustion of the jet is essentially as vigorous as with pure sodium. With 60 mole % mercury, the combustion is just noticeably less vigorous. With 60 to 72 mole % mercury, the rate of combustion decreases rapidly until with 72 and greater mole %, no fire is observed in the jet, although a small amount of white smoke is formed.

It is possible that the compound $NaHg_2$, which occurs at 66.7 mole % mercury, is important in this rather sudden change in combustibility with composition. $NaHg_2$ is the most stable of the sodium-mercury compounds; it has a melting point of 360°C and a heat of formation at 375°C of about 3.2 kcal/gram-atom.

## BRAZING

P. Patriarca G. M. Slaughter

### High-Conductivity-Fin Heat Exchanger

One of the metallurgical problems associated with the use of high-conductivity fin materials for heat exchangers has been the selection of suitable brazing alloys. For a limited preliminary study the following variables were arbitrarily fixed:

1. The fin material would be 10-mil-thick copper clad on both sides with 2 mils of Inconel. (The fabrication of this material by roll-cladding techniques is described in the following section on "Fabrication.")
2. The Inconel tubing would be 0.188 in. in outside diameter with 0.020-in. wall thickness.

[6] D. D. Williams, *A Study of the Sodium-Hydrogen-Oxygen System*, NRL Memorandum Report No. 33 (June 1952).

[7] M. D. Banus, report at the Hydroxide Committee Meeting held at Beverly, Mass. in August 1953.

[8] D. D. Williams (as reported by R. R. Miller), *Fourth Progress Report*, NRL Problem No. 32C-11-061 (1952).

3. The configurations to be studied would be a longitudinal fin, referred to here as a Delta design, and a radial fin consisting of the popular punched-fin and a multitude of tube-to-fin joints.

4. The service environment would consist of (*a*) sodium at 816°C within the tubes and (*b*) air at 816°C on the exterior of the tubes and on the fin surfaces.

In order to satisfy the corrosion requirements of resistance to both sodium and air at 816°C, the search for a suitable brazing alloy was confined to alloys with a nickel-chromium base. Since the melting point of the copper core would be about 1080°C, the maximum suitable brazing alloy flow temperature was chosen as 1050°C. A nickel-chromium-iron-silicon-boron brazing alloy manufactured by the Wall Colmonoy Corporation and known as "Low-Melting Nicrobraz" (LMNB) was found to have suitable flowability on Inconel when brazed in −57°C dew-point hydrogen at 1050°C. A nominal composition of this alloy is given in Table 22, along with that of standard Nicrobraz (NB). As may be seen, the basic difference involved a change in the nickel and chromium contents of the two alloys.

**TABLE 22. COMPOSITION OF NICROBRAZ AND "LOW-MELTING NICROBRAZ"**

| CONSTITUENT | COMPOSITION (nominal wt %) | |
|---|---|---|
| | LMNB (flow point, 1050°C) | NB (flow point, 1150°C) |
| Nickel | 80 | 70 |
| Chromium | 5 | 15 |
| Iron | 5 | 5 |
| Silicon | 5 | 5 |
| Boron | 5 | 5 |

A major problem in the fabrication of the tube-to-fin joints was the protection of the exposed copper to prevent selective oxidation of the core. Figure 27 shows a series of Inconel clad copper fins as brazed to an Inconel tube. As can be seen, the copper core is adequately protected from attack by an oxidation-resistant brazing alloy fillet. The fin material was prepared by punching holes, nominally 0.190 in. ID, and leaving a lip to provide

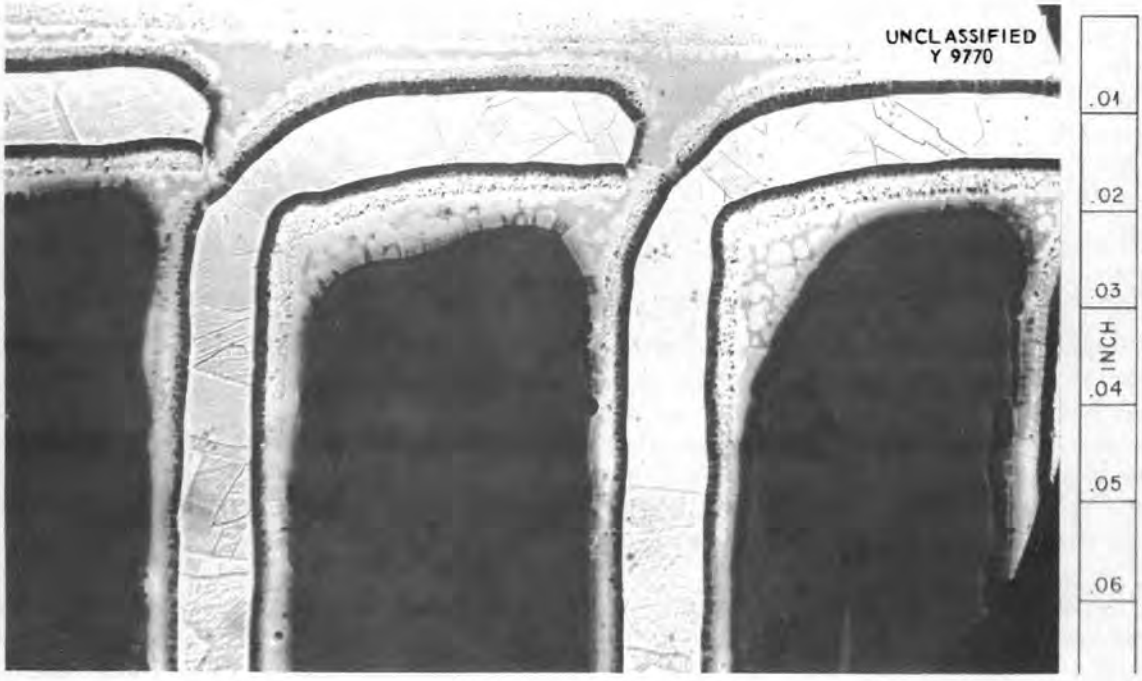


**Fig. 27. Section of Tube-to-Fin Joint Brazed with Low-Melting-Point Nicrobraz.** Tube material, Inconel; fin material, copper (10 mils thick) clad on both sides with 2 mils of Inconel. 50X

a 15-fin-per-inch spacing. The brazing alloy was preplaced as wire around the outer diameter of the fin lip and cemented with commercial Nicrobraz.

The techniques used for fabrication of the LMNB wire are presented here, since they are applicable to a large group of brazing alloys which must be initially prepared as a powder. The procedure used is, briefly, the following: (1) 50 g of alloy powder, preferably −100 to −200 mesh, is mixed with approximately 25 $cm^3$ of Rohm and Haas Acryloid B-7 to provide a thick homogeneous slurry; (2) excess binder is driven off by baking for 10 min at 200°C to a hard cake; (3) this composite is softened with a small quantity of acetone and kneaded to the consistency of putty; (4) the billet thus formed is extruded on a hydraulic press through a 0.060-in.-ID Lavite die and wound on a $^3/_{16}$-in.-dia mandrel rotated at approximately 60 rpm by a variable-speed motor; (5) the mandrel is set aside for curing at room temperature for a minimum of 1 hr; (6) the brazing-alloy helix is removed from the mandrel and stored in 1-in. over-all lengths until cut with a knife to supply individual rings.

Examination of the joints shown in Fig. 27 at higher magnification revealed that no significant diffusion had occurred to affect the properties of the core material. The dark lines delineating the copper core were attributed partially to the presence of a heavy precipitate in the clad material and partially to relief polishing. The precipitate is characteristic of dilution and diffusion effects observed in nickel-base alloys and stainless steels brazed with the high-boron, high-silicon Nicrobraz alloys.

A quantity of LMNB wire, as extruded, was permitted to cure in straight lengths for use in experiments for determining the feasibility of the Delta fin design. Inconel-clad copper sheet was preformed into 6 in. lengths of the Delta configuration and brazed into the basic unit, a section of which is shown in Fig. 28, by preplacing LMNB wire along the full length of one side of each tube with Nicrobraz cement. The success of the brazing operations confirmed the ability of this cement to hold brazing alloy wire in place until a temperature of 800 to 900°C is reached, at which time sintering of the wire to the base material becomes pronounced. The most critical joint of the basic Delta fin was considered to be the one shown in the lower right corner of Fig. 28, where the sheared and therefore exposed edges of the fin mated with each other and with the Inconel tube. Previous experiments had verified that LMNB did not flow on copper. Fortunately, preplacing a LMNB wire on the inside and another on the outside of the Delta fin effectively reduced the joint design to two T joints. One joint consisted of Inconel cladding against Inconel cladding and the other of Inconel cladding against Inconel tubing.

Figure 29, an enlargement of the critical joint, illustrates the wetting of the joint walls and the tube walls and reveals the complete protection of the exposed copper. The basic Delta fin shown was oxidized for 500 hr at 800°C in static air. Examination of the joint and the clad core indicates that adequate protection was achieved. However, the effects of the 500-hr oxidation treatment on the copper core are evident. These effects are similar to those reported in detail in the following section on "Fabrication." Briefly, the effects were the formation of voids in the copper core, diffusion of nickel into the core, and diffusion of copper into the cladding. Thus it appears that Inconel clad

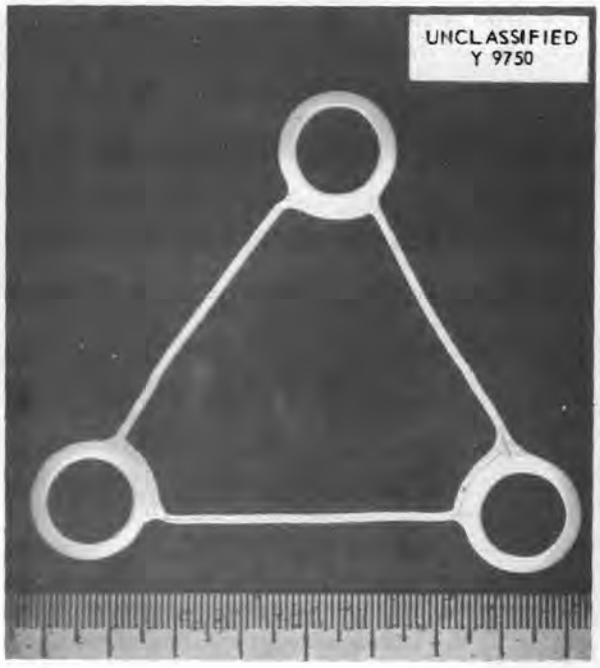


**Fig. 28. Section of Delta Fin Brazed to Inconel Tubes with Low-Melting-Point Nicrobraz and Oxidized for 500 hr at 800°C in Static Air.** Tube material, Inconel; fin material, copper (10 mils thick) clad on both sides with 2 mils of Inconel. 10X

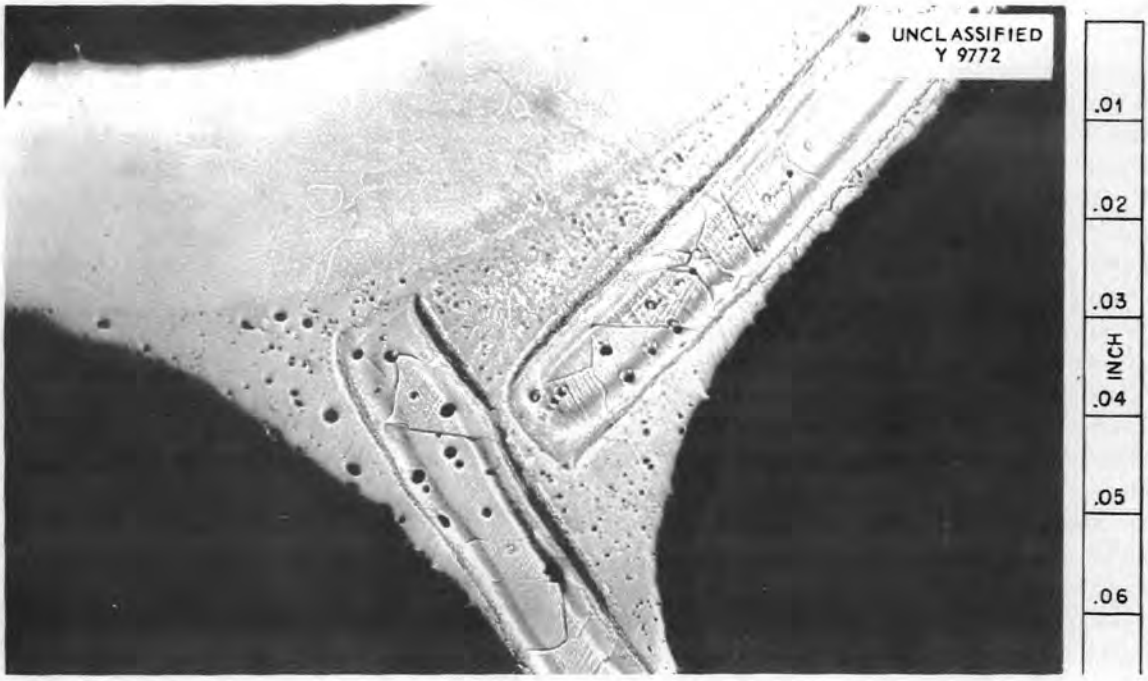


**Fig. 29. Section of Joint Shown in Lower Right Corner of Delta Fin of Fig. 28. 50X**

on copper will not be entirely suitable for high conductivity fins, at least not without diffusion barriers. However, the results of this brazing study are believed to be applicable to other cladding materials.

### Nickel-Phosphorus and Nickel-Chromium-Phosphorus Brazing Alloys

The nickel-phosphorus and nickel-chromium-phosphorus systems are being studied, at the suggestion of other investigators, to determine their suitability as elevated-temperature brazing alloys. The evaluation of these systems is in preliminary stages, but the results indicate that phosphorus additions are extremely effective in lowering the melting point of nickel and nickel-chromium alloys. Phosphorus is especially suitable for reactor applications because of its low cross section for absorption of thermal neutrons. Alloys of the approximate compositions given in Table 23 have been prepared from a master nickel-phosphorus alloy (87% Ni–13% P).

Stainless steel T joints brazed with these alloys exhibited excellent flow and wetting properties. As was anticipated, however, the joints were quite brittle. It is expected that diffusion treatments may improve the ductility of these alloys so that they will be comparable to the Nicrobraz and G-E No. 62 alloys and will therefore retain the obvious advantages of low melting point and low cross section.

**TABLE 23. COMPOSITIONS AND MELTING POINTS OF SEVERAL BRAZING ALLOYS**

| ALLOY COMPOSITION | APPROXIMATE MELTING POINT (°C) |
|---|---|
| 87% Ni–13% P | 900 |
| 79% Ni–12% P–9% Cr | 1000 |
| 72% Ni–11% P–17% Cr | 1050 |
| 67% Ni–10% P–23% Cr | 1100 |

A survey of the recent literature revealed the current interest in the use of an "electroless" method of nickel plating that was developed several years ago at the Bureau of Standards. It was noted that by this method a high-phosphorus-content nickel plate is deposited. Briefly, the method involves reduction of a nickel salt to metallic nickel. A hypophosphite is converted to the phosphite with subsequent deposition of phosphorus-containing nickel. An obvious advantage

of this method is the possibility of depositing a uniform plate on a complex surface without experiencing the difficulties introduced by variations in the "throwing power" of the electrolytic methods.

Since the phosphorus content of the "electroless" plate was reported to be about 10%, it became apparent that the plate might serve as a brazing alloy, as plated. The possibility of preplacing this brazing alloy for fabrication of complex ANP heat exchangers appeared to justify an investigation. Accordingly, a series of type 316 stainless steel strips $\frac{1}{2} \times 3 \times \frac{1}{16}$ in. were submitted to the ORNL Research Shops for "electroless" plating with a nominal thickness of 1 mil of nickel-phosphorus in a 7-hr period by using procedures based on the method developed by the Bureau of Standards.

Standard T joints were made for flowability tests by using a plated stainless steel strip against an unplated stainless steel strip. Excellent wetting was observed when the specimens were brazed in dry hydrogen at 900°C; this indicated that the approximate composition of 90% Ni–10% P, as reported, was correct.

Since it was anticipated that the oxidation resistance of the "electroless" nickel-phosphorus brazing alloy could be improved by alloy addition of chromium, a series of stainless steel test strips was prepared with approximately 0.2 mil of chromium (deposited by conventional electrolytic plating methods) on 1 mil of "electroless" nickel-phosphorus alloy. These test strips were brazed at 1000°C, and they exhibited the same excellent flow as observed with the "electroless" nickel-phosphorus alloy.

The nickel-chromium-phosphorus specimen is shown in Fig. 30. The dark line between the chromium and the nickel-phosphorus layers is believed to be due to relief polishing as a result of the differences in the hardnesses of the materials. Figure 31 shows a section of an as-brazed T joint made by using the nickel-chromium-phosphorus plated specimen shown in Fig. 30.

Figure 32 shows a section of the T joint shown in Fig. 31 after having been subjected to static air for 500 hr at 800°C. As may be seen, the oxidation resistance of this alloy is favorable. What appear to be voids in the brazing alloy matrix

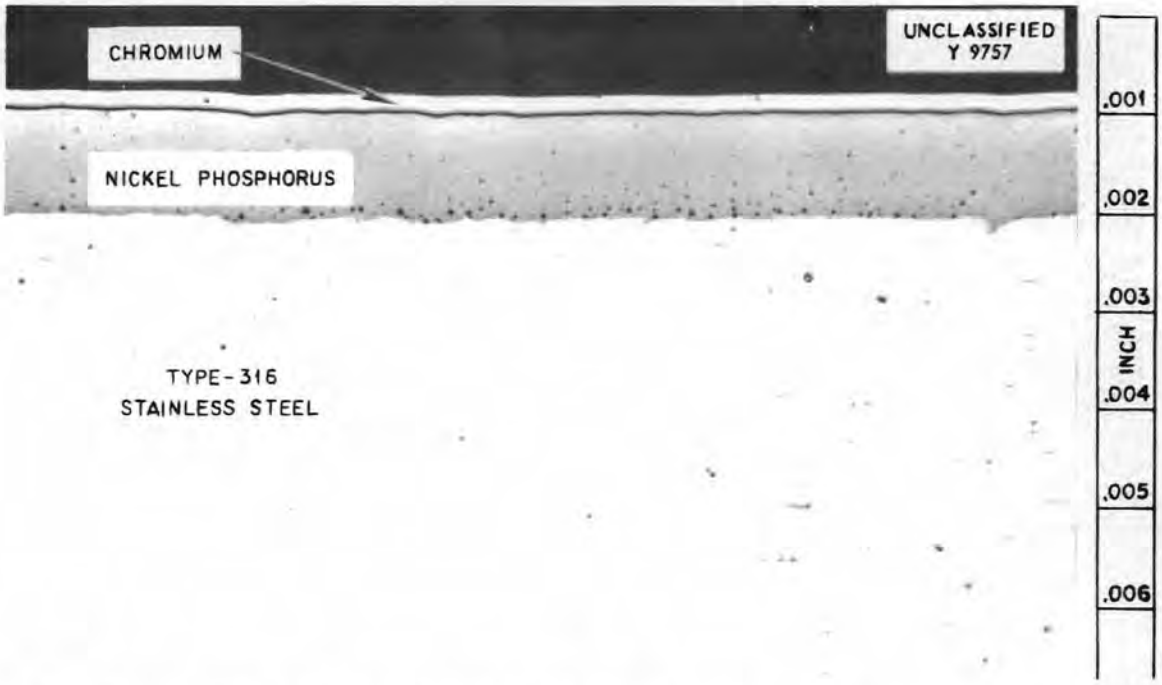


**Fig. 30. Section of Type 316 Stainless Steel As Plated with Approximately 1 mil of "Electroless" Nickel-Phosphorus and Approximately 0.2 mil of Chromium for Fabrication of a Nickel-Phosphorus-Chromium Brazed T Joint. 500X**

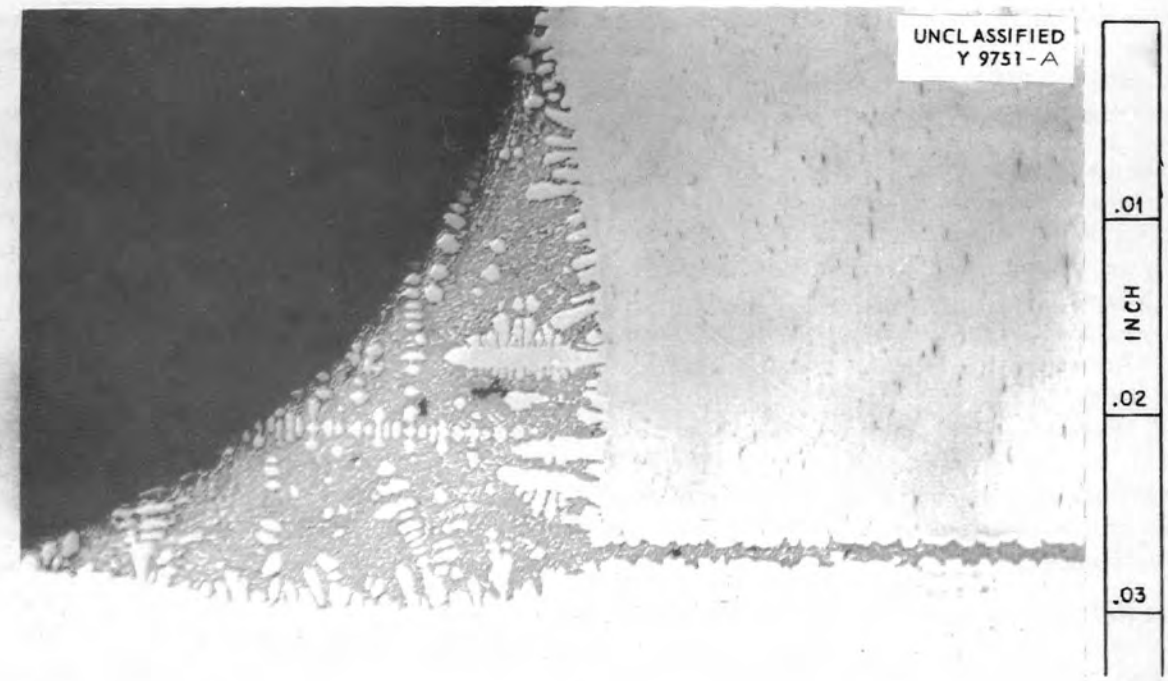


Fig. 31. Section of a T Joint Made by Brazing at 1000°C the Specimen Shown in Fig. 30. 100X

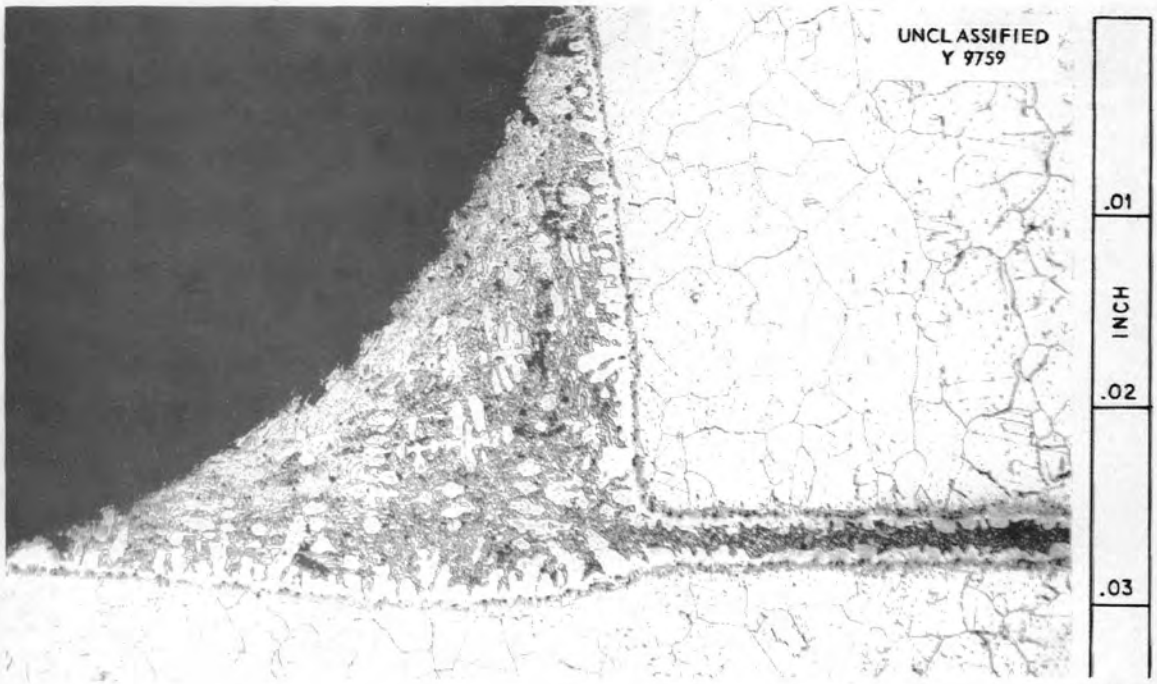


Fig. 32. Section of T Joint Shown in Fig. 31 After Having Been Subjected to Static Air for 500 hr at 800°C. 100X

were found to be polishing pits, and the irregularities at the brazing alloy fillet surface can be attributed to oxidation.

Figure 33 shows a section of a T joint made by using "electroless" nickel-phosphorus plated type 316 stainless steel without a chromium plate after having been subjected to static air for 500 hr at 800°C. Although the oxidation resistance of the "electroless" nickel-phosphorus brazing alloy appears to be inferior to that of the nickel-chromium-phosphorus alloy, the results are considered encouraging. The voids at the interface in the T are believed to be due to removal of constituents during polishing, and the undercut and the irregularities of the fillet surface are believed to be due to oxidation.

A series of "electroless" nickel-phosphorus and nickel-chromium-phosphorus T-joint specimens were subjected to corrosion tests in sodium for a 100-hr period. The results of these tests are presented above in the section on "Static Corrosion."

The results of the investigations made to date indicate that the nickel-chromium-phosphorus system shows promise both as applied conventionally and as applied by "electroless" plate methods. Preliminary remelt tests indicate that remelt temperatures of 1250°C can be achieved by treatment at 1000°C for times as short as 10 min because of the relatively high diffusivity of phosphorus. The physical tests conducted to date are inconclusive, but there is evidence that ductility can be improved by control of brazing temperature and time.

### Heat Exchanger Fabrication

As has been indicated in previous reports, efforts to apply Nicrobraz as an elevated-temperature brazing alloy for fabrication of ANP sodium-to-air heat exchangers have been complicated by a number of factors. The results of numerous experiments conducted on laboratory-scale test specimens and on full-size heat exchanger assemblies have shown that the rate of heating to the brazing temperature is of great importance.

**Slow Heating.** Although early experiments indicated that difficulties in brazing did not arise from diffusion of constituents from the brazing alloy during heating with a consequent loss in flowability at the brazing temperature, later tests gave contrary indications. With tests using Nicrobraz in the form of flat washers prepared by stamping from sheet rolled or extruded from powder mixtures, it was found that during slow heating

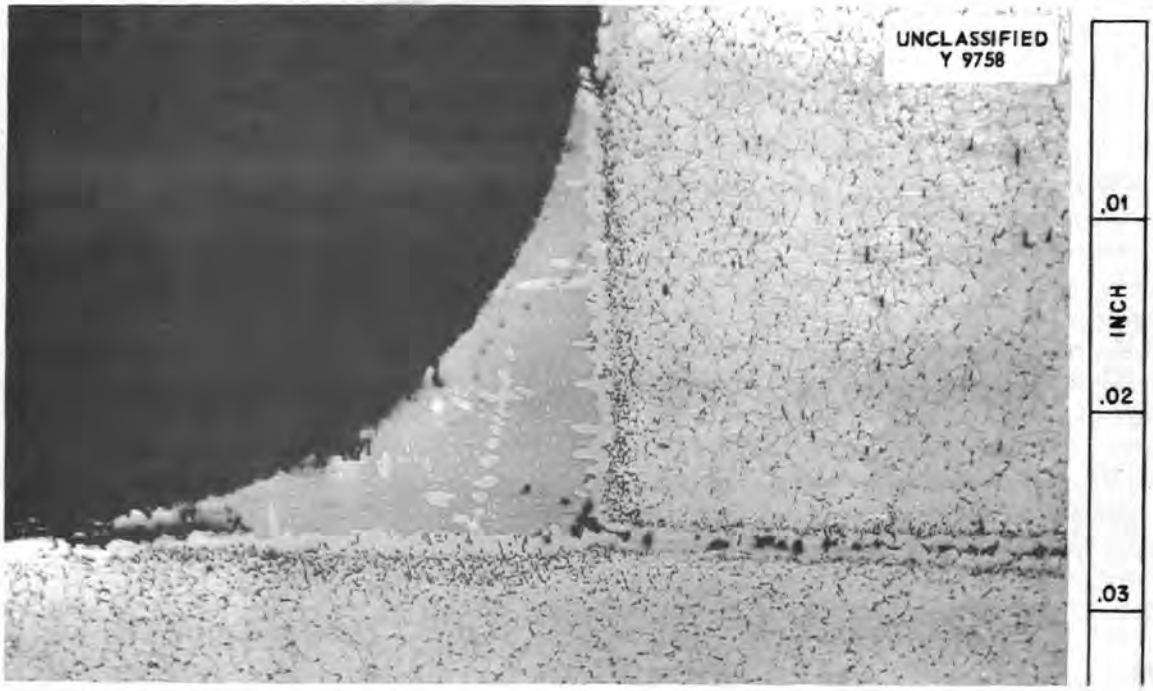


**Fig. 33. Section of "Electroless" Nickel-Phosphorus Brazed Type 316 Stainless Steel T Joint After Having Been Subjected to Static Air for 500 hr at 800°C.** 100X

sufficient boron diffused from the brazing material to appreciably increase the melting point of the brazing alloy and thereby prevent the flow needed to produce a satisfactory joint.

**Fast Heating.** A remedy to brazing difficulties seemed to be fast heating to the brazing temperature to minimize diffusion and subsequent lack of flow. The other possible alternative, that of increasing the brazing temperature, was found to be ineffective because dilution and undercutting also increased materially with temperature.

Rapid heating to the brazing temperature was found to introduce associated problems. As would be expected, unequal heating occurred, with the thin fin material reaching the furnace temperature before the tubes did. In addition to increasing distortion, this condition resulted in "stealing" of preplaced brazing alloy; that is, the alloy would flow on the fin surface and would consequently be unavailable for adequate wetting of the tube wall when the temperature equalized. Since the remedy for this effect would be a preheat and since preheating would permit diffusion, there appeared to be no remedy for the situation unless diffusion could be decreased. This was accomplished by using extruded Nicrobraz rings, as described in the preceding section on "High-Conductivity-Fin Heat Exchangers." Experiments revealed that 60-mil wire formed into rings for preplacement was relatively unaffected by rate of rise to temperature because of the relatively small contact area afforded for diffusion. The production of a large quantity of these rings was initiated on a laboratory scale for future experiments and for possible use in a test heat exchanger.

Along with the study of Nicrobraz as a brazing alloy, simultaneous tests were conducted with the G-E No. 62 alloy (69% Ni–20% Cr–11% Si). Each experiment revealed that this alloy was relatively independent of the complicating factors that influence the behavior of Nicrobraz. The dilution, diffusion, and heating-rate studies indicated that the boron-free G-E alloy could be preplaced in any convenient form and that preheat could be applied without impeding subsequent flow. Seven pounds of this alloy as –200 mesh powder was obtained and is being used for a study of suitability for brazing heat exchangers. A heat exchanger with 1000 tube-to-fin joints was fabricated by using this alloy preplaced as a slurry and subjected to the following brazing cycle: (1) heat to 900°C at an average rate of 50°C per minute; (2) hold at 900°C for 30 min to equalize fin and tube temperatures; (3) heat to 1150°C at an average rate of 30°C per minute; (4) hold at 1150°C for 60 min, furnace cool to black, and air cool to room temperature. Examinations of this test radiator indicated that adequate flow and wetting had occurred, and it was found to be leak free, as determined by a helium leak detector.

In order to evaluate the cracking tendencies of this alloy, the test radiator was subjected to 10 thermal cycles from 1000°C to room temperature with average cooling rates as high as 300°C per minute. Since no leaks developed in the 36 tube-to-header joints, the radiator was water quenched from 1000°C and examined. One small leak was detected and subsequently repaired by rebrazing.

To further evaluate the effect of thermal cycling, a 180 tube-to-fin joint section will be examined metallographically and the number of cracks recorded. This number will be compared with the number of cracks present after treatment of similar 180-joint sections at 1500°F in static air for 100-, 200-, 300-, and 500-hr periods followed by a water quench.

In anticipation of adequate resistance to cracking, a heat exchanger with 6000 tube-to-fin joints has been assembled and will be brazed following manual inert arc welding of the 180 tube-to-header joints. The joints were made accessible by splitting the headers. Each weld will be backed up with brazing alloy as a precaution against possible leaks in the welded joints as a result of stresses set up during the brazing cycle. It is believed that the brazing of tube-to-header joints may be accomplished with consistency by using the G-E alloy; however, the added strength of a welded joint and the additional insurance against the necessity for rebrazing justify serious consideration of the use of welded joints in heat exchanger fabrication.

## FABRICATION

E. S. Bomar J. H. Coobs
H. Inouye

### ANP Radiator

The investigation of high-thermal-conductivity fins is continuing. During this period, the fin thicknesses were reduced to a maximum of 2 mils of cladding or plate on each side of 4 mils of

copper. The feasibility of fabricating such thin composites is encouraging in view of the results reported below.

**Roll Cladding of Copper.** The problems associated with the roll cladding of copper with 2 mils of oxidation-resistant alloy are mainly those of maintaining uniform core and cladding thicknesses and of producing a cladding that is free of pinholes or breaks.

High reduction per pass and cold rolling in excess of about 40% between anneals result in variations of between 1 and 3 mils when a thickness of 2 mils is desired. The pinholes are usually caused by hard particles on the rolls and working or cold rolling too severely between anneals.

The claddings tested to date were made by hot rolling an evacuated capsule at 1000°C in several passes. These capsules were heated in an atmosphere of hydrogen to reduce scaling. The percentages of hot reduction necessary to obtain a bond were approximately 35% for Inconel cladding, 50% for type 310 stainless steel, and greater than 50% for type 446 stainless steel. The thicknesses of clad copper fabricated and tested were 2 mils of cladding on each side of 4 mils of copper and 2 mils of cladding on each side of 10 mils of copper.

**Oxidation and Evaluation of Clad Copper.** Cladding thicknesses were obtained by metallographic measurements of the composite or by measuring the copper core after it was stripped with nitric acid. Pinholes and cladding-thickness variations were found. By suitable fabrication techniques, clad variations were held to within +0.5 mil, and the pinholes were reduced to a few in several square inches of the composite.

Oxidation tests were made in slowly flowing air without edge protection of the test pieces. The oxidation of the exposed copper in 500 hr at 1500°F was to a depth of approximately 10 mils. Pinholes, when they occurred, resulted in the formation of copper oxide nodules. The affected area under the pinhole seemed to be restricted to the size of the nodule.

**Inconel Cladding on Copper.** Tests made for a period of 100 hr at 1500°F on Inconel-clad copper showed that defects, when they occurred, were restricted to the formation of copper oxide nodules about $\frac{1}{32}$ in. in diameter at the site of existing pinholes or near failures in the cladding. Slight warpage of the test pieces occurred. Metallographic examination of the cross section of a test piece showed a diffusion zone of about 3 mils and the formation of numerous voids in the core near the original copper-Inconel interface.

Specimens tested for 500 hr at 1500°F showed surface defects similar to those found after the 100-hr tests, except that there was noticeable roughness. Metallographic examination of the cross section of a specimen showed that a copper-rich phase penetrated to the surface of the cladding. The roughness was probably due to the oxidation of the resultant alloy. The voids found after the 100-hr tests became larger and were randomly distributed throughout the specimen. In these tests, the 10-mil copper core is altered by diffusion products from the cladding, and there is an expansion of 1 to 2 mils in the composite thickness.

Clad material made by the General Plate Division, Metals and Controls Corporation, showed the same results, except that pinhole oxidation was more severe.

**Type 310 Stainless Steel Cladding on Copper.** Several tests for 100 and 500 hr at 1500°F showed that surface failures of type 310 stainless steel-clad copper were limited to the formation of copper oxide nodules, as described previously; warpage was slight. Examination of the copper-stainless interface showed the appearance of islands of a dark phase in the cladding up to 0.5 mil. The effect of increasing the time of exposure from 100 to 500 hr was an increase in the number of these islands in the cladding but not in their depth of penetration. The copper core did not appear to be affected.

**Type 446 Stainless Steel Cladding on Copper.** Surface failures of type 446 stainless steel-clad copper were similar to the failures in other claddings, except that severe warping of the composite occurred. No noticeable change was noted upon examination of the interface after 100 hr at 1500°F. In 500 hr, a dark discontinuous phase precipitates at the interface that is about 0.2 mil thick.

**Aluminum-Bronze Cladding on Copper.** It was indicated previously that the aluminum-copper alloy (5% Al–95% Cu) oxidized locally. Oxidation tests of aluminum-copper alloys with 6 and 8% aluminum at 1500°F resulted only in a slight discoloration of a polished surface. An aluminum-copper alloy with 10% aluminum increased in weight and dimensions because of the formation of a rather thick film of $Al_2O_3$.

These alloys are being investigated primarily because of their expected high thermal conductivity (estimated to about six times that of Inconel and types 310 and 446 stainless steel at 1500°F), ease of fabrication, and resistance to oxidation.

Ingots of aluminum-copper alloys with 6 and 8% aluminum were made and rolled into sheet. Attempts to roll clad the alloys onto copper at 900°C resulted in bonding on one side only. The incompleteness of the bond was probably due to the formation of $Al_2O_3$ during the welding of the capsule.

**Evaluation of Copper Core.** The results of numerous tests on the claddings of Inconel and of stainless steels show that OFHC copper is better for the core material than are the commercial grades of copper. This conclusion is based on the following factors. (1) The number of voids appearing at the copper-Inconel interface was greater when the cores were of commercial copper than when they were of OFHC copper. (2) Metallurgical bonds were consistently obtained during the roll-cladding operation when the core was OFHC copper. (3) The brazes successfully used to make tube-to-fin joints necessitated the use of hydrogen. Copper that contained residual copper oxide caused the formation of blisters within the composite.

**Study of Diffusion Barriers Between Inconel and Copper.** Although types 446 and 310 stainless steel seem to be satisfactory as clad materials for copper at 1500°F, diffusion barriers for use between Inconel and copper will be investigated so that Inconel can be used for the cladding if ultimately required. For this study, refractory metals and those elements and/or alloys which are known to have low solubility in copper will be used. Final composite thicknesses of 8 mils will be made to determine the rolling characteristics and the warpage which may occur under a thermal test.

**Vapor Plated Chromium and Nickel on Copper.** Several samples of copper plated by the thermal decomposition of the carbonyls of chromium and nickel were supplied by the Commonwealth Engineering Corporation. The coatings were applied both as codeposits and as separate layers of chromium on nickel on copper. Bright smooth deposits were limited to small areas, which were brittle and failed to protect copper from oxidizing at 1500°F. The plate thicknesses tested were between 0.2 and 1.6 mils. No further work on these materials is contemplated.

**Chromium Plate on Copper.** Samples of "ductile" chromium plate 1 mil thick have been received from the Ductile Chrome Process Company. Cracking of the plate is not evident except by metallographic examination and oxidation tests. Alteration of the copper core does not occur as a result of diffusion.

### Special Alloys

**Inconel-Type Alloys.** Seven vacuum melts of approximately 30 lb each have been made; the nominal compositions are given in Table 24. Two extrusion billets 3 in. OD and 4 in. long were machined from each ingot. Ingots 14 through 18 are to be made into tubing for corrosion studies, and ingots 19 and 20 are to be extruded as rod for physical testing. Thus far, the bottom halves of all the melts have been extruded, except ingot 18, which failed to extrude at 2200°F. Higher temperatures and lower extrusion rates will be used to fabricate the top halves of the ingots.

TABLE 24. COMPOSITIONS OF SEVERAL INCONEL-TYPE ALLOYS

| INGOT NO. | NOMINAL COMPOSITION (wt %) | | | |
|---|---|---|---|---|
| | Ni | Cr | Fe | Mo |
| 14 | 75 | 18 | 7 | |
| 15 | 75 | 10 | 15 | |
| 16 | 75 | 5 | 20 | |
| 17 | 83 | 10 | 7 | |
| 18 | 75 | 5 | 10 | 10 |
| 19 and 20 | 78 | 15 | 7 | |

**Nickel-Beryllium Alloy.** Nickel-beryllium alloy (97.5% Ni–2.5% Be), which is age-hardenable, was cast into a 1-in. rod and swaged at room temperature to $\frac{1}{8}$-in. rod. Since difficulties had been experienced previously with this alloy because of cracking, attempts were made to determine the cause of this brittleness. Several sections of an ingot were annealed in hydrogen and in air and either water quenched or air cooled. It was found that water quenching produced no cracks, as was previously reported.[9] The samples annealed in

[9] R. Rimbach and A. J. Michel (trans.), *Beryllium, Its Production and Application*, The Chemical Catalog Co., p. 267-279, 1932.

hydrogen at 1100°C cracked when cold rolled 5%, and those annealed at 900°C in hydrogen cracked at about 50% reduction. The samples annealed in air at 900 or 1100°C rolled satisfactorily. Air cooling or water quenching did not affect the fabrication.

**Sigma-Phase Alloys.** Corrosion studies of several alloys in liquid metals indicate that those alloys containing sigma-phase material are superior in reducing the amount of mass transfer. In order to verify this, the following metals and alloys are being made into tubing: (1) cobalt, (2) 55% Co–45% Cr, (3) 45% Fe–40% Cr–15% Ni.

Attempts to hot roll these alloys at 850, 1000, and 1200°C were unsuccessful because these alloys are decidedly "hot short." A second series of these alloys has been made with additions of manganese and aluminum[10] to the cobalt and to the 55% Co–45% Cr alloy. A 1 wt % addition of a master alloy of nickel, titanium, manganese, and aluminum was added to the iron-chromium-nickel ingot. These alloys have not been rolled.

### Columbium Research

Programs have been outlined for investigating recrystallization of columbium and diffusion of columbium into oxidation resistant alloys. Atmosphere purification studies are being made for conducting creep tests. No significant results have been obtained.

### Tubular Fuel Elements

Additional tubular fuel elements are being prepared by drawing. Twelve tubes containing cores of type 302 stainless steel, iron, and nickel with 20 and 30% $UO_2$ are being reduced from 0.750 in. in diameter with a 0.042-in. wall to a final size of 0.250 in. in diameter with a 0.015-in. wall or a total reduction in area of 87%. Plug drawing, as suggested by Mr. Giacobbe of the Superior Tube Company, is being tried in preference to drawing on a mandrel because the latter process applies a shear stress to the core. The shear stress may have contributed to the failure of the core material in many of the tubes drawn at the Superior Tube Company during earlier experiments.[11] The plans call for the reduction of six tubes on each of two schedules in steps of 15 and 20% reduction per pass, respectively.

The results for the first three passes with the 15% schedule were quite encouraging. Six tubes were processed through four steps of the schedule without difficulty. All six tubes have excellent inside and outside finishes, with no evidence of "rippling" or folding in the core region. However, on the fifth step, reduction became very erratic because of difficulty in holding the plug in position in the die. As a result, one tube failed in tension and the remaining four were not reduced sufficiently to conform to the schedule.

A sixth reduction step was tried on the remaining four tubes and the results were disastrous. Three tubes failed in tension, and in processing the fourth tube the plug did not pull into the die and the wall thickness was thus not reduced. In most cases, failure occurred at the trailing end of the core, and therefore this may be the weakest part of the tube. The major cause of failure, however, was inability to keep the plugs positioned in the die properly; as a result, the reductions did not conform to the schedule. Thus the reductions on the sixth pass were much more than 15%. Galling occurred in the dies on the fifth and sixth passes also and may have contributed to the failure. However, the galling may, in turn, have been caused by the increased reduction on these passes.

In addition, three of the six tubes were processed through two steps of the 20% schedule, with discouraging results. All three failed – one on the first pass and two during the second. Also, slight "rippling" was evident at the leading end of the core. Evidently this schedule is quite severe for reduction of laminated tubes by plug drawing. However, it is planned to continue drawing the remaining tubes until the schedule is finished or until they fail completely.

### G-E Control Rod

After conferring with W. Baxter of the General Electric ANP program, a decision was made to abandon attempts to fabricate a control rod by brazing segments of hot-pressed 56% $B_4C$–44% Fe absorber into a stainless steel tube. A rod 30 in. long prepared by this method was quite satisfactory from a reactivity standpoint, but attempts to establish a continuous bond between absorber and tube wall were unsuccessful. Also, it was

[10] F. G. Foote and J. F. Schumar, *Metallurgy Division Quarterly Report April, May, and June 1952*, ANL-4860.

[11] E. S. Bomar and J. H. Coobs, *Met. Quar. Prog. Rep. Jan. 31, 1952*, ORNL-1267, p. 93.

felt that the thermal conductivity of the absorber was much too low for this application.

Several prototype control rods were fabricated by an alternate method which consists of filling a tube with a mixture of Al-$B_4C$ or Cu-$B_4C$ powder and hot swaging to consolidate the mixture and to form a bond between the matrix and tube wall. Mixtures containing 47% Al–53% $B_4C$ and 75% Cu–25% $B_4C$ were prepared by mixing –100 mesh atomized aluminum and grade C electrolytic copper powders with metallurgical grade $B_4C$ for 1 hr in an oblique blender. The $B_4C$ was ground for 16 hr and contained about 60% –325 mesh particles. The tap densities of these mixtures were: $B_4C$-Al mixture, 63%; $B_4C$-Cu mixture, 50%.

It was decided that the $B_4C$-Al mixture could be used with $\frac{5}{8}$-in.-dia tubing with a total reduction of 40%. However, the $B_4C$-Cu mixture would require more reduction for complete consolidation, so it was loaded into a $\frac{3}{4}$-in.-dia tube and reduced a total of 58%. The final size of the finished rods was $\frac{1}{2}$ in. in diameter, as requested.

The tubes used for both mixtures were AISI type 304 stainless steel with an original wall thickness of 0.049 inch. They were bright annealed in dry hydrogen, loaded by tapping for 3 to 5 min, sealed, and evacuated through a porous sintered-metal plug. The $B_4C$-Al rods were reduced at 600°C in two steps, while the $B_4C$-Cu rods were reduced at 1000°C in four steps.

Seven experimental rods were prepared, including one of each material and 20 in. long, for reactivity tests in the LITR. In each rod, the core material was consolidated to 95% or more of theoretical density, and good distribution of the $B_4C$ was obtained. The $B_4C$-Cu core material showed good bonding to the stainless tube wall, as swaged, while the $B_4C$-Al mixture did not. However, after being heated to 700°C for 15 min, the $B_4C$-Al exhibited excellent bonding.

The stainless steel tube wall was increased during swaging to a final thickness that varied from 0.053 to 0.057 in., or somewhat less than the required 0.065-in. wall. However, if the original wall thickness had been 0.058 in., an increase in the same proportion would have given a final thickness very close to that required.

Several short sections, about 6 in. long, of each type of rod were submitted to General Electric for thermal conductivity and strength tests.

### ARE Pump Seals

The small experimental compacts of the compositions used for the face seal rings of the ARE pump were prepared from copper, silver, and 95% Ag–5% Cu with 14 vol % of $MoS_2$. In general, these compacts had excellent microstructures. In the compacts prepared with electrolytic copper or precipitated silver, with or without 5% copper, the flake-like particles of $MoS_2$ were oriented perpendicular to the direction of pressing and were distributed at random in the continuous, homogeneous, and highly dense matrix.

On the other hand, the compacts prepared with coarse, granular silver had rather poor structure in which the $MoS_2$ was distributed exclusively at the particle boundaries. This resulted in poor interparticle bonding and poor physical properties.

An additional order was received from W. C. Tunnell of the Experimental Engineering Group for a number of rings of the copper plus 8% $MoS_2$ composition, which seemed to have the best physical properties of the group. These rings were for a V-ring seal for the shaft of a fluoride pump. Six cylinders $1\frac{3}{4}$ in. OD, $1\frac{1}{8}$ in. ID, and 2 in. long were prepared from which sufficient rings could be machined for two tests on a $1\frac{3}{16}$-in.-dia shaft. In addition, four more cylinders $3\frac{3}{8}$ in. OD, $2\frac{1}{8}$ in. ID, and 2 in. long were prepared for machining rings for a $2\frac{1}{2}$-in.-dia shaft. In fabricating these cylinders, it was found that densities as high as 97.5% of theoretical could be attained by hot pressing at 950 to 960°C and cooling under pressure.

The series of compacts of stainless steel and 9% $MoS_2$ was examined by metallographic and x-ray techniques to determine the extent of reaction between the components. The sulfide phase seemed to be interspersed with a metallic phase which became more prominent as the pressing temperature was increased from 1030 to 1225°C. Examination by a magnetic etching technique revealed that much of the austenite had been converted to ferrite by reaction with the $MoS_2$. In the sample pressed at 1225°C, only isolated grains of stainless steel retained their austenitic structure. This conversion to ferrite was confirmed by x-ray diffraction analysis; however, the sulfide phase could not be identified.

In spite of the unfavorable reaction of the components, it was decided that the stainless steel

and $MoS_2$ composition should be tested, since the copper and $MoS_2$ composition might not be sufficiently resistant to chemical attack for use in the V-ring seals. Two cylinders $1\frac{11}{16}$ in. OD, $1\frac{3}{16}$ in. ID, and 2 in. long were prepared from –325 mesh type 304 stainless steel with 9% $MoS_2$. These were fabricated by hot pressing in an $Al_2O_3$-lined graphite die at 1225°C; they had an average density of 93.5%. It is interesting to note that under identical conditions of temperature and pressure straight stainless steel powder is only consolidated to 87% of theoretical density.

Attempts to form $MoS_2$ on the surface of molybdenum have been continued. The pyrex reaction vessel used initially was replaced with material that permitted the use of a higher temperature. Also, $H_2S$ was used in one experiment in place of sulfur vapor.

For the experiment in which $H_2S$ was used, the molybdenum was introduced in the form of an 18 in. long, 0.057-in.-dia wire. The wire was suspended in a vertical tube furnace with a temperature gradient from room temperature to 1020°C. Hydrogen sulfide was passed through the tube at the rate of 1 liter per minute during an exposure of $1\frac{1}{2}$ hr at temperature. This exposure was terminated because of the escape of $H_2S$ as a result of plugging of the gas outlet with condensed sulfur.

Data[12] on the free energy of formation of $H_2S$ indicate that at 1000°C the equilibrium pressure of $S_2$ gas is about 0.08 atmosphere. An appreciable portion of decomposed $H_2S$ must have been swept out of the reaction chamber before recombination could take place. The molybdenum wire reacted with the gaseous atmosphere at temperatures from 535 to 1020°C. X-ray diffraction patterns identified the reaction layer as $MoS_2$. The difficulty outlined above, plus the psychological and physiological hazards associated with the escape of $H_2S$, makes the use of sulfur vapor more attractive.

Two furnaces were arranged to permit heating of a molybdenum sample contained in a tube to one temperature and a sulfur reservoir at the other end to a lower temperature. Type 446 stainless steel tubing was used for the container. Four runs were made with this arrangement. Table 25 summarizes the information obtained from the four exposures.

These tests indicate that a $MoS_2$ layer can be formed by exposure to sulfur vapor and that a degree of control may be exercised by varying the molybdenum temperature and the sulfur vapor pressure. Further checks will be made to determine whether the temperature at which the $MoS_2$ is formed has an appreciable effect on the nature of the compound formed.

[12] H. J. T. Ellingham, *J. Soc. Chem. Ind. (London)* 63, 125-133 (1944).

**TABLE 25. REACTION OF MOLYBDENUM WITH SULFUR VAPOR**

| SULFUR TEMPERATURE (°C) | SULFUR VAPOR PRESSURE* (mm Hg) | MOLYBDENUM TEMPERATURE (°C) | TIME AT TEMPERATURE (min) | REMARKS |
|---|---|---|---|---|
| 445 | 760 | 800 | 60 | No $MoS_2$ formed |
| 490 | 1441 | 900 | 120 | Complete conversion of a 4-g Mo sample; layer of FeS formed on inner surface of tube |
| 490 | 1441 | 900 | 8 | Powdery $MoS_2$ $\frac{1}{16}$ in. thick on Mo compact |
| 460 | 948 | 900 | 10 | Porous Mo sample had $\frac{1}{16}$-in. layer of $MoS_2$; dense Mo sample showed slight reaction |

*N. A. Lange, *Handbook of Chemistry*, 6th ed., p. 1421, Handbook Publishers, Sandusky, Ohio, 1946.

### Shield Plates

Six shield plates of a 70% Fe–30% $B_4C$ composition were fabricated by hot pressing at 950°C. Fairly coarse $B_4C$, –140 +325 mesh, was used to inhibit solution of the boron so that the plates could be machined before they were used by the Solid State Division.

## MECHANICAL PROPERTIES OF INCONEL

R. B. Oliver J. W. Woods
D. A. Douglas, Jr. K. W. Reber

A compilation of creep and stress-rupture data for both coarse- and fine-grained Inconel tested in fluoride fuel at 815°C has been completed in the range of stresses from 7500 to 2500 psi. Additional specimens, which are being stressed at 1500 and 2000 psi, have been in test for 1500 hours. Data for fine-grained Inconel tested in argon at 815°C are complete for the range of stresses from 7500 to 3500 psi, and specimens have been in test at 1250 psi for about 1500 hours. Figure 34 summarizes the data on heat 8004 of sheet Inconel, which is currently being tested. This new heat of Inconel exhibits roughly twice the rupture life observed for the original heat 4511 tested. The improved properties are thought to result from the larger amounts of the minor alloying elements present in heat 8004 as compared with heat 4511.

Fine-grained Inconel sheet is currently being tested at 704°C and at 899°C. These tests are being made in argon and in fuel to observe the effects of temperature on the properties in these two environments. The results, to date, do not indicate that the attack of the fuel is increased as a function of temperature.

A series of tube-burst tests at 815°C on Inconel tubes loaded with fuel and surrounded with argon

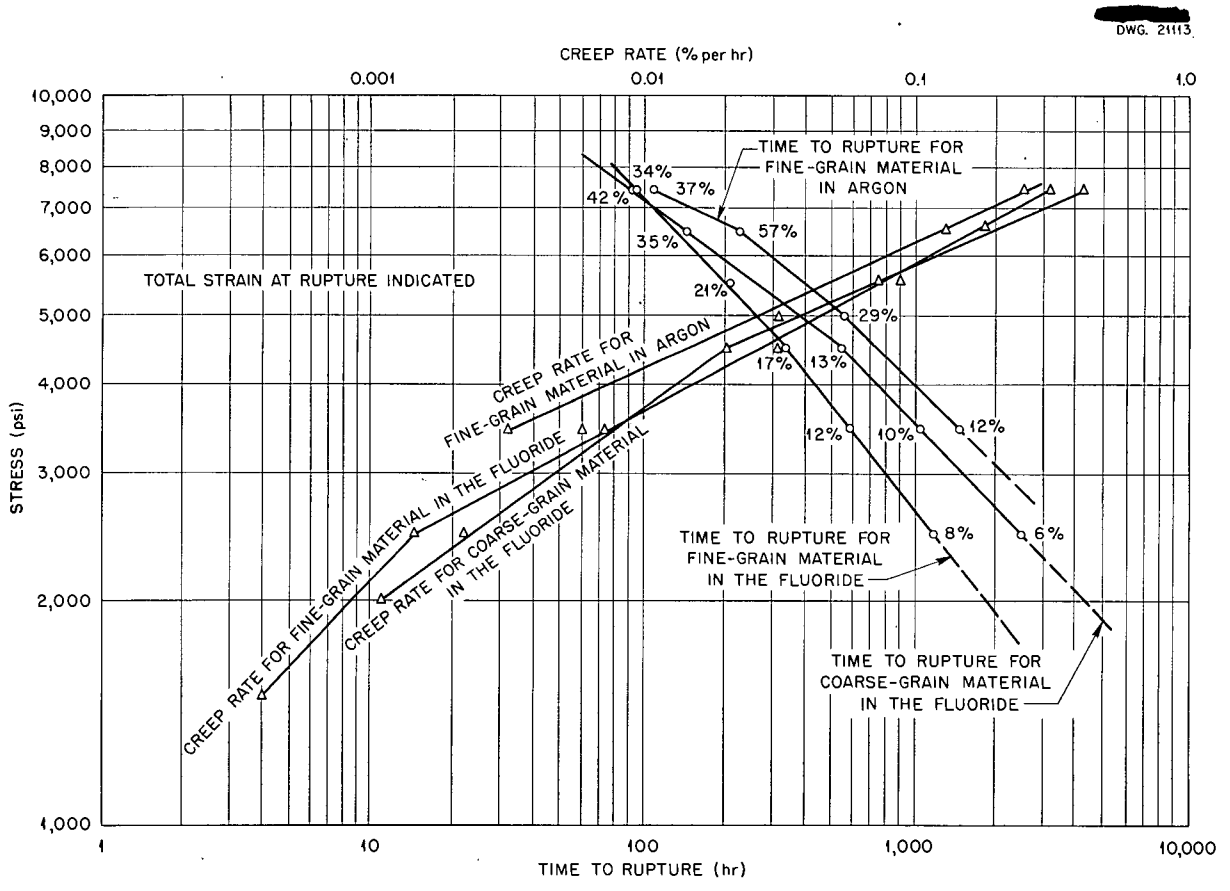


**Fig. 34. Creep and Stress-Rupture Data for 65-mil Inconel Sheet Tested in Argon and Fluoride 27 at 1500°F.**

has been completed in the range of tangential stresses from 2500 to 3500 psi. The times-to-failure for these 10-mil tubular specimens are approximately the same as the time required for the 65-mil sheet specimen to deform 2% when tested in fuels at similar stresses.

It is interesting to note that in these tests not only is the longest rupture life observed in air, but the greatest extensions are found when oxygen is present either in the gaseous atmosphere or as an oxide film. The shortest rupture life and the least ductility is observed in hydrogen, while intermediate values are found in the other environments. Also, the total elongation at rupture is more regular and reproducible for specimens tested in fuel than for those tested in the other environments.

Metallographic examination of specimens after test indicates that, in the absence of corrosive attack, the intergranular cracking which ultimately results in failure is initiated below the surface of the specimen. Specimens tested in fuel at stresses above 3000 psi have cracks that originate at the surface and follow the corrosive attack into the specimen. Specimens tested at stresses below 3000 psi, while showing greater corrosive attack, have internal intergranular cracks of a size and distribution similar to those observed for specimens tested in argon. Specimens tested in air show a very high frequency of tiny intergranular cracks. These cracks appear to originate at the interior of the specimen, and they also appear to be filled with a metal oxide.

---

## UPR METALLURGY

J. E. Cunningham

Activity on the program to assist North American Aviation, Inc. in demonstrating technical feasibility on their proposed thorium-uranium converter reactor (UPR) continued during the period April 1 through July 1, 1953. The scope of the metallurgical effort was limited to the development of reliable techniques for manufacturing the thorium feed loadings needed in operation of the reactor for the production of sizable quantities of $U^{233}$.

Previous development work[1] on the program indicated that (1) thorium can be metallurgically bonded with aluminum by roll cladding in air at a temperature of 450°C with a total reduction in thickness of 8 to 1; (2) the combination of lower rolling temperature (260°C), smaller diameter rolls, and 52S-grade aluminum cladding tends to minimize the thick-core, thin-clad defect at the plate ends. This so-called "end effect" is caused by the difference in plasticity of the two metals. Results of short-time diffusion tests conducted on thorium-aluminum couples under controlled conditions indicate that initial diffusion and subsequent compound formation start at the 300 to 350°C temperature level.

Additional diffusion studies have been performed in an attempt to find a barrier material that can be sandwiched between thorium and aluminum to prevent formation of the brittle compound layer. The thermal stability of the clad-plate product at 150 and 200°C and the methods of assembly necessary to provide the desired component configuration were also investigated.

Work on this program was terminated as of July 1, 1953.

### DIFFUSION STUDIES ON BARRIER MATERIALS

J. A. Milko

The diffusion behavior of several barrier materials in direct contact with aluminum and thorium was investigated at 500 and 600°C temperature levels. The time of test, except where indicated, was 4 hr and the tests were conducted according to the procedure previously described.[1] Results of the tests are discussed briefly in the following paragraphs.

#### Silicon-Aluminum Alloys as Barriers

An alloy of 0.65% silicon with aluminum showed a minor effect in reducing the diffusion layer thickness between thorium and aluminum. To

[1] J. A. Milko, *Met. Semiannual Prog. Rep. Apr. 10, 1953*, ORNL-1551, p. 68-72; R. J. Beaver, *ibid.*, p. 72-75.

determine whether greater amounts of silicon would tend to further minimize the diffusion of aluminum into thorium, experiments were performed with alloys of 1.3 and 4% silicon with aluminum. Unfortunately, the results tend to show an adverse effect. The silicon-aluminum alloy barrier containing 1.3% silicon appears to be responsible for an increase in the diffusion layer thickness of nearly twice that of the straight thorium-aluminum, that is, 0.095 mm compared with 0.051 mm for the thorium-aluminum couple at 500°C. Similar trends were obtained for the silicon-aluminum alloy barrier containing 4% silicon. The Knoop hardness value of the diffusion layer was about 450, or about the same as that for the silicon-aluminum alloy barrier containing 0.065% silicon.

### Barriers Containing Beryllium

It has been reported that in one commercial process for coating low-carbon steel sheet with aluminum the presence of small amounts of beryllium in the bath improves the resultant coating. Hence, the possibility of minimizing the diffusion layer between thorium and aluminum by using beryllium was investigated. Alloys of beryllium and aluminum and beryllium and thorium were prepared and tested.

The presence of about 1.7% beryllium in the thorium had no effect in minimizing the diffusion of aluminum. The diffusion layer thickness was about 0.053 mm as compared with 0.051 mm for the thorium-aluminum diffusion layer. Similarly, the presence of about 1% beryllium in the aluminum had no significant effect in decreasing the diffusion. Knoop hardness values of the diffusion layers of these couples were about the same as those of the straight thorium-aluminum couples.

### 52S Aluminum Alloy as a Barrier

The reported lack of complete bonding in the experimental roll cladding of thorium with 52S aluminum (nominal composition: 2.5% Mg, 0.25% Cr, balance Al) gave an indication of the probable usefulness of 52S aluminum as a barrier material. Thorium–52S aluminum and thorium–52S aluminum–aluminum diffusion couples were prepared and tested at 500 and 600°C for 4 hours. The diffusion layer thickness of such couples was two to three times that of the straight thorium-aluminum couple, depending on temperature.

### SAP Aluminum Alloy as a Barrier

Sintered aluminum powder containing up to 25% aluminum oxide (SAP) in a well-dispersed pattern was considered as a possible barrier material. A test conducted at 500°C for 4 hours indicated that no direct benefit could be derived from using this material to minimize diffusion of aluminum into thorium.

### Magnesium as a Barrier

Although it is well known that magnesium forms compounds with thorium, it was of interest to evaluate the approximate rate of diffusion of magnesium into thorium because it apparently does not tend to diffuse into uranium in the temperature range of 400 to 600°C. Diffusion couples of thorium-magnesium and thorium-magnesium-aluminum tested in the temperature range of interest, 400 to 600°C, developed unusually large thicknesses of a brittle layer that was, in some cases, eight times the thickness of the straight thorium-aluminum diffusion layer.

### Chromium Alloys as Barriers

Chromium additions to both thorium and aluminum provide no beneficial effect in reducing the diffusion layer thickness. In some cases, the thickness of the layer was about four times greater than that of the straight thorium-aluminum diffusion layer.

### Cerium Alloys as Barriers

It has been reported in the classified technical literature[2,3] that cerium is probably the only element which forms an appreciable solid-solution phase with thorium. On this premise, it was of interest to determine whether such a solid solution would be effective in decreasing the amount of aluminum diffusion into thorium. An iodide thorium–cerium alloy containing 5% cerium and an aluminum-cerium alloy containing 11% cerium were made. Cerium in this amount appears to form a eutectic with aluminum. Diffusion couples were prepared from these alloys and heated in direct contact for 4 hr at 500 and 600°C.

---

[2] J. G. Feibig, *Water Corrosion of Alloys of Thorium and of Uranium*, CT-2715 (Apr. 25, 1945).

[3] A. B. Grenginger, *Metallurgy Division Report for April 1945*, CT-2925.

The diffusion layer of the thorium–5% cerium alloy–aluminum couple was 0.076 mm thick after heating at 600°C, whereas the thorium-aluminum diffusion layer thickness was 0.051 mm under similar conditions. The diffusion layer thickness of the thorium–11% cerium–aluminum alloy couple was about the same as that of the straight thorium-aluminum couple.

### Nickel as a Barrier

Sylvania Products, Inc.,[4] reported some success with the use of nickel as a barrier to prevent diffusion between uranium and aluminum. Although it is well known that nickel and thorium form at least three compounds, it was of interest to measure nickel's diffusion tendency. A couple of thorium-nickel-aluminum was heated for 4 hr at 600°C. Examination of the diffusion layer indicated not only severe diffusion into the thorium but also diffusion into the aluminum.

### Alloys of Vanadium, Columbium, and Molybdenum with Thorium as Barriers

Diffusion couples were prepared from aluminum and alloys of thorium with 8 wt % of vanadium, columbium, or molybdenum and tested in intimate contact for 4 hr at 500 and 600°C. Examination of the couples showed the presence of diffusion layer thicknesses equivalent to those of straight thorium-aluminum couples.

### Alloy of Tin with Thorium as a Barrier

Tin was considered as a barrier material because of its reported insolubility with aluminum. Although its addition to the thorium was thought to result in compound formation, it was considered possible that the transport of aluminum atoms into the thorium would be impeded. Couples treated at 500 and 600°C for 4 hr showed diffusion layer thicknesses equivalent to those of straight thorium-aluminum couples.

### Titanium as a Barrier

Titanium was considered as a possible barrier material mainly because certain alloys of titanium with aluminum were reported to not possess an unusually high hardness. Arc-melted iodide titanium was prepared into sheet and annealed, and diffusion couples of titanium with thorium and with aluminum were studied.

In the thorium-titanium couple no definite diffusion occurred until a temperature of 650°C was reached. Small diffusion layer thicknesses, 0.002 to 0.003 mm, were found after heating for 4 hr at 850°C. The diffusion layer was indeed small.

On the other hand, diffusion couples of titanium with aluminum showed thicknesses of 0.028 to 0.043 mm after heating for 4 hr at 600°C. At 500°C, no measurable diffusion layer thickness was observed. These observations merit further study and evaluation.

## ROLL CLADDING STUDIES

R. J. Beaver

Qualitative mechanical tests, such as repeated bending and twisting, and metallographic examination of alclad thorium plates have indicated that metallurgical bonding, without formation of intermetallic compounds, is obtained in the temperature range of 260 to 400°C. Photomicrographs of the 2S aluminum-thorium interface of plates rolled at 260, 400, and 450°C are shown in Fig. 35. No intermetallic compound formed in the plate rolled at 260°C, and only isolated clumps of intermetallic compound are present in the plate rolled at 400°C. However, in the plate rolled at 450°C, a thin discontinuous layer of intermetallic compound appears. It is apparent that if compound formation at the bond interface is to be eliminated, fabrication of alclad thorium plates must be confined to a temperature range of 260 to 400°C.

The results obtained from rolling a series of 20 plates at 260°C with cladding thicknesses ranging from 10 to 35 mils have revealed that the differential thickening of the thorium and thinning of the aluminum can be drastically reduced. The rolling practice is to apply a 40% "sticking" pass early in the reduction sequence and to finish the rolling with 25 or 40% passes. Bonding has been obtained at 80% total reduction. A comparison of the "end effect" in plates rolled at various temperatures is shown in Fig. 36.

### Heat Treatment of Alclad Thorium Plates at 150 and 200°C

A possible source of failure of the alclad thorium plate under operating conditions is the formation and growth of the brittle intermetallic compound

[4] *Monthly Technical Progress Report for March 20 to April 20, 1953*, SEP-124 and *Monthly Technical Progress Report for April 20 to May 20, 1953*, SEP-126.

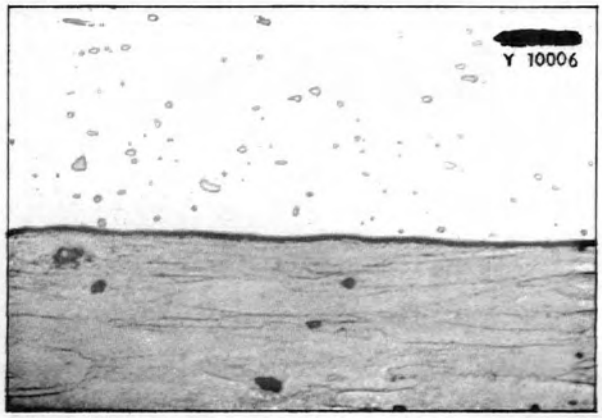


ROLLED AT 260°C

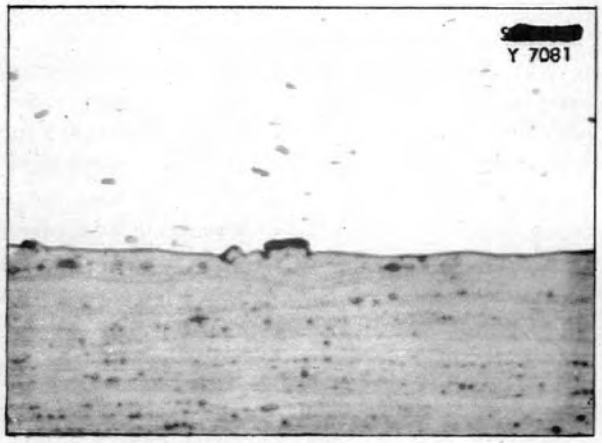


ROLLED AT 400°C

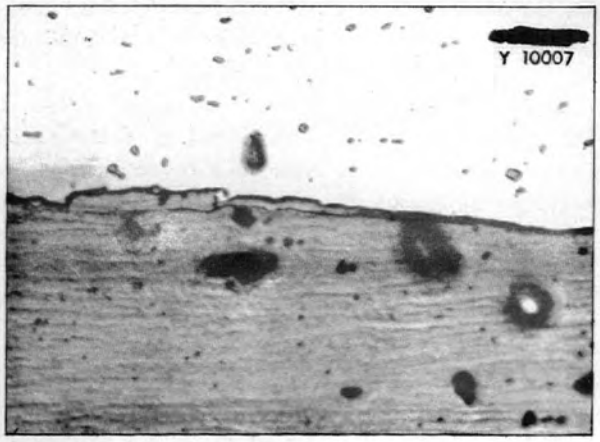


ROLLED AT 450°C

**Fig. 35. Influence of Rolling Temperature on Formation of Intermetallic Compounds in Alclad Thorium Plates.** Etchant: perchloric acid and alcohol. 1000X

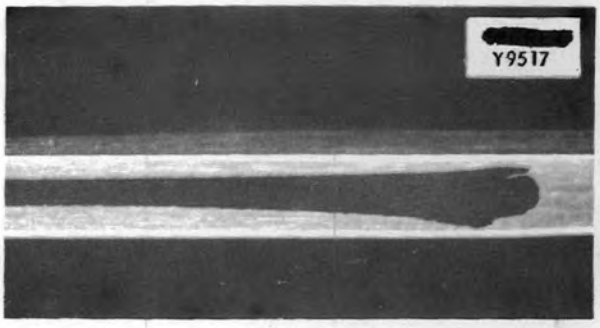


ROLLED AT 600°C

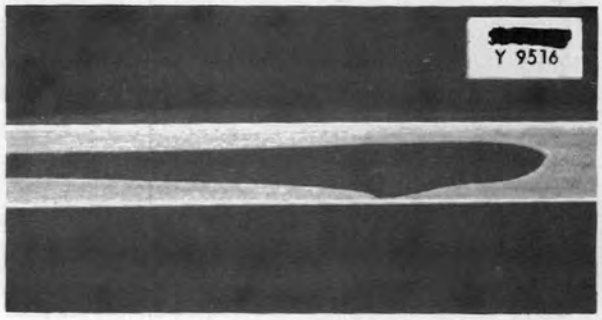


ROLLED AT 450°C

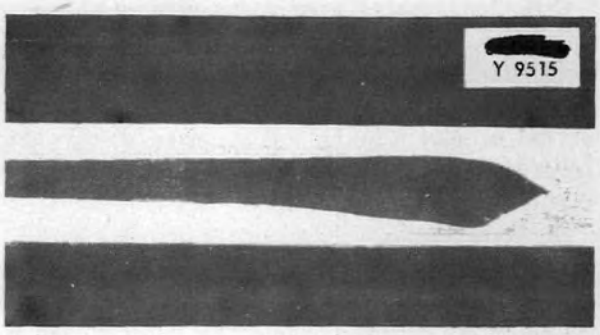


ROLLED AT 340°C

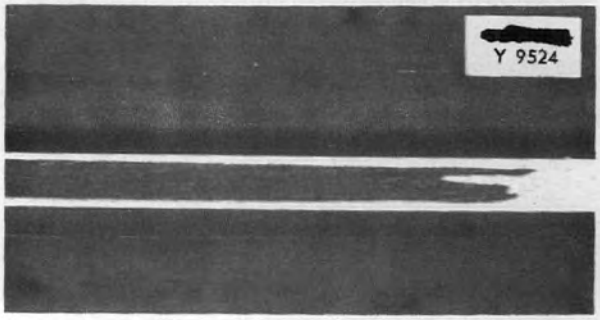


ROLLED AT 260°C

**Fig. 36. Influence of Rolling Temperature on "End Effect" in Thorium Plates Clad with Type 52S Aluminum.** Etchant: 50% HCl–50% $H_2O$. 2X

layer at the bonded thorium-aluminum interface. An investigation has been completed to determine whether formation and growth of the intermetallic compound occurs during a ten-week period of heating at 150 and 200°C.

Thirteen alclad thorium plates were rolled at 450°C. Unfortunately, metallographic examination of the as-rolled plate revealed that the plates were rolled at too high a temperature and a thin, discontinuous intermetallic compound was present. The most representative thickness appeared to be 0.0002 mm, but there were isolated clumps of intermetallic compound that were as thick as 0.009 mm. Qualitative physical testing indicated that the plate was satisfactorily bonded. Six of the plates were heated at 150°C and six at 200°C. At the end of each 7, 14, 28, 42, 56, and 70-day period, a plate was removed from each furnace and examined qualitatively for bond strength and metallographically for intermetallic compound formation and growth. The results of the diffusion treatment are given in Table 26, in which the most representative compound layer thicknesses are shown, as well as the maximum thicknesses. The maximum thicknesses represent measurement of the isolated clumps of intermetallic compound that were scattered along the bonded interface.

A comparison of the compound layer in the as-rolled plates and in the plates treated at 150 and 200°C for 70 days is shown in Fig. 37. Although a clear-cut conclusion cannot be drawn because of the presence of compound formation at the interface in the as-rolled plates, it is apparent that growth occurred during the diffusion treatment. It appears that this condition is not very serious in plates treated at 150°C. However, the results for plates treated at 200°C for 56 and 70 days are somewhat discouraging. Each plate was subjected to severe bending after the designated heat treatment. In no case did the interface fail in a brittle fashion. However, the bond in the plate treated at 200°C for 70 days appeared to have been weakened by the compound layer.

### Assembly of Thorium Feed Components

In addition to the thorium metal for the shim safety control rod, the UPR calls for two thorium feed components. Conceptional cross sectional views of these components are shown in Fig. 38. The square box is designed primarily to house the fuel element in the active core, while the parallel-plate type of unit is for use in the thorium blanket

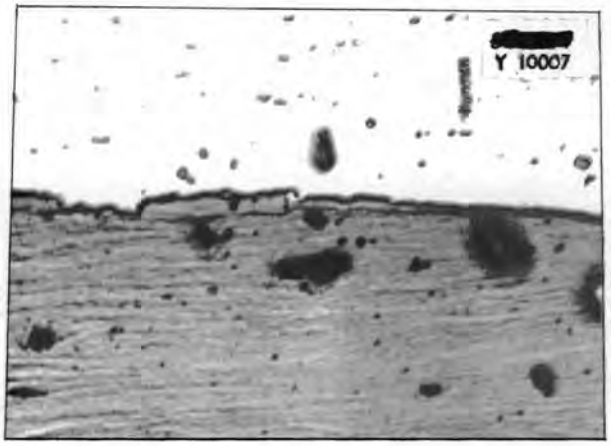


AS-ROLLED PLATE, ROLLED AT 450°C

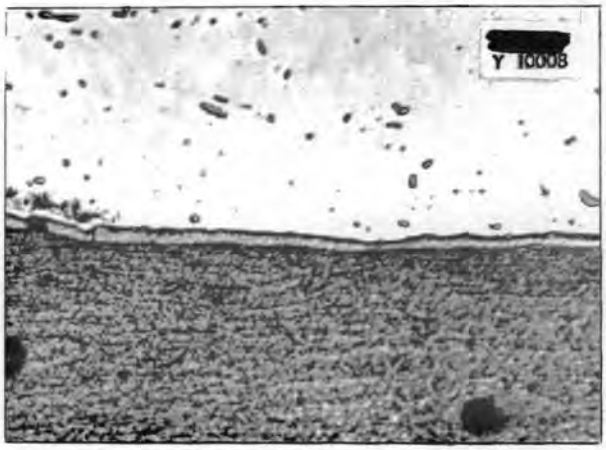


TREATED AT 150°C

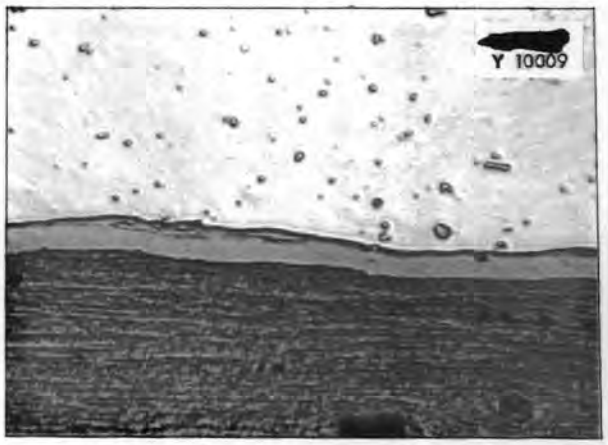


TREATED AT 200°C

**Fig. 37. Comparison of the Intermetallic Compound Layer in As-Rolled Alclad Thorium Plate and That in Similar Plates Treated at 150 and 200°C for 70 Days.** Etchant: perchloric acid and alcohol. 1000X

DWG. 21817

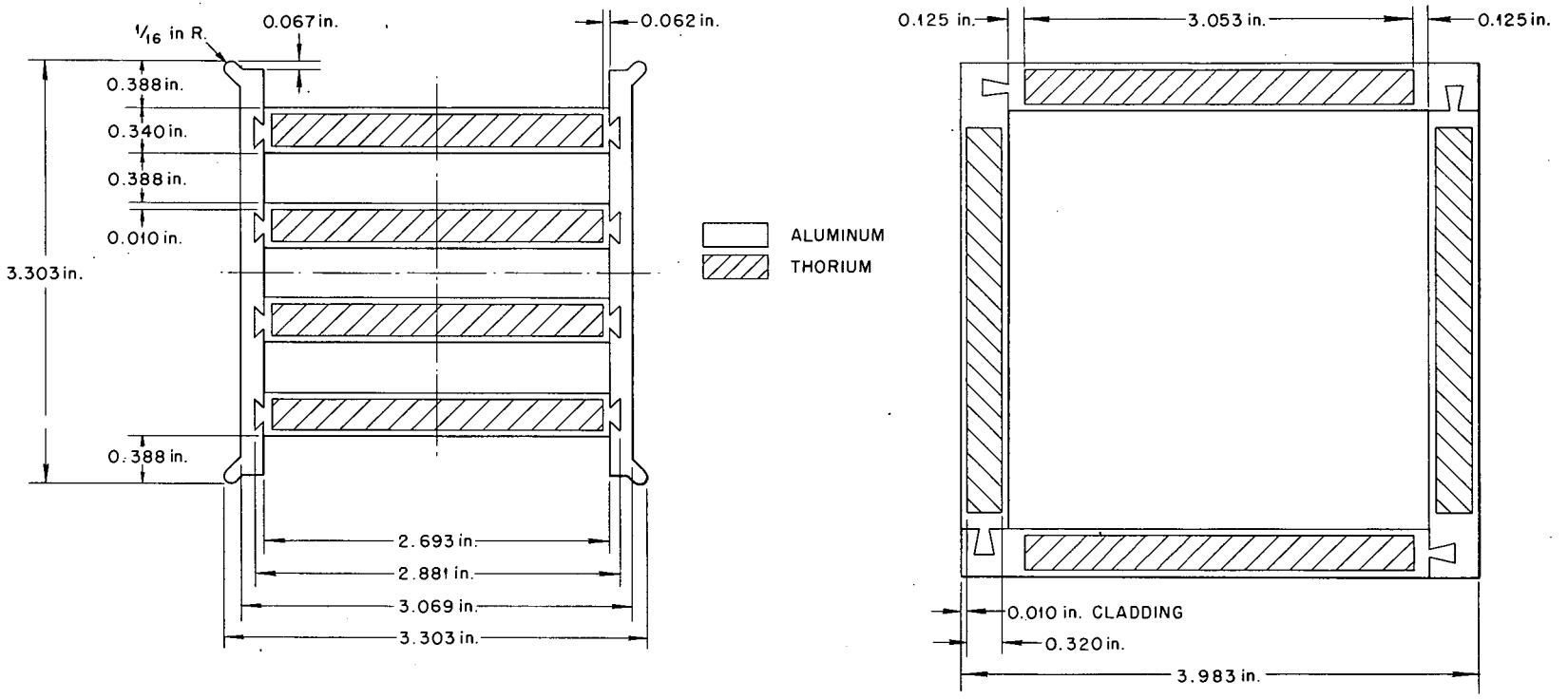


ALCLAD THORIUM BLANKET ASSEMBLY
LENGTH 30 in.

ALCLAD THORIUM BOX ASSEMBLY
LENGTH 78 in.

**Fig. 38. Cross Section of Thorium Feed Components Proposed for NAA-UPR.**

TABLE 26. RESULTS OF THERMAL TREATMENT OF ALCLAD THORIUM PLATES AT 150 AND 200°C

| TIME AT TEMPERATURE | | INTERMETALLIC COMPOUND LAYER THICKNESS (mm) | | | |
|---|---|---|---|---|---|
| | | Most Representative | | Maximum | |
| Days | Hours | At 150°C | At 200°C | At 150°C | At 200°C |
| 0 | 0 | 0.0002 | | 0.009 | |
| 7 | 168 | 0.0008 | 0.0018 | 0.003 | 0.007 |
| 14 | 336 | 0.0011 | 0.0022 | 0.007 | 0.007 |
| 28 | 672 | 0.0012 | 0.0026 | 0.005 | 0.007 |
| 42 | 1008 | 0.0013 | 0.0031 | 0.006 | 0.006 |
| 56 | 1344 | 0.0014 | 0.0034 | 0.005 | 0.015 |
| 70 | 1680 | 0.0016 | 0.0039 | 0.004 | 0.009 |

surrounding the active lattice. Details of these components are described fully in NAA-SR-207.

Alclad thorium plates cannot be assembled by conventional aluminum brazing techniques because of the instability of the bond at elevated temperatures. Heating the clad plates to 600°C for 1 hr, equivalent of the Al–Si brazing cycle, resulted in failure of the bond because of excessive compound formation at the bond interface.

Alternate methods of joining are mechanical means or welding if the welding operation does not impair the bond or cause excessive warpage. The dovetail type of joint appears impractical because galling occurs when attempts are made to slide closely machined aluminum parts over the long assembly required.

Joining of parallel thorium plates to aluminum side plates by means of a simple block-type joint and plug welding appears to be not only technically sound but a cheap method of construction, as well. This joining method permits gang milling and multiple drilling of the side plates. The thorium-bearing plates require no special machining. The component parts could be readily assembled, firmly clamped in a welding jig, and plug welded on both sides with a consumable-electrode Aircomatic gun. After welding, the desired contours on the plates could be machined with a single contour cutter. A unit with closely finished dimensions should result.

Initial attempts to produce this type of construction were extremely encouraging. The component parts of a full-sized dummy parallel plate unit were machined and assembled as illustrated in Fig. 39. The holes for the plug welding were $\frac{1}{4}$ in. in diameter with a $\frac{3}{4}$-in.-dia chamfer. As shown, thermocouples were provided at distances of $\frac{1}{8}$, $\frac{3}{8}$, $\frac{7}{8}$, and $1\frac{7}{8}$ in. below the plug welds at the ends of the plate to measure the temperature distribution beneath the weldment during the welding operation. Because of lack of equipment for Aircomatic welding, heliarc welding with a $\frac{1}{4}$-in.-dia 2S aluminum filler rod was substituted. Results of the time-temperature relationships beneath the plug welds are shown in Fig. 40. The maximum temperature at $\frac{1}{8}$-in. depth is approximately 470°C, but the heat dissipates rapidly and there is not sufficient time for it to cause

**Fig. 39. Dummy Aluminum Assembly Prior to Plug Welding.**

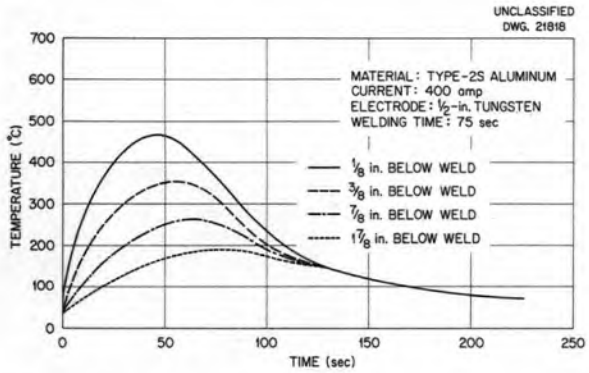


**Fig. 40. Relationship Between Temperature and Time at Various Distances Below Weld During Plug Welding.**

appreciable intermetallic compound formation and growth between the aluminum and the thorium. Measurement of the assembly after plug welding revealed that the maximum distortion was 0.040 inch. It is felt that the distortion was due to improper clamping and could be lessened by the use of a permanent welding fixture. No measurement of change in plate spacing was made. After the plug welding, the side plates of the welded assembly were machined to approximately the contour specified in the design. The finished assembly is illustrated in Fig. 41.

Unfortunately, thorium box assemblies of the types shown in Fig. 42 are not easily constructed by welding because the internal dimensions are critical and the inner surfaces cannot be easily machined after welding. Numerous mechanical joints for permanently fastening thorium-clad plates into the box configuration were evaluated. Factors of compressive and hydrostatic strength and dimensional reproducibility and stability, as well as cost of fabrication, were considered.

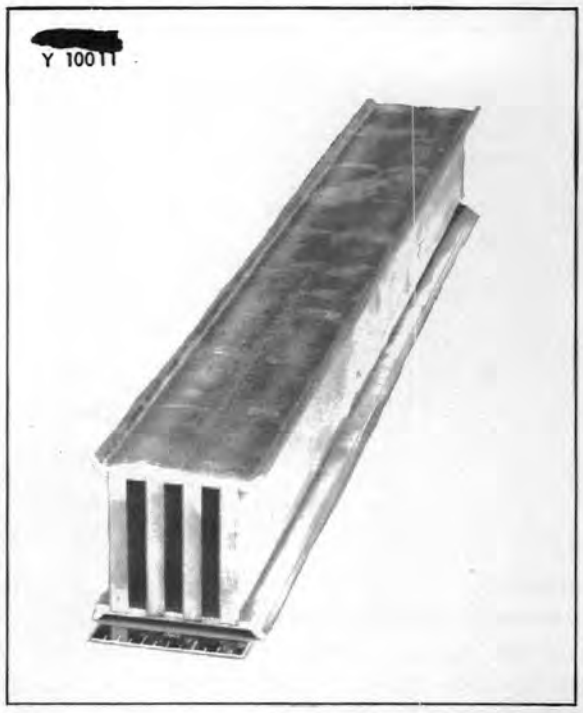


**Fig. 41. Finished Thorium Blanket Assembly.**

The four most promising joint designs were selected and full-scale cross sectional, but short length, boxes of each type of design were fabricated for further study. The finished test boxes are illustrated in Fig. 42. Testing is incomplete, but Table 27 presents the preliminary findings for these four mechanical joints compared with those for the NAA window-box design.

The spun head rivet, miter cross pin lock, and shear rivet joint designs all have the undesirable feature of using either pins or rivets. This type of construction is objectionable because of the possibility of a pin or rivet loosening in service and getting into the water system or lodging somewhere in such a way as to prevent removal of the elements.

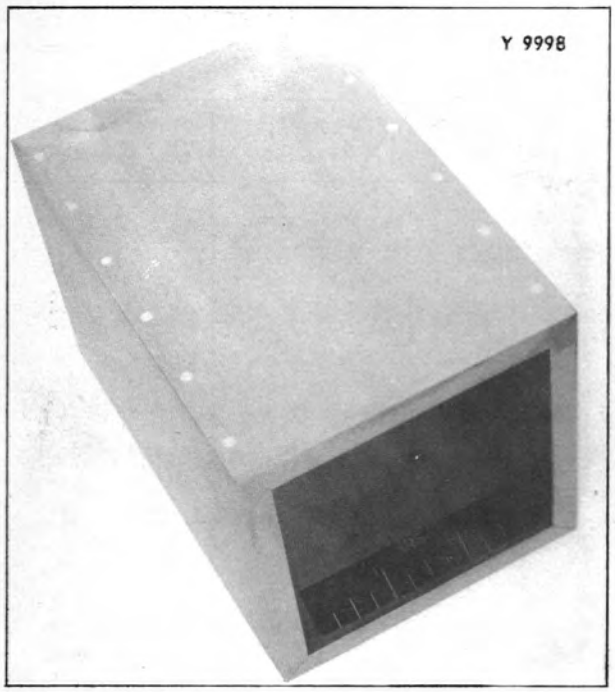


MITER CROSS PIN LOCK

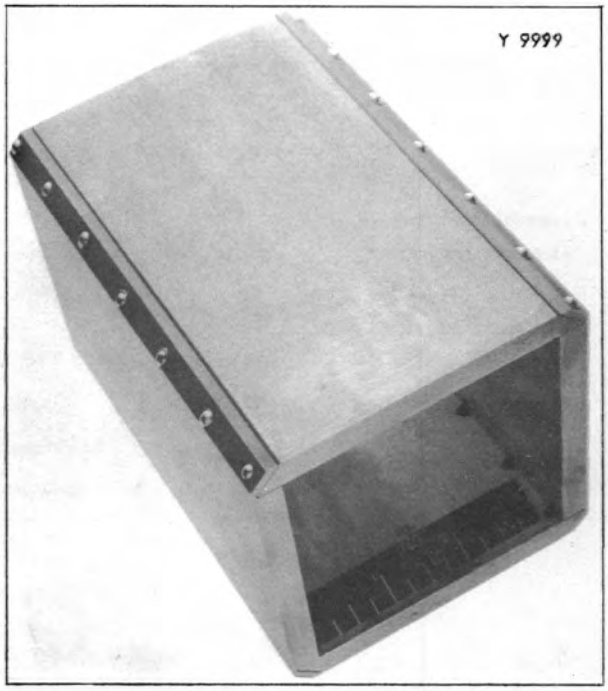


SHEAR RIVET ASSEMBLY

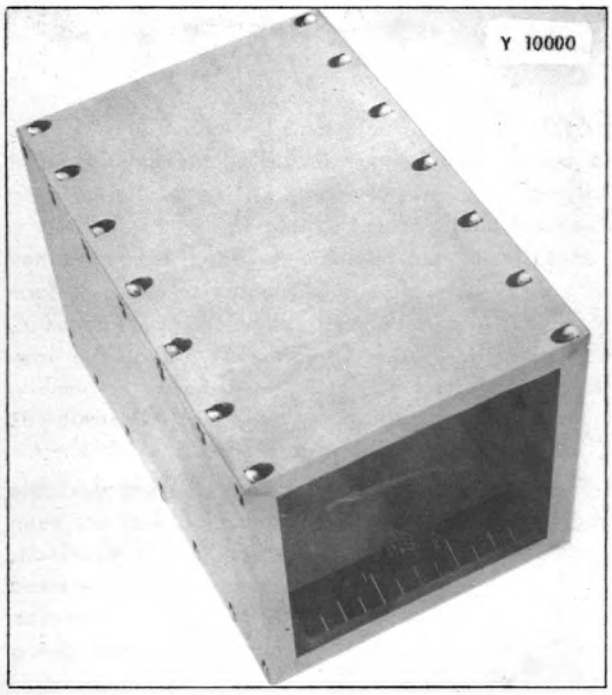


SPUN HEAD RIVET

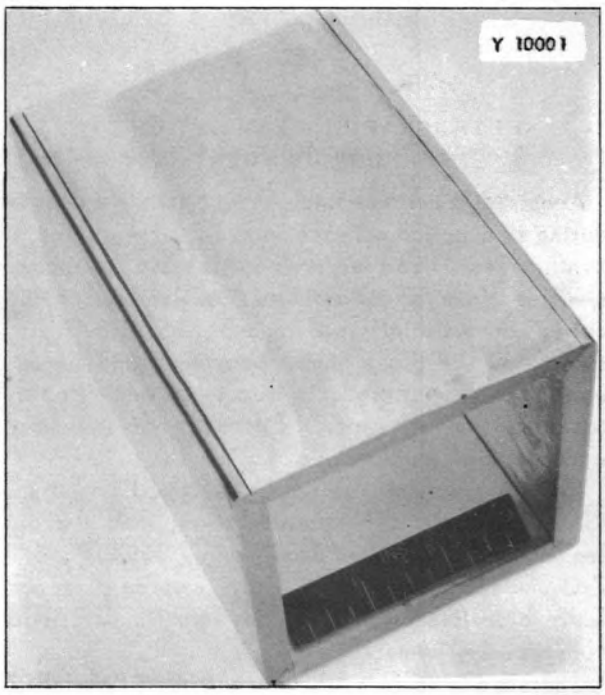


SPUN LOCK JOINT

**Fig. 42. Possible Mechanical Joint Designs for Construction of the UPR Thorium Box Component.**

TABLE 27. PRELIMINARY EVALUATION OF VARIOUS MECHANICAL JOINT DESIGNS

| | JOINT DESIGN | | | | |
|---|---|---|---|---|---|
| | Spun Head Rivet | Spun Lock Joint | Miter Cross Pin Lock | Shear Rivet Assembly | NAA Window Box Assembly |
| Diagonal compressive strength, load in lb | 320 | 795 | 380 | 530 | |
| Internal structure can withstand 50-psi pressure | Yes | Yes | Yes | Yes | |
| Dimensional tolerance | Good | Good | Good | Fair | Good |
| Dimensional stability | Excellent | Satisfactory | Excellent | Excellent | Satisfactory |
| Cost of fabrication | Intermediate | Lowest | Intermediate | Intermediate | Highest |

## CERAMICS

J. M. Warde
L. M. Doney
J. R. Johnson
S. D. Fulkerson
C. E. Curtis
A. J. Taylor
G. D. White

### PETROGRAPHIC EXAMINATION OF FLUORIDE FUELS

About 1500 petrographic examinations were made during this period. These included examination of synthesized fluoride compounds and quenched samples from phase studies, evaluation of the purity of materials and phases in ARE fuels, evaluation of glass pump packings, and examination of reduction products from loops and filtration residues and filtrates. Examples of the work accomplished are given below.

Fuel 31 consists primarily of $NaZrF_5$ and E2 ($3NaF \cdot 4ZrF_4$?). The powder taken from the dip leg of an Inconel pot was mainly $Na_3ZrF_7$ and $ZrO_2$. This shows that $ZrF_4$ will oxidize and leave a deficiency of $ZrF_4$ and that $Na_3ZrF_7$ will subsequently form.

There are indications that the so-called "$NaZrF_5$" can vary in composition with corresponding changes in refractive indices.

There was a marked change in the composition of fuel 30 after it had been run in a loop for 3000 hr in that the refractive indices of the solid solution were markedly lower at the end of the run than those of the solid solution in normal fuel 30. This is believed to be due to $CrF_3$ entering the solid solution. More information will be available when chemical analyses are completed.

Results of petrographic examinations combined with x-ray data show that the low-temperature form of $Na_2UF_6$ is hexagonal rather than orthorhombic, as reported in the literature.[1] Also, the low-temperature form of $K_3UF_7$ is either orthorhombic, monoclinic, or triclinic, whereas Zachariasen gives $K_3UF_7$ as either cubic or tetragonal.

Fuel irradiated in the MTR showed an appreciable quantity of $UO_2$, but unirradiated fuel has not been made available for examination and comparison.

A number of fluoride compounds were synthesized by Barton's group, and their optical properties have been determined. These data are being collected for a formal report.

A considerable amount of work was done on the identification of minerals present in raw materials.

[1] J. J. Katz and E. Rabinowitch, *The Chemistry of Uranium*, NNES Div. 8, Vol. 5, p. 381, McGraw-Hill, New York, 1951.

### INSULATING END CAP DEVELOPMENT

Work continued in cooperation with the Fuel Survey, Fuel Technology Subsection at Hanford on the development of insulating end caps for Hanford-type fuel slugs. Additional specimens were prepared and sent to Hanford for evaluation.

Cylindrical end caps that have a cavity filled with bubble alumina were machined from 2S aluminum rod. The end caps were 1.25 in. in diameter and 0.4375 in. thick. The cavities were 1.25 in. in diameter and 0.250 in. deep. The cavity in each end cap was covered with a lid 0.0625 in. thick that was welded in place. The bubble alumina used was −20 mesh +50 mesh material from the Carborundum Company.

Compacts are being prepared by hot pressing a mixture of 60 wt % aluminum powder and 40 wt % bubble alumina in a "sandwich" between layers of aluminum powder. The finished specimen will consist of cylinders 1.25 in. in diameter with ¼-in. layers of the aluminum-alumina mixture between ¼-in. layers of aluminum. These compacts will be sent to Hanford for thermal conductivity measurements.

### CERMETS

For more than a year there has been a program for making a cermet fuel element which might perform in a gas-cooled power system. A practical system must use materials which are available and economical and which have nuclear characteristics that will permit conversion or breeding. A graphite-moderated reactor that would use nitrogen as a working gas was suggested to the ORSORT students as a possible system. A group of students headed by J. Gallagher and advised by W. Jordan designed a package reactor system of this kind that used SiC-Si cermet fuel elements. The power system of their design appears to be entirely practical provided the fuel elements do not suffer too great radiation damage and do not lose too much of the generated fission products. High-temperature operation lessens the total equilibrium damage, but, unfortunately, it also increases the diffusion and permeation rates of the fission products generated in the element. The general investigation program includes producing the cermet fuel elements and testing them to determine the extent of the above phenomena.

The SiC-Si material was chosen for the following reasons: (1) it has a reasonably low neutron absorption cross section (~0.15 barn); (2) it has suitable physical properties at high temperatures; (3) it is made of inexpensive, available materials; (4) a similar material has been made commercially by the Carborundum Company, who invented it.

The physical properties which indicate its use are: (1) tensile strength of the order of 10,000 psi, which slightly increases up to 2000°F; (2) usefulness up to 2450°F (silicon sweats out at 2550°F); (3) thermal conductivity of 0.04 (cgs), which is about the same as for some stainless steels; (4) low thermal expansion, $2.5 \times 10^{-6}$ per °C, similar to that of graphite; (5) low porosity (depending on the fabrication process); (6) excellent oxidation resistance.

Two shapes have been considered so far: a cross-shaped element and a tubular element. Cross-shaped elements have been made with $UO_2$ additions. The fuel portion is the same SiC-Si material to which 10% (over-all cross wt %) $UO_2$ was added. It is surrounded completely by nonfuel-bearing SiC-Si.

The cermet is made by pressing mixed powders of graphite and volatile materials such as wheat flour, napthalene, Carbowax, or some plastics into the desired shape. The compact is then heated in an inert atmosphere to 1000°C to drive off the volatile components and leave a porous carbon shape. This is then dipped in molten silicon at 1800°C, where an infiltration with silicon and an exothermic reaction that creates SiC occur simultaneously. A rough coating of $SiO_2$ forms on the surface when the dip is carried out in air, and silicon may adhere in droplets at various places. A final grinding to remove the external blemishes must be carried out, preferably with a diamond-wheel surface grinder.

A simulated service test has been designed, and equipment is being constructed which will blast nitrogen over a hot fuel element at 100 to 200 fps. The element will be heated electrically by its own resistance. The apparatus is designed so that it can be inserted in the ORNL graphite reactor, the LITR, or the MTR for radiation tests; however, initial tests will not be made under radiation. A number of "static" radiation tests are planned. Elements will be exposed for short periods in the ORNL graphite reactor in sealed aluminum tubes. They will then be heated to various temperatures of up to 2200°F to determine the rate of fission-product loss as a function of temperature. A

number of elements will be sliced, following high-temperature exposure only, to determine whether the uranium migrates. An element containing enriched uranium will be exposed in the LITR for stability testing. If necessary, the elements can then be tested in-pile in the apparatus described above to give a simulated service test that includes radiation exposure.

Limited radiation studies of SiC, conducted by Primak at Argonne, showed that the damage anneals out almost completely between 1000 and 1200°C. Although his tests were carried out with hexagonal SiC, while the material in SiC-Si is cubic, and experience indicates that damage is less when exposure is made at higher temperatures, it would seem probable that the total equilibrium radiation damage at the proposed operating temperatures (1500 to 2200°F) will be tolerable.

Gaseous fission products will probably diffuse through and escape from the fuel elements, to some extent, at high temperatures, even though the fuel elements are nonporous. The tests outlined should reveal semiquantitatively the extent of such losses.

### $UO_2$ INVESTIGATIONS

Further work was carried out on the fabrication of $UO_2$ rods 0.3 in. in diameter and 2 in. long to be clad in 20-mil zirconium and placed in an aluminum sheath. This work is being done in cooperation with the Westinghouse Atomic Power Development Division (WAPD) and is in connection with WAPD investigations of fuel elements for the PWR (formerly CVR) reactor.

Three rods of $UO_2$ 2 in. long and 0.3 in. in diameter fabricated by hydrostatic pressing (1000 psi), fired to 1750°C, and held for 5 hr (hydrogen atmosphere) were prepared. The density of the packed material was 83% of theoretical. The rods were clad in 20-mil zirconium tubing with zirconium end plugs ½ in. long welded in place.

A 30-mil zirconium tube with an inside diameter of approximately 0.300 in. and with a zirconium end plug ½ in. long welded in place was packed with fused $UO_2$. A Syncron vibrator was used for packing the $UO_2$. The length of the packed section was approximately 2 inches. The density of the packed material was 70% of theoretical. After the tube had been packed, a zirconium plug ½ in. long was welded in place in the open end.

These specimens were evaluated by WAPD, and it was decided to proceed with the fabrication of the rods of $UO_2$ and to attempt to obtain maximum density of the fused $UO_2$ by hydrostatic pressing and firing to 1750°C. The first rod fabricated from the fused oxide had a density of 10.47 g/cm$^3$ (96.3% of theoretical), and it was nonporous. This rod has been machined to 0.300 in. in diameter and 2 in. in length; the material is quite brittle but not so brittle as the hot-pressed material. A spectroscopic analysis of the finished rod indicated the presence of 0.08% iron, less than 0.15% chromium, less than 0.08% nickel, and 0.12% silicon, presumably picked up in milling.

### $ThO_2$ INVESTIGATIONS

It has been found that thorium oxide with a density approaching theoretical (10.0) can be obtained by the addition of only 1% CaO and firing to 1800°C. Normal $ThO_2$ attained only 80% of theoretical density under the same conditions.

X-ray patterns and petrographic examinations indicate that CaO is taken into solid solution with $ThO_2$ up to about 25 mole %. The addition of small amounts of CaO will create oxygen deficiencies and promote the formation of "holes." Holes in structures are generally believed to influence the sintering mechanism in such a way that in this case a greater degree of sintering might be expected. Borie has found no change in $ThO_2$ lattice parameters with up to 40% CaO addition. A check for free lime showed none in the 12.5% CaO sample but that a small amount might be present in the 25% CaO sample.

The ionic radii of $Ca^{++}$ and $Th^{4+}$ are approximately the same (~1.00 Å). Only $Sr^{++}$, for which the ionic radius is reasonably close to that of $Th^{4+}$, shows an effect similar to that of $Ca^{++}$ in the densification of $ThO_2$. $Be^{++}$, $Mg^{++}$, $Ba^{++}$, $Na^{+}$, $Si^{4+}$, and $Al^{3+}$ have little or no effect.

For a thoria breeding blanket, thoria pellets approximately ⅛ in. in diameter with comparatively low density would be required. Strong bars of sintered thoria have been produced with a little over one half theoretical density (5.3). Still lower densities will be attained, and it is proposed to test pellets of the light-weight material for rate of wear by abrasion such as would occur in a mobile fuel bed, in water, or in other liquids.

### RARE EARTH OXIDE INVESTIGATIONS

Work with the rare earth oxide $Sm_2O_3$ shows that dry-pressed bars acquire optimum density and

strength at 1500°C. The fired bars disintegrated in boiling water to a white powder, and thus there was indication of the formation of a hydrate. X-ray studies of the evaporated solution showed a phase entirely different from that of the original $Sm_2O_3$. Dry-pressed bars fired at this temperature will be tested for thermal expansion, corrosion resistance, melting point, x-ray diffraction, and other properties on which there is no information in the literature.

### CERAMIC CONTAINERS FOR RADIOACTIVE STRONTIUM

A ceramic container for radioactive strontium is needed to provide for safe use of the material. The container or seal must not absorb too much of the beta activity. An enamel coating over a layer of $Sr(NO_3)_2$ on copper was tried. The decomposition of the nitrate prevented successful adherence. An admixture of a strontium compound in powdered glass will be pressed and sintered. Also, a low-melting glass containing strontium will be glazed onto a glass disk.

### GLASS-TYPE PUMP SEALS (ANP)

A suitable, viscous, high-temperature seal material was requested by the Experimental Engineering Group of ANP. Limited experiments had shown a $NaBeF_3$ mixture to have promise when used with a number of metal washers which served to isolate rings of the melt. The ring voids were filled with the powdered fluoride mix. Scoring of the housing was observed.

The need was for a glassy substance with appropriate viscosity for the temperature range involved that would also have stability against devitrification. To provide a freely flowing viscous seal, it is believed that a viscosity gradient of $10^2$ poises in the hot end to $10^{15}$ poises or higher in the cold end should be established. Softening of the whole seal should be carried out first so that wetting will take place on the shaft, housing, and metal spacers. Devitrification, or crystallization in the glass, will lead to a fluid containing relatively hard crystals which will act as an abrasive on the metal parts.

Beryllium fluoride is a glass former that produces a structural network of randomly oriented $BeF_4^{--}$ ion tetrahedra that is analogous to the silica-glass network. Alkali and alkaline earth ions serve similar functions in the fluoride network as they do in the oxide systems.

Very few data are available on the physical properties of the fluoride glasses; however, on the basis of similarity to oxide glasses, it is possible to predict their general behavior. Thus, for a glass with little tendency to devitrify and with reasonable stability against atmospheric attack, $Mg^{++}$ or $Ca^{++}$ and $Al^{3+}$ ions should be included. A glass which softens to a viscosity of the order of $10^8$ poises at 250°C is desirable. The addition of alkali ions such as $Na^+$ or $K^+$ will produce the desired viscosity. The glass composition proposed is the following:

| COMPOSITION (wt %) | MATERIAL |
|---|---|
| 50 | $BeF_2$ |
| 25 | KF |
| 16 | $MgF_2$ |
| 9 | $AlF_3$ |

This glass was found to melt satisfactorily, and it did not devitrify in the handling operations. The glass was melted in platinum at about 900°C and cast into a graphite die to form the desired ring shape. It was not possible to cool the rings in the open without cracking. By slow cooling in a blanket of glass wool, most cracking was avoided, and it can be eliminated by furnace cooling and annealing.

Future work will include studies of other compositions ranging from pure $BeF_2$ to mixtures containing various proportions of Na, K, Ca, F, and Al fluorides. Attempts to impregnate very porous graphite with these glasses will also be made.

### CERAMIC CONTAINER FOR USE IN FUEL STUDIES (ANP)

A ceramic container for use in the investigations of the electrical resistivity of the fluoride fuels was requested by the Heat Transfer and Physical Properties Group of ANP. Beryllium oxide was selected as a promising material for the service required, and as a pilot experiment, a hot-pressed beryllium oxide block was drilled straight through. This beryllium oxide block was satisfactory for use as the container required. Longer blocks are desired, so future work will involve making isostatically pressed and sintered beryllium oxide blocks which can be formed in longer shapes and still have uniform density.

# METALLOGRAPHY

R. J. Gray
R. S. Crouse
T. M. Kegley, Jr.
T. K. Roche

In the metallographic examination of Inconel, the alloy being considered for applications in the aircraft reactor program, there is question concerning the carbide precipitation at various temperatures. In the case of Inconel specimens subjected to radiation in the cyclotron or the graphite reactor, the question arises as to whether observed carbide precipitation is a radiation effect or a thermal effect. On various occasions, the Metallography Section has been asked for photomicrographs that exhibit the carbide precipitation range for Inconel. Because of the lack of a previous definitive study, a program has been outlined for heat-treating Inconel stock of varying carbon content at various temperatures to provide for a metallographic survey of carbide precipitation.

The materials chosen for the study were high-purity Inconel (0.012% carbon) and commercial Inconel (nominal 0.02 and 0.076% carbon). The Inconel with 0.012% carbon was prepared at the Laboratory by melting together high-purity ferrochromium and electrolytic nickel. The casting was fabricated by hot extrusion followed by cold swaging to individual rods reduced 35, 56, and 65% in area relative to the extruded product. At present, the carbide study is being conducted on the material that received the greatest reduction in area. In addition, recrystallization data will be obtained for all three swaged rods.

The Inconel with nominal 0.02% carbon was taken from commercial pipe stock and the Inconel with 0.076% carbon was taken from ½-in. commercial rod stock.

Specimens from the as-swaged high-purity rod and specimens from the commercial stocks in the as-received condition were heat treated for 100 hr over the temperature range from 800 to 1800°F at 100°F intervals. Specimens from the as-swaged high-purity rod and from the 0.076% carbon commercial rod were also given a solution treatment at 2100°F for 2 hr prior to the 100-hr heat treatment. Heat treating was carried out in a helium atmosphere, and all specimens were water quenched from temperature.

Although metallographic examination of the heat-treated specimens is incomplete, Figs. 43 through 46 illustrate some results of the study. Figures 43 and 44 show the Inconel with 0.012% carbon that was heat treated after the 2-hr solution anneal at 2100°F. The carbides precipitated at 1200°F and redissolved at 1800°F. Figures 45 and 46 show the commercial Inconel stock with nominal 0.02% carbon heat treated in the as-received condition. Carbide precipitation can be observed at 1200°F and resolution occurred at 1800°F.

Microscopic examination of the Inconel stock with 0.076% carbon heat treated at the various temperatures after the 2100°F solution treatment revealed large amounts of precipitated carbides both at the grain boundaries and within the grains in the temperature range of 1200 to 1600°F. At 1700 and 1800°F, a coalescence and probable partial solution of the carbides were observed. The complete solution of the carbides at 1800°F for the lower carbon stock leads to the possible conclusion that, upon increasing the carbon content of the Inconel, the precipitation range is broadened.

A type 321 stainless steel pin specimen was exposed to uranyl sulfate solution in a loop. Metallographic examination of the specimen showed a phase which was attacked preferentially. This phase proved to be ferromagnetic (probably ferrite), as shown in the series of photomicrographs in Fig. 47. The procedure used in identifying ferromagnetic constituents was described previously.[1] Figure 47*a* shows the specimen as polished. Figure 47*b* shows the specimen after the application of the colloidal iron solution. Even without energizing the electromagnet, there was enough residual magnetism in the specimen to cause the colloidal particles to outline faintly the magnetic phase. Upon energizing the electromagnet, the magnetic phase was clearly defined, as shown in Fig. 47*c*. Figure 47*d* shows the specimen as chemically etched.

[1] R. J. Gray, R. S. Crouse, and T. K. Roche, *Met. Quar. Prog. Rep. Apr. 30, 1952*, ORNL-1302, p. 105-119.

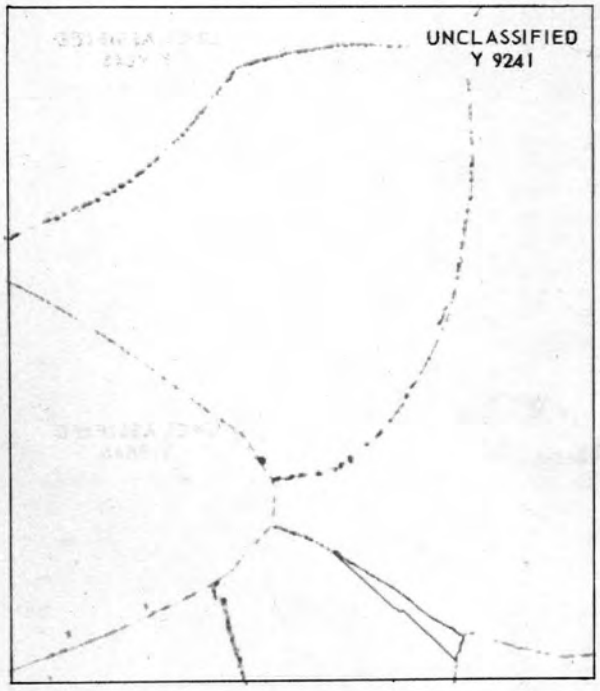


**Fig. 43. Inconel (0.012% C) Homogenized for 2 hr at 2100°F and Heat Treated for 100 hr at 1200°F.** Etchant: aqua regia. 500X

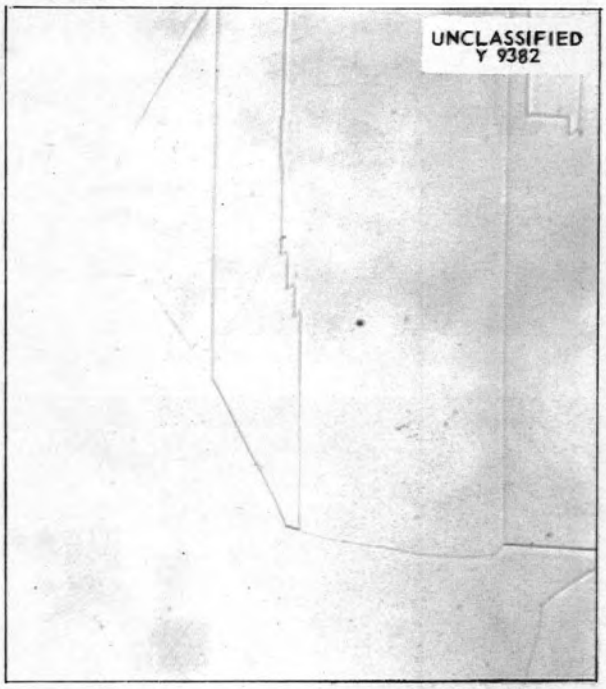


**Fig. 44. Inconel (0.012% C) Homogenized for 2 hr at 2100°F and Heat Treated for 100 hr at 1800°F.** Etchant: aqua regia. 500X

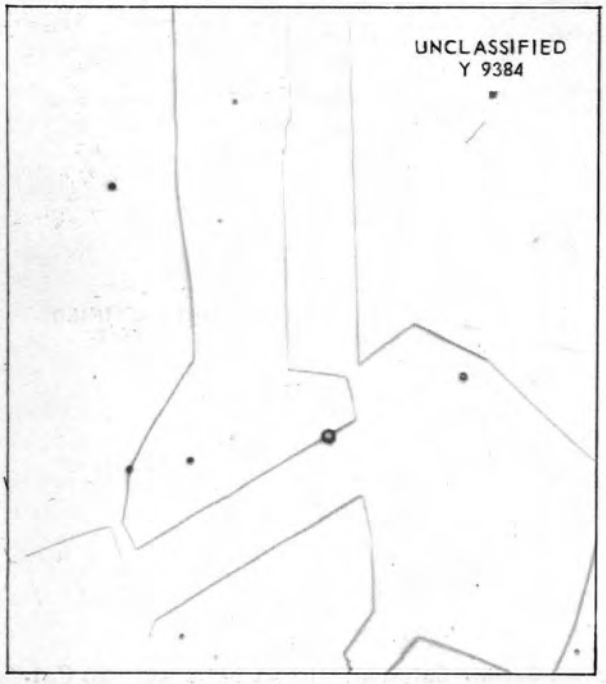


**Fig. 45. Inconel (0.02% C) Heat Treated for 100 hr at 1200°F.** Etchant: aqua regia, 500X

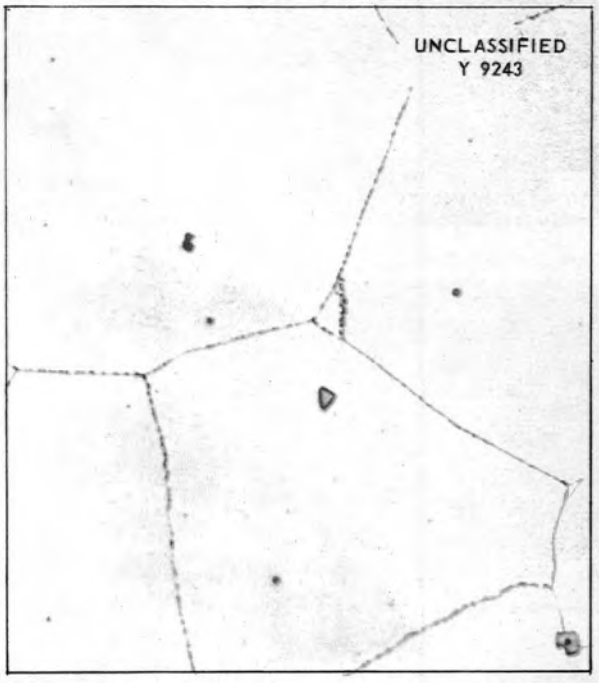


**Fig. 46. Inconel (0.02% C) Heat Treated for 100 hr at 1800°F.** Etchant: aqua regia. 500X

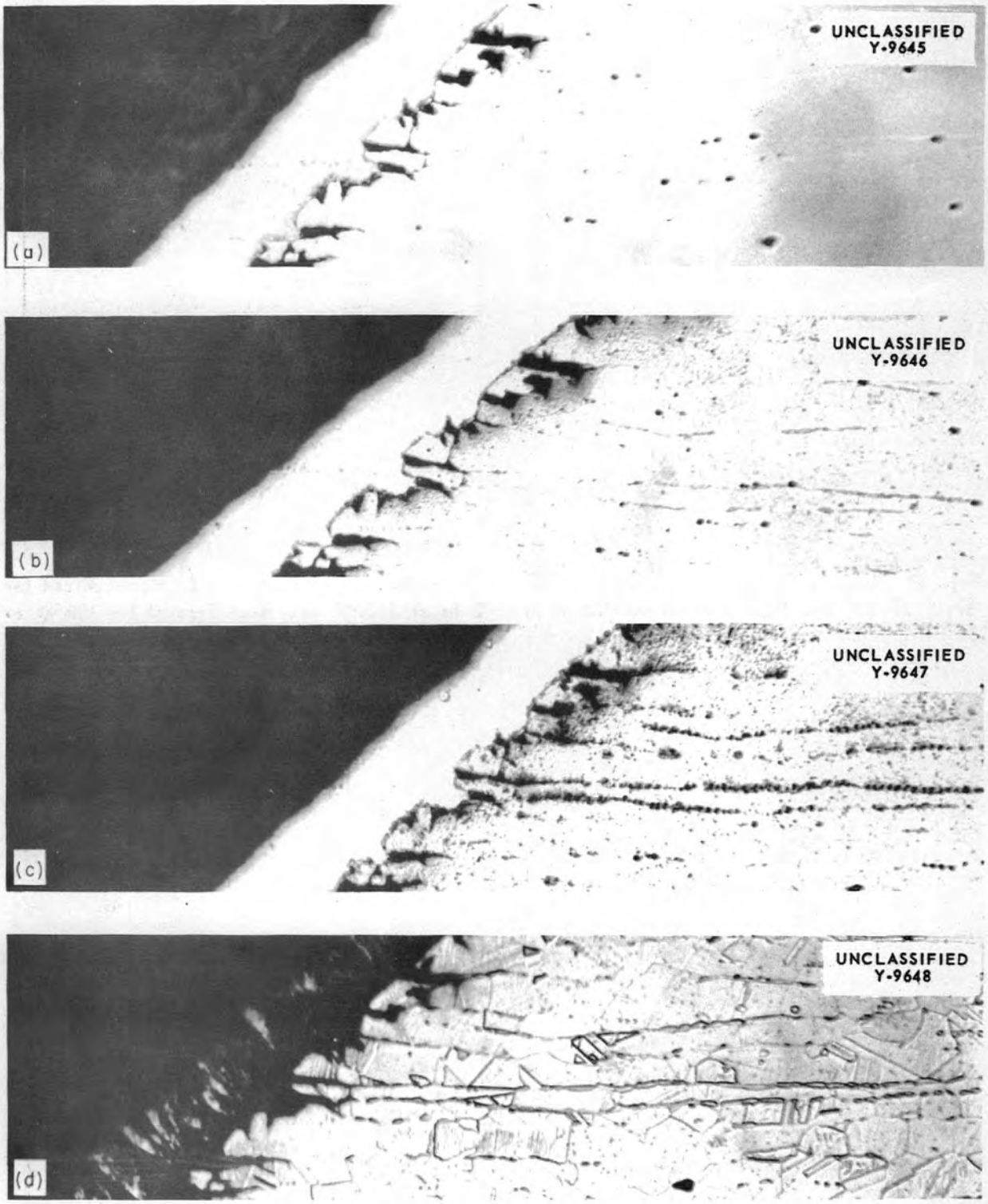


**Fig. 47. Type 321 Stainless Steel Pin Exposed to Uranyl Sulfate Solution. (a) As polished. (b) Collodial iron applied. (c) Magnet energized. (d) Etched with glyceria regia. 500X**

# FABRICATION METALLURGY

J. E. Cunningham

## MTR EXPERIMENTAL STUDIES

Design analyses and fabrication studies continue on the MTR fuel element. The purpose of the work is to enhance operational performance of the reactor and to reduce fabrication and chemical processing costs.

Exploratory work indicated that braze-clad material could be used in the construction of MTR fuel elements and that a worthwhile saving in fabrication and chemical processing costs would result. Additional brazing tests were performed to determine the exact specifications required for the braze-clad material to produce sound brazed joints and to meet the stringent dimensional tolerances specified for the fuel element. Side-plate material clad with silicon-aluminum alloy (12% Si–88% Al) on one side was prepared according to the schedule given in Table 28 and was then tested.

The composite containing approximately 19 mils (15% of the 125-mil gage thickness) consistently gave the best results during brazing and was therefore selected for use in construction of future MTR fuel elements. Details of the brazed joints fabricated with the new product are illustrated in Fig. 48.

Arrangements have been completed for Alcoa to supply the desired clad product, which will be designated as brazing sheet M-315. The M-315 product will be available in most commercial gages, and the specifications call for a 12% silicon–88% aluminum alloy clad on one side of either 2S- or 3S-grade aluminum. The cladding thickness of the braze metal is specified as 15% of the total gage thickness.

Results of the brazing studies were encouraging. Preplacement of the brazing alloy not only simplified the assembly operation but also permitted a reduction in the amount of aluminum-silicon alloy required in fabrication of the element. This latter factor is important because silicon interferes with dissolution and subsequent chemical processing of the fuel elements.

Table 29 presents materials and performance data on several fuel element designs. Elements of design types I, II, and III have already been in service in the MTR and are described purely for comparative purposes. The designs of the last three elements listed in Table 29, namely, II-A, III-A, and IV, are based on the use of braze-clad side-plate material in construction. The amount of silicon added during brazing has been greatly reduced from the amount used for the type I design. The reduction in the amount of silicon should markedly facilitate chemical processing.

Another source of silicon, however, is in the 2S-grade aluminum cladding which nominally contains a maximum of 1% (Fe + Si). The amount of silicon from this source is also being reduced because less aluminum is used in the fabrication of the new types of elements. The high-purity aluminum (99.75% aluminum, minimum) used in preparation of the enriched uranium–aluminum alloy melts contains very little silicon.

TABLE 28. SPECIFICATIONS FOR BRAZE-CLAD MATERIAL TESTED

| TOTAL COMPOSITE THICKNESS (mils) | ALUMINUM BASE METAL THICKNESS (mils) | Al-Si BRAZE METAL THICKNESS (mils) | SILICON CONTENT PER ELEMENT (g) |
|---|---|---|---|
| 125 | 95 | 30 (24%*) | 10.4 |
| 125 | 100 | 25 (20%) | 8.8 |
| 125 | 106 | 19 (15%) | 6.6 |
| 125 | 112.5 | 12.5 (10%) | 4.4 |

*Percentage of the 125-mil gage thickness.

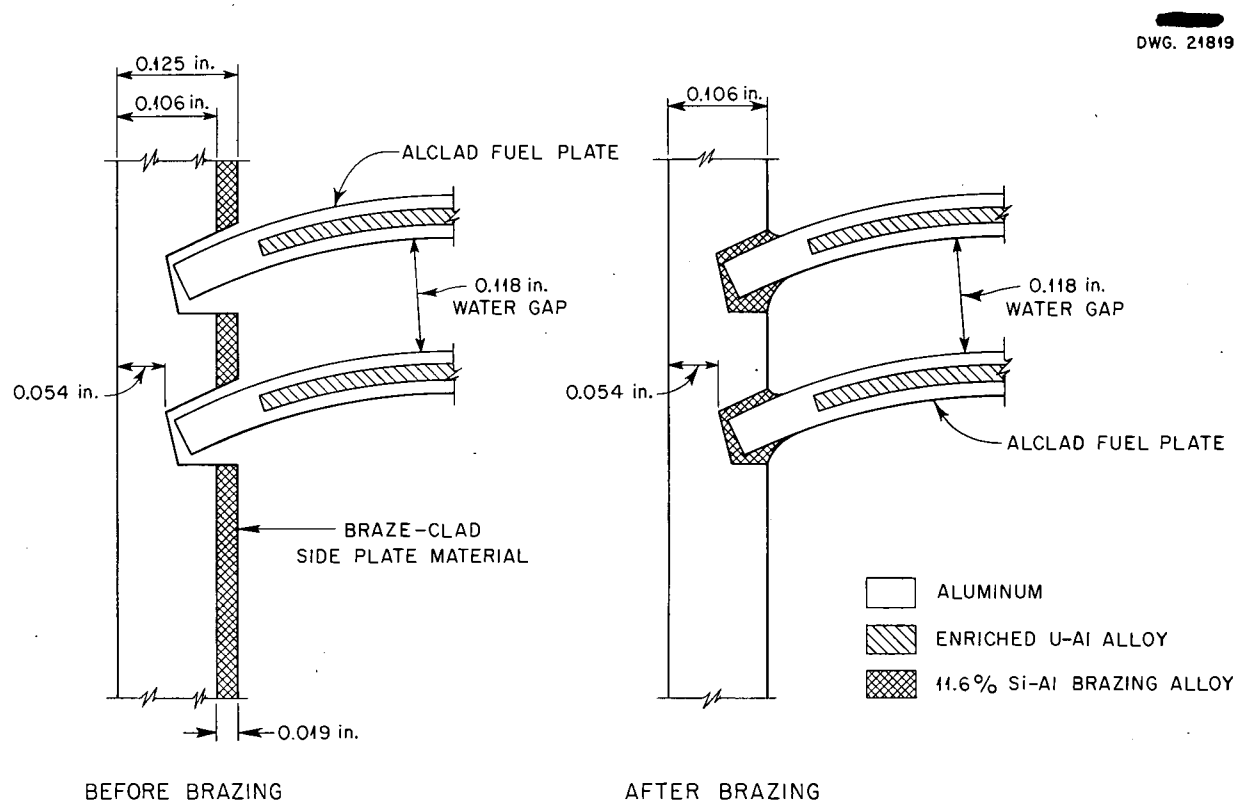


**Fig. 48. Brazing Details for MTR Fuel Element Joints Made by Using Braze-Clad Side Plate Material.**

The aluminum-to-water ratios for 3 by 9 slab loading arrangements of the new element designs, types II-A, III-A, and IV, are 0.656, 0.562, and 0.477, respectively. These ratios correspond to percentage gains in excess reactivity (based on $\Delta k/k = 0$ for the type I design) of 0.9, 2.3, and 3.7, respectively. If these gains are taken in terms of longer life, the same over-all performance can be obtained with fewer fuel elements. This is certainly worthwhile because, with current fabrication and chemical processing costs running at approximately $2 and $7 per gram, respectively, this increase in operational performance represents a sizable monetary saving.

Unfortunately, the present MTR water system is limited in total capacity to about 25,000 gpm. This limitation imposes a real problem in operation of the reactor with the type IV fuel elements because the water flow area is increased approximately 20% with the new element compared with that required for the type I element. Operation of the reactor with the type I fuel elements required a water flow rate of approximately 21,000 gpm. It appears that measures must be taken to either increase the capacity of the present water system or to operate the reactor at a slightly elevated power level.

## ALCLAD $UO_2$ AND ALUMINUM POWDER FUEL PLATES

E. S. Bomar

The feasibility of fabricating MTR fuel plates with sintered $U_3O_8$-aluminum powder mixture cores has been demonstrated.[1] Alclad plates containing uranium concentrations as high as 40 wt % equivalent as $U_3O_8$ in the core mixture have been successfully fabricated. The interest in fuel elements with higher uranium investment than is currently specified for the MTR arose because slightly enriched uranium is being considered in the construction of a proposed university-type reactor. Additional work was performed to evaluate the quality of the finished product.

[1] E. S. Bomar, *Met. Semiannual Prog. Rep. Apr. 10, 1953*, ORNL-1551, p. 76.

TABLE 29. MATERIALS AND PERFORMANCE DATA ON SEVERAL MTR FUEL ELEMENT DESIGNS

| FUEL UNIT DESCRIPTION | | | | | | |
|---|---|---|---|---|---|---|
| Element designation | I | II | III | II-A | III-A | IV |
| Number of fuel plates | 18 | 18 | 19 | 18 | 19 | 20 |
| Side-plate thickness, mils | 188 | 125 | 125 | 106[a] | 106[a] | 106[a] |
| Clad-core-clad thickness, mils | 20-20-20 | 20-20-20 | 15-20-15 | 20-20-20 | 15-20-15 | 10-20-10 |
| Water-gap spacing, mils | 117 | 117 | 118 | 117 | 118 | 118 |
| Al-to-$H_2O$ ratio[b] | 0.723 | 0.645 | 0.548 | 0.634 | 0.527 | 0.432 |
| AREAS, VOLUMES, AND MASSES OF MATERIALS IN FUEL ELEMENT | | | | | | |
| Total metal | | | | | | |
| Area, $cm^2$ | 26.34 | 24.61 | 22.25 | 24.32 | 21.66 | 18.96 |
| Volume, $cm^3$ | 1580.37 | 1476.64 | 1337.60 | 1458.98 | 1300.14 | 1137.70 |
| Mass, g | 4402 | 4136 | 3761 | 4091 | 3561 | 3223 |
| Water[b] | | | | | | |
| Area, $cm^2$ | 36.03 | 37.76 | 40.12 | 38.05 | 40.71 | 43.41 |
| Volume, $cm^3$ | 2161.80 | 2265.60 | 2407.20 | 2283.00 | 2502.60 | 2604.60 |
| Increase in area, % | | 4.80 | 11.35 | 5.60 | 12.98 | 20.48 |
| Aluminum | | | | | | |
| Area, $cm^2$ | 26.05 | 24.34 | 21.97 | 24.11 | 21.45 | 18.75 |
| Volume, $cm^3$ | 1563.17 | 1460.40 | 1320.00 | 1446.60 | 1287.60 | 1125.0 |
| Mass, g | 4236 | 3957 | 3577 | 3920 | 3489 | 3049 |
| Total uranium[c] | | | | | | |
| Area, $cm^2$ | 0.16 | 0.16 | 0.16 | 0.16 | 0.16 | 0.16 |
| Volume, $cm^3$ | 9.52 | 9.52 | 9.52 | 9.52 | 9.52 | 9.52 |
| Mass, g | 180 | 180 | 180 | 180 | 180 | 180 |
| Silicon[d] | | | | | | |
| Area, $cm^2$ | 0.13 | 0.15 | 0.12 | 0.05 | 0.05 | 0.05 |
| Volume, $cm^3$ | 7.68 | 8.89 | 7.08 | 2.86 | 3.02 | 3.18 |
| Mass, g | 17.1 | 14.9 | 15.7 | 6.6 | 7.0 | 7.4 |
| Decrease in mass, % | | 12.9 | 8.2 | 61.5 | 59.0 | 56.8 |
| CHANGES IN Al-TO-$H_2O$ RATIO AND REACTIVITY FOR THE 3 BY 9 SLAB LOADING ARRANGEMENT[e] | | | | | | |
| Al-to-$H_2O$ ratio | 0.734 | 0.666 | 0.581 | 0.656 | 0.562 | 0.477 |
| $\Delta k/k$ in per cent[f] | | +0.8 | +2.0 | +0.9 | +2.3 | +3.7 |

[a]Thickness remaining after brazing with 125-mil braze-clad side-plate material (106 mils of aluminum plus 19 mils of aluminum-silicon alloy).

[b]Includes one half of the water spacing between adjacent units.

[c]Total uranium content includes 168 g of $U^{235}$, 1.7 g of $U^{234}$, and 10.3 g of $U^{238}$.

[d]Based on silicon contained in 11.6% Si–88.4% Al alloy only; 2S grade aluminum contains a maximum of 1% (Fe + Si).

[e]The 3 by 9 active lattice consists of 23 fuel units and 4 control rods positioned with the fuel sections completely "in." Area and volume measurements based on one half the water gap between the beryllium reflector and the lattice being assigned to the active lattice. The active lattice dimensions are 9.139 by 28.674 in. with an effective depth of 26.622 inches.

[f]Taken from plot $\Delta k/k$ vs. Al-to-$H_2O$ ratio in document IDO-16083-PPCo (Mar. 16, 1953), p. 15, by H. L. McMurray. $\Delta k/k = 0$ at $Al/H_2O = 0.732$ for the type I fuel element design.

**Transverse Tensile Strength of Core Material**

Tensile specimens were prepared by brazing aluminum pull bars to coupons cut from several alclad plates to determine the strength of the core material in the direction transverse to rolling. Aluminum-silicon eutectic alloy and Eutector 190 brazing flux were used for brazing. The samples and pull bars were jigged for proper alignment, brazed, and machined in the region of the test coupon to a diameter of 0.505 inch. Results are summarized in Table 30.

The core material with higher concentrations of pressed powder shows inferior strength to that of the 17% uranium–83% aluminum alloy core. Since the core material in most reactors is not a load-bearing member, this strength difference is probably not an important factor.

**Density of Core Material**

Measurements were made to determine the density of the core stock containing the equivalent of 20, 30, and 40 wt % uranium as $U_3O_8$-aluminum powder. Six clad-core-clad disks approximately 1 in. in diameter were punched at random along the length of the finished plates. The over-all density was determined on each composite. The values obtained on samples taken from the same plate showed surprisingly good agreement.

To obtain the density of the core material, it was necessary to accurately measure the cladding thickness. This was done by measuring the clad-core-clad thickness on a given sample at several fields under the microscope to obtain an average value. Table 31 gives the core density of the sample selected from each plate.

Unfortunately, the cladding prevented a direct check on the density of the core material. To check the accuracy of these observed-calculated values, however, a comparison of the observed and the theoretical density of $U_3O_8$ was made. The following assumptions were used in making the comparison: Uranium was present in core material as $U_3O_8$, and the weight percentages were those of the starting material. The observed value of 5.93 g/cm$^3$ found for $U_3O_8$ is somewhat smaller than the range of values reported by Katz and Rabinowitz,[2]

[2] J. J. Katz and E. Rabinowitz, *The Chemistry of Uranium*, NNES Div. 8 Vol. 5, Table 11.13, p. 272, McGraw-Hill, New York, 1951.

TABLE 30. TRANSVERSE TENSILE STRENGTH OF ALUMINUM–$U_3O_8$ OR ALUMINUM–URANIUM ALLOY CORES

| SAMPLE DESIGNATION | TEST MATERIAL | MAXIMUM LOAD (psi) | REMARKS |
|---|---|---|---|
| 17-1 | Alclad 23.6 wt % $U_3O_8$–Al powder plate | 3,150 | Failed through core |
| 17-2 | Alclad 23.6 wt % $U_3O_8$–Al powder plate | 6,150 | Failed through core |
| 17-3 | Alclad 23.6 wt % $U_3O_8$–Al powder plate | 4,500 | Failed through core |
| 18-1 | Alclad 35.4 wt % $U_3O_8$–Al powder plate | 2,275 | Failed through core |
| 18-2 | Alclad 35.4 wt % $U_3O_8$–Al powder plate | 2,875 | Failed through core |
| 18-3 | Alclad 35.4 wt % $U_3O_8$–Al powder plate | 3,050 | Failed through core |
| 19-1 | Alclad 47.2 wt % $U_3O_8$–Al powder plate | 1,200 | Failed through core |
| 19-2 | Alclad 47.2 wt % $U_3O_8$–Al powder plate | 2,225 | Failed through core |
| 19-3 | Alclad 47.2 wt % $U_3O_8$–Al powder plate | 1,250 | Failed through core |
| 1 | Alclad 17 wt % U–Al alloy plate | 10,950 | Failed through core |
| 2 | Alclad 17 wt % U–Al alloy plate | 11,000 | Failed through braze joint |
| 3 | Alclad 17 wt % U–Al alloy plate | 11,675 | Failed through core |
| 4 | Alclad 17 wt % U–Al alloy plate | 13,075 | Failed through core |

TABLE 31. DENSITY VALUES FOR ALUMINUM-$U_3O_8$ CORE MATERIAL

| TEST DISK NO. | TEST MATERIAL | DENSITY ($g/cm^3$) |
|---|---|---|
| 17-10 | 23.6 wt % $U_3O_8$–Al powder core | 3.09 |
| 18-10 | 35.4 wt % $U_3O_8$–Al powder core | 3.31 |
| 19-10 | 47.2 wt % $U_3O_8$–Al powder core | 3.66 |

that is, 7.19 to 8.34 $g/cm^3$. In addition, the density of the starting $U_3O_8$ used in this work was found to be 8.40 $g/cm^3$, as determined by x-ray diffraction.

### Segregation in Core Material

On initial examination, both radiography and density determinations indicated that the cores were of uniform blend along the plate length. Chemical analysis by the potentiometric titration method failed to show similar results. Gross variations in the analytical results were traced to residues in the sample solution prior to titrating. Since "aquadag" was used in the preparation of these plates to prevent bonding of the cladding, graphite may have combined with oxygen to form carbon monoxide during rolling. The presence of CO may have caused a partial reduction of $U_3O_8$ to $UO_2$.

A second set of plates was prepared with the omission of the graphite layer, and samples were taken for chemical analysis. Again, a dark residue remained after acid treatment prior to titrating. This residue was identified as $UO_2$, and it occurred in quantities that would be capable of causing the variations shown by analysis of the previous samples. A second set of samples dissolved completely after a small addition of nitric acid to the 5 to 1 mixture of sulfuric and hydrochloric acids normally employed for dissolving. Results of analyses by both potentiometric and activation methods are given in Table 32.

The larger values of uranium content and the smaller deviation for the second set of potentiometric analyses are obviously the result of more complete solution of the samples. The variations found are probably due to the error in the analytical determination, variation in the core thickness, and/or segregation of the oxide. The analytical accuracy was reported to be ±0.5%.

TABLE 32. RESULTS OF POTENTIOMETRIC AND ACTIVATION ANALYSES OF CORE MATERIALS

| PLATE NO. | POTENTIOMETRIC ANALYSIS NO. 1 | | POTENTIOMETRIC ANALYSIS NO. 2* | | ACTIVATION ANALYSIS | |
|---|---|---|---|---|---|---|
| | Uranium Content** | Deviation From Mean (%) | Uranium Content** | Deviation From Mean (%) | Uranium Content** | Deviation From Mean (%) |
| 17 | 582*** | –7.9 | 751 | –2.8 | 616 | –9.0 |
| | 658 | +4.1 | 790 | +2.2 | 690 | +1.9 |
| | 655 | +3.8 | 777 | +0.5 | 725 | +9.2 |
| 18 | 1009 | +16.1 | 1135 | –3.9 | 1152 | +9.2 |
| | 791*** | –9.2 | 1209 | +2.5 | 1030 | –4.8 |
| | 808 | –7.1 | 1192 | +1.1 | 1065 | –5.3 |
| 19 | 1493 | 15.8 | 1638 | –2.1 | 1673 | –4.9 |
| | 1313*** | 1.1 | 1703 | +1.8 | 2077 | +18.0 |
| | 1087 | 17.1 | 1674 | +0.4 | 1529 | –16.0 |

*Samples for Potentiometric No. 2 completely dissolved.

**Milligrams of uranium per milligram of sample $\times 10^{-4}$.

***Samples showing heaviest residue in each group of three samples tested.

In conclusion, it was found that variations in uranium content as high as 4% existed along the length of the plate. It was not established whether these variations were due to segregation or differences in core thickness. Such variations would have no effect on the total uranium content present in a given plate, however, because this is limited only by the accuracy of the weighing of the core mixture prior to compacting.

## URANIUM-ALUMINUM ALLOY PRODUCTS

J. H. Erwin

### MTR Replacement Fuel and Control Rod Elements

Since March 1, 1953, ten complete core loadings have been fabricated and delivered to the MTR site. A complete loading for the 3 by 9 lattice arrangement consists of 23 thin-side-wall fuel elements and 2 cadmium-uranium control rod elements. One additional loading, the balance of the current order, is being constructed and should be completed and delivered prior to October 1, 1953. This total number of elements is sufficient to operate the reactor through the end of the calendar year and to maintain two core loadings in reserve.

Included in the above shipments was one complete fuel loading of the thin-side-wall 19-plate elements. The observed gain in $\Delta k/k$ for the reactor loaded with the new elements in the clean state was measured as 0.96% over the thin-side-wall 18-plate element or a gain of 1.56% over the original 18-plate, $^3/_{16}$-in. side-plate unit. The gain was somewhat lower than the calculated value of 2%. Complete operating performance for the 19-plate element, which decreased the Al-to-$H_2O$ ratio in the active core to 0.581, has not yet been reported. The ORNL engineering drawings which give the details of the thin-side-wall 19-plate element are given below:

| DRAWING TITLE | DRAWING NO. |
|---|---|
| Side plate and comb | D-16621 |
| Standard fuel plate | C-16623 |
| Outside fuel plate | C-16622 |

An experimental MTR control rod which features the substitution of an aluminum extrusion for the lower stainless steel bearing section was completed and transferred to the Reactor Experimental Engineering Division for testing. A dummy control rod element for the proposed Research Reactor was constructed for mechanical and hydraulic testing.

Recent improvements in the manufacturing process have made it possible to increase the rate of production of MTR type fuel elements to approximately 2.5 units a day. A recent survey showed that the actual unit costs of fabricating the fuel and control rod elements during the first six months of 1953 were $325.00 and $2830.00, respectively. These figures include costs incurred in handling and recovering the $U^{235}$ material.

An over-all material balance is drawn on each batch of enriched uranium metal processed. The inventory balance is completed only after the uranium contained in the dross, samples, crucibles, stirring rods, etc. is recovered. Inventory results on the last nine batches of material processed are shown in Table 33.

TABLE 33. INVENTORY RESULTS ON ENRICHED URANIUM MATERIAL PROCESSED

| AMOUNT OF $U^{235}$ PROCESSED (kg) | LOSS OR GAIN (g) | CHANGE (%) |
|---|---|---|
| 8.5 | +8 | 0.09 |
| 7.0 | +9 | 0.14 |
| 8.5 | +10 | 0.12 |
| 9.0 | +44 | 0.50 |
| 7.5 | +0.26 | |
| 8.0 | −8 | 0.09 |
| 13.0 | −9 | 0.07 |
| 12.0 | −6 | 0.05 |
| 7.0 | −14 | 0.20 |

It is felt that this slight discrepancy is due somewhat to the chemical analyses on which the uranium contents are based. It is suspected that better agreement in the material balances would result if the uranium content were based on the intended melt composition and the chemical analysis were used as a secondary check. A study of metallurgical data obtained previously is now being made to determine the validity of such a basis for material balances.

### LITR Replacement Fuel and Control Rod Elements

The ten "sweetened" fuel elements and three "sweetened" control rods needed for operation of the LITR at the 3-megawatt power level were fabricated and delivered to the Operations Division.

### Fuel Elements for BORAX

The 28 special elements needed by ANL for the boiling experiments were completed and forwarded to Arco. The unit was a modified MTR type of element containing only ten active plates. The fuel content of each unit was specified as 157 ± 1 g of $U^{235}$.

### BSR Fuel Elements

The ten standard 140-g fuel assemblies and three cadmium-lead control rods needed to complete a cold loading of elements for operation of the Bulk Shielding Reactor at a power level of 100 watts or less were completed.

### Fuel and Control Elements for the Tower Shielding Facility

Fabricational work was started on the initial loading of 36 fuel units required for startup of the Tower Shielding Facility. These elements are scheduled for completion by November 1, 1953.

### Extrusion of Enriched Uranium-Aluminum Alloy Rod Stock for "J" Slugs

Twenty-four enriched 7.5 wt % uranium–aluminum alloy rods were fabricated[3] and delivered to the processing group in Building 9212 at Y-12. The stock was needed for completion of an order for 200 experimental extruded "J" slugs for Hanford. The canning, irradiation, and chemical dissolving characteristics of extruded slugs will be evaluated for comparison with the behavior of similar slugs prepared by casting.

Castings 4 in. in diameter and 11 in. long were prepared by conventional methods at Y-12 and transferred to X-10 for extrusion. The fabrication schedule used for breaking down the casting to 1.375-in.-dia wrought rod is given in Table 34.

The rods were straightened in the Medart straightener between the intermediate and final draw, as well as after the final draw. The final diameter of the rods was intentionally left 0.012 in. oversize to permit machining to final slug size. There was not sufficient time available to tool-up to remove the objectionable 0.001-in. ridges left by the Medart straightener.

In conclusion, it was found that converting the 4-in.-dia 7.5 wt % uranium–aluminum alloy castings into 1.375-in.-dia wrought stock presented no difficult fabricational problems. The nature of the alloy is such that the alloy can be readily cold or hot worked. The yield of metal from fabricating cropped castings into finished extruded and drawn rod stock was better than 99%.

### Fabrication of Alclad Uranium-Aluminum Alloy Tube for Chalk River

The possibility of fabricating an alclad enriched uranium-aluminum alloy tube for service in the NRX reactor was investigated. Preliminary work[4] conducted on a 20% normal uranium alloy indicated that a tube, 1.36 in. in outside diameter with a 0.125-in. wall thickness, clad inside and out with 0.0625-in.-wall aluminum tubing, could easily be fabricated.

[3] J. E. Cunningham and J. H. Erwin, *Extrusion of Enriched Uranium-Aluminum Alloy Rod Stock for Preparation of Hanford "J" Slugs*, ORNL CF-53-6-240 (June 26, 1953).

[4] J. H. Erwin, *Work Done by D. E. Rosson – Preliminary Studies on Fabrication of Alclad U-Al Alloy Tube for Chalk River*, ORNL CF-53-6-132 (June 17, 1953).

TABLE 34. EXTRUSION AND DRAWING SCHEDULE

| WORK PIECE DIAMETER (in.) | REDUCTION IN AREA PER PASS (%) | TEMPERATURE (°C) | REMARKS |
|---|---|---|---|
| 4.0 | | | As-received U-Al casting |
| 1.5 | 86 | 500 | As extruded |
| 1.415 | 11 | Room temperature | Initial cold draw at 5 fpm |
| 1.386 | 4 | Room temperature | Intermediate draw at approximately 25 fpm |
| 1.375 | 2 | Room temperature | Final draw at approximately 25 fpm |

## MISCELLANEOUS FABRICATIONAL WORK

Approximately one thousand normal uranium and one thousand uranium–0.1% thorium miniature slugs were prepared for dissolving studies by the Chemical Technology Division.

About 2000 lb of lead-bismuth alloy was made for the ANP group at Y-12.

Small amounts of enriched-uranium foil were fabricated for MIT and the ORNL Criticality Group.

Work was started on the fabrication of a 28-in.-dia uranium disk, $\frac{1}{16}$ in. thick, to be used by the Physics Division as a new source plate in the Lid Tank Facility.